DTIC FILE COPY

(4)

AD-A216 465

RADC-TR-89-202
In-House Report
October 1989

THE INTERACTION OF POLYCRYSTALLINE COPPER FILMS WITH DILUTE AQUEOUS SOLUTIONS OF CUPRIC CHLORIDE

Lois Harper Walsh

DTIC
ELECTE
JAN 0 4 1990
S D
D

APPROVED FOR PUBLIC RELEASE; DISTRIBUTION UNLIMITED.

ROME AIR DEVELOPMENT CENTER
Air Force Systems Command
Griffiss Air Force Base, NY 13441-5700

90 01 04 071

This report has been reviewed by the RADC Public Affairs Office (PA) and is releasable to the National Technical Information Service (NTIS). At NTIS it will be releasable to the general public, including foreign nations.

RADC TR-89-202 has been reviewed and is approved for publication.

APPROVED:

JOSEPH B. BRAUER, Chief
Microelectronics Reliability Division
Directorate of Reliability and Compatibility

APPROVED:

JOHN J. BART
Technical Director
Director of Reliability and Compatibility

FOR THE COMMANDER:

JAMES W. HYDE III
Directorate of Plans and Programs

If your address has changed or if you wish to be removed from the RADC mailing list, or if the addressee is no longer employed by your organization, please notify RADC (RBRE) Griffiss AFB NY 13441-5700. This will assist us in maintaining a current mailing list.

Do not return copies of this report unless contractual obligations or notices on a specific document requires that it be returned.

UNCLASSIFIED
SECURITY CLASSIFICATION OF THIS PAGE

REPORT DOCUMENTATION PAGE

Form Approved OMB No. 0704-0188

1a. REPORT SECURITY CLASSIFICATION UNCLASSIFIED	1b. RESTRICTIVE MARKINGS N/A
2a. SECURITY CLASSIFICATION AUTHORITY N/A	3. DISTRIBUTION/AVAILABILITY OF REPORT Approved for public release; distribution unlimited.
2b. DECLASSIFICATION/DOWNGRADING SCHEDULE N/A	
4. PERFORMING ORGANIZATION REPORT NUMBER(S) RADC-TR-89-202	5. MONITORING ORGANIZATION REPORT NUMBER(S) N/A
6a. NAME OF PERFORMING ORGANIZATION Rome Air Development Center 6b. OFFICE SYMBOL (If applicable) RBRE	7a. NAME OF MONITORING ORGANIZATION Rome Air Development Center (RBRE)
6c. ADDRESS (City, State, and ZIP Code) Griffiss AFB NY 13441-5700	7b. ADDRESS (City, State, and ZIP Code) Griffiss AFB NY 13441-5700
8a. NAME OF FUNDING/SPONSORING ORGANIZATION AFOSR 8b. OFFICE SYMBOL (If applicable) RBRE	9. PROCUREMENT INSTRUMENT IDENTIFICATION NUMBER N/A
8c. ADDRESS (City, State, and ZIP Code) AFOSR Bolling AFB DC 20332-6600	10. SOURCE OF FUNDING NUMBERS PROGRAM ELEMENT NO. 61102F; PROJECT NO. 2306; TASK NO. J4; WORK UNIT ACCESSION NO. 09

11. TITLE (Include Security Classification) THE INTERACTION OF POLYCRYSTALLINE COPPER FILMS WITH DILUTE AQUEOUS SOLUTIONS OF CUPRIC CHLORIDE

12. PERSONAL AUTHOR(S)
Lois Harper Walsh

13a. TYPE OF REPORT	13b. TIME COVERED	14. DATE OF REPORT (Year, Month, Day)	15. PAGE COUNT
In-House	FROM Sep 87 TO Mar 89	October 1989	184

16. SUPPLEMENTARY NOTATION
Also submitted in partial fulfillment of requirements for degree of Doctor of Philosophy in Solid State Science and Technology at Syracuse University.

17. COSATI CODES			18. SUBJECT TERMS (Continue on reverse if necessary and identify by block number)
FIELD	GROUP	SUB-GROUP	
13	08		Dissolution, Copper, Microelectronics, Etch
20	12		

19. ABSTRACT (Continue on reverse if necessary and identify by block number)

The dissolution of copper in a dilute aqueous cupric chloride solution was studied to achieve an understanding of the role microstructure plays in the dissolution process. A multi-technique approach was taken using combinations of solution chemistry, computer modeling, and microstructural characterization techniques to analyze as-received samples and to monitor the dissolution process. This latter approach allowed reaction rates and activation energies to be calculated from speciation concentrations derived from computer modeling of known thermochemical reactions. In conjunction with the solution analysis, surface techniques were used to analyze the concentration distribution of the various elements after sample exposure to the etchant.

An important conclusion from this research is that the etching characteristics of the polycrystalline thin copper films are dependent on the film's microstructure and must be reported with any quantitative reaction rates and activation energies to be useful members of the data base begun with this research. A procedure is suggested that will aid future researchers in the (Cont'd)

20. DISTRIBUTION/AVAILABILITY OF ABSTRACT ☐ UNCLASSIFIED/UNLIMITED ☒ SAME AS RPT. ☐ DTIC USERS	21. ABSTRACT SECURITY CLASSIFICATION UNCLASSIFIED
22a. NAME OF RESPONSIBLE INDIVIDUAL LOIS HARPER WALSH	22b. TELEPHONE (Include Area Code) (315) 330-4055 22c. OFFICE SYMBOL RADC(RBRE)

DD Form 1473, JUN 86 Previous editions are obsolete. SECURITY CLASSIFICATION OF THIS PAGE
UNCLASSIFIED

19 (Cont'd). correlation of microstructure and dissolution characteristics of different copper samples prior to mass production of metallization for microelectronic circuits. In other words, it is shown that with knowledge of the surface and the bulk structure of the copper sample, one can predict how the sample will react to an etchant and, therefore, exercise control over the dissolution process.

Accesion For
NTIS CRA&I ☑
DTIC TAB ☐
Unannounced ☐
Justification
By
Distribution /
Availability Codes
Dist | Avail and / or Special
A-1

ABSTRACT

The dissolution of copper in a dilute aqueous cupric chloride solution was studied to achieve an understanding of the role microstructure plays in the dissolution process. A multi-technique approach was taken using combinations of solution chemistry, computer modeling, and microstructural characterization techniques to analyze as-received samples and to monitor the dissolution process. This latter approach allowed reaction rates and activation energies to be calculated from speciation concentrations derived from computer modeling of known thermochemical reactions. In conjunction with the solution analysis, surface techniques were used to analyze the concentration distributions of the various elements after sample exposure to the etchant.

XRD results demonstrated that differently deposited samples had a variation in preferred orientation ranging from strong (111) to strong (100). In a closed system the apparent activation energy for the dissolution reaction on the strongly oriented (100) electroless samples is $48 kJ \cdot mol^{-1}$ and $79 kJ \cdot mol^{-1}$ for the slightly (111) oriented evaporate sample. This increase in activation energy occurs despite a small decrease in the average grain size of these samples as determined by SEM and TEM analysis. A decrease in nucleation sites due to a decrease in average grain size is proposed to account for the decrease in dissolution rate. Auger Electron Spectroscopy mapping and

depth profiling were used to determine the composition of the surface film resulting from the exposure of copper to the 0.01M cupric chloride solution. It was found that chloride deeply penetrated the sample while the oxide concentration decreased with increasing distance from the sample's surface. Similar findings were reported for the vapor phase halogenation of copper and provides the basis for comparing these two reaction systems.

The Cu_2^+/Cu_3^+ cluster ratios were determined for the samples by secondary ion mass spectroscopy(SIMS). The slightly (111) oriented evaporate film had the lowest cluster ratio while the (100) oriented film, with a more open structure, had higher ratios. The activation energies measured for these two types of sample increased with increasing degree of (111) character. The SIMS results, therefore, further confirm the importance of crystallographic orientation on the dissolution kinetics of copper samples in dilute copper chloride electrolytes.

An important conclusion from this research is that the etching characteristics of the polycrystalline thin copper films are dependent on the film's microstructure and must be reported with any quantitative reaction rates and activation energies to be useful members of the data base begun with this research. A procedure is suggested that will aid future researchers in the correlation of microstructure and dissolution characteristics of different copper samples prior to mass production of

metallization for microelectronic circuits. In other words, it is shown that with knowledge of the surface and the bulk structure of the copper sample, one can predict how the sample will react to an etchant and, therefore, exercise control over the dissolution process.

PREFACE

Thanks are due to many individuals for their support and asssitance in the completion of this dissertation. First and foremost, thanks to my family for their long suffering patience. Thanks to my husband, Doug, for his faith in my abilities. Thanks to my children, Richard and Patricia, for their coping with a mommy in school. Especially, thanks for accompanying me on the midnight trips to the laboratory.

Thanks to John Hassett for his words of encouragement and many discussions on water chemistry during our hours of commuting back and forth to Syracuse.

I thank my friends at IBM, Endicott for their support in this project. The encouragement received from Nadia Tonsi and Natalie Feilchenfeld to bring an idea to a research proposal. Thanks to Ralph Paonessa who, as supervising engineer, aided with supplies and equipment to bring the research proposal to an actual project. Special thanks to Kim Blackwell, Ron McHatton, Rich Weale, and Oscar Moreno who supplied copper samples from IBM for this research. Also thanks to Frank Emmi for the initial Auger spectroscopy work.

Thanks also to my adivsor, Dr. Jim Schwarz, who was willing to supervise this research projeect. Appreciation is also given to Dr. Yoshi Oshida for the x-ray diffraction data and Dr. Robert Huang for his advise in computer modelling.

Sincere appreciation is expressed to all of my friends at the Rome Air Development Center. Especially thanks to David Roberts, Bela Vastag, Donald Calabrese, Eugene Blackburn, Terry Oxford, and Ivars Irbe for help with analysis techniques, reading rough drafts and translating the German article. Special thanks go to Marie St. Thomas for her expert typing. Finally, I wish to thank Dr. Robert Thomas for his generous support and understanding during this research project.

CONTENTS

Page

LIST OF TABLES.....vi

LIST OF FIGURES.....vii

CHAPTER

I. INTRODUCTION..... 1

II. OBJECTIVE OF RESEARCH..... 13

III. EXPERIMENTAL PROCEDURE 16

IV. RESULTS AND DISCUSSION..... 25

V. SUMMARY..... 61

VI. CONCLUSIONS AND RECOMMENDATIONS..... 65

BIBLIOGRAPHY.....161

LIST OF TABLES

TABLE	TITLE	PAGE
1	PHI 600 Multiprobe parameters	67
2	Surface techniques	68
3	Colorimetric Results	69
4	Qualitative correlation of color change and oxide thickness	70
5	XRD:original electroless	71
6	XRD:original electroplate	72
7	XRD:original evaporate	73
8	XRD:original sputter	74
9	Deposition parameters and film characteristics	75
10	pH: summary of long etch results (0.01M $CuCl_2$ at 45°C open system)	76
11	Chemical equations and equilibrium constants at 25°C	77
12	Microql matrix for an open system	78
13	Microql matrix for a closed system	79
14	Equilibrium constants calculated for each experimental temperature	80
15	Microql output for copper species in the Electroless, 45°C open system	81
16	Experimental reaction rates	82
17	Experimental activation energies	83
18	Reaction rates calculated from Sesselmann's experimental diffusion constants	84
19	Activation energies calculated from Sesselmann's experimental diffusion constants	85
20	Activation energy versus preferred orientation ratio	86
21	Comparison of activation energy with film thickness/grain size and grain size	87
22	SEM: SUMMARY	88
23	AES: SUMMARY	89
24	SIMS: SUMMARY	90

LIST OF FIGURES

FIGURE	TITLE	PAGE
1	GRAVIMETRIC: room temperature	91
2	GRAVIMETRIC: ice bath	91
3	OPTICAL: original electroless	92
4	COLORIMETRIC: electroless after 1.8 hours exposure to 0.001M $CuCl_2$ at room temperature	92
5	OPTICAL: original electroplate	93
6	COLORIMETRIC: electroplate after 1.8 hours exposure to 0.001M $CuCl_2$ at room temperature	93
7	OPTICAL: original evaporate	94
8	COLORIMETRIC: evaporate after 1.8 hours exposure to 0.001M $CuCl_2$ at room temperature	94
9	OPTICAL: sputter	95
10	COLORIMETRIC: sputter after 1.8 hours exposure to 0.001M $CuCl_2$ at room temperature	95
11	SEM: original electroless	96
12	SEM: original electroplate	96
13	SEM: original evaporate	97
14	SEM: original sputter - 1000X	98
15	SEM: original sputter - 5000X	98
16	SEM: ion beam etch electroless 1.5 minute	99
17	SEM: ion beam etch electroplate 30 minute	99
18	SEM: ion beam etch evaporate 78 minute	100

19 SEM: ion beam etch sputter 34 minute.....100

20 AES: original electroless.....101

21 AES: original electroplate.....101

22 AES: original evaporate.....102

23 AES: original sputter.....102

24 AES: electroless 1.0 min. ion beam etch.....103

25 AES: electroless 1.5 min. ion beam etch.....103

26 AES: electroplate 1.0 min. ion beam etch.....104

27 AES: evaporate 1.0 min. ion beam etch.....104

28 AES: evaporate 2.0 min. ion beam etch.....105

29 AES: sputter 1.0 min. ion beam etch.....105

30 SIMS: original electroless.....106

31 SIMS: original electroplate.....106

32 SIMS: original evaporate.....107

33 SIMS: original sputter.....107

34 SIMS: comparison of original films 108

35 pH: blank 1.....109

36 pH: blank 2.....109

37 pH: blank 3.....110

38 pH: blank 4.....110

39 pH: blank 5.....111

40 pH: electroless 45°C closed.....111

41 pH: electroless 45°C open.....112

42 pH: electroless 20°C closed.....112

43 pH: electroless 10 C open.....113

44 pH: electroless 3 C closed.....113

45 pH: electroplate 45 C closed.....114

46 pH: electroplate 45 C open.....114

47 pH: electroplate 10 C open.....115

48 pH: electroplate 3 C closed.....115

49 pH: evaporate 45 C closed.....116

50 pH: evaporate 45 C open.....116

51 pH: evaporate 10 C open.....117

52 pH: evaporate 45 C closed no light.....117

53 pH: evaporate 20 C closed.....118

54 pH: evaporate 20 C open.....118

55 pH: evaporate 3 C closed.....119

56 pH: sputter 45 C closed.....119

57 pH: sputter 45 C open.....120

58 pH: sputter 10 C open.....120

59 SEM: electroless short etch.....121

60 SEM: electroplate short etch.....121

61 SEM: evaporate short etch.....122

62 SEM: evaporate short etch.....122

63 SEM: electroless short etch.....123

64 AES MAP: electroless short etch - chlorine....123

65 AES MAP: electroless short etch - copper.....124

66 AES MAP: electroless short etch - oxygen.....124

67 SEM: electroplate short etch.....125

68 AES MAP: electroplate short etch - chlorine...125

69 AES MAP: electroplate short etch - copper.....126

70 AES MAP: electroplate short etch - oxygen.....126

71 AES MAP: electroplate short etch - carbon.....127

72 AES MAP: evaporate short etch - chlorine.....127

73 AES MAP: evaporate short etch - copper.....128

74 AES MAP: evaporate short etch - oxygen.....128

75 AES: electroless short etch.....129

76 AES: electroplate short etch.....129

77 AES: evaporate short etch.....130

78 ADP: electroless 45°C short etch.....131

79 SIMS: electroless short etch.....132

80 SIMS: electroplate short etch.....132

81 SIMS: evaporate short etch.....133

82 SIMS: comparison short etch.....133

83 SEM: electroless long etch.....134

84 SEM: electroplate long etch.....134

85 SEM: electroplate long etch.....135

86 SEM: evaporate long etch.....135

87 SEM: electroplate long etch.....136

88 SEM: sputter long etch.....136

89 SEM: electroless long etch.....137

90 AES: electroless long etch.....137

91 SEM: electroless long etch.....138

92 AES: electroless long etch point 1.....138

93 AES: electroless long etch point 2.....139

94 AES: electroless long etch.....139

95 SEM: electroplate long etch.....140

96 AES: electroplate long etch (area survey).....140

97 AES: electroplate long etch at point 1.....141

98 AES: electroplate long etch at point 2.....141

99 AES: electroplate long etch at point 3.....142

100 AES: electroplate long etch at point 4.....142

101 AES: electroplate long etch at center.....143

102 AES: evaporate long etch.....143

103 AES: sputter long etch.....144

104 AES: electroplate long etch
after 0.5 min. ion beam sputter.....145

105 AES: electroplate long etch
after 1.0 min. ion beam sputter.....145

106 AES: electroplate long etch
after 1.5 min. ion beam sputter.....146

107 AES: evaporate long etch.....147

108 AES: evaporate long etch.....147

109 AES: evaporate long etch.....148

110 AES: sputter long etch at point 1.....148

111 AES: sputter long etch at point 2.....149

112 AES: sputter long etch at point 3.....149

113 AES: sputter long etch at point 4.....150

114 AES: sputter long etch at point 5.....150

115 AES: sputter long etch at point 6.....151

116 AES MAP: sputter long etch - chlorine.....151

117 AES MAP: sputter long etch - copper.....152

118 AES MAP: sputter long etch - oxygen.....152

119 AES MAP: sputter long etch - carbon.....153

120 ADP: evaporate long etch 45°C closed system...154

121 AES: fracture cross-section line profile.....155

122 SIMS: electroless long etch.....156

123 SIMS: electroplate long etch.....157

124 SIMS: evaporate long etch.....157

125 SIMS: sputter long etch.....158

126 SIMS: comparison long etch.....158

127 SIMS: comparison all electroless.....159

128 SIMS: comparison all electroplate.....159

129 SIMS: comparison all evaporate.....160

130 SIMS: comparison all sputter.....160

I. INTRODUCTION

In the electronics industry, thin films of copper deposited on substrates are used as electrically conductive paths to interconnect semiconductor devices and other computer components. Electronic circuits are mass produced to obtain product uniformity and lowest manufacturing cost. For mass production to be effective all raw materials used in the manufacturing process must have identical critical properties regardless of their source. For example, in general, copper thin films would be considered as a single raw material regardless of their deposition type. In particular, the mass production assumption is that all copper metal, regardless of origin, will chemically, physically, and electrically respond in the same way in an electronic circuit. Unfortunately, interchangeability rarely applies to systems that require such exacting process control as metal deposition.

The interchangeability assumption is not valid for copper since the copper metal's basic character or microstructure will vary depending on origin. Variations in microstructure such as grain size and preferred grain orientation are not considered in mass produced circuits, but these properties are critical to characterization of the copper metal. Also, in general, the metal deposition technique is dictated by the size of the substrate rather than by the desired final metal characteristics. Large

substrates or circuit boards are plated in aqueous baths which are easily scaled to accommodating sizes. Small circuits, such as decals, can be easily inserted into vacuum systems for either evaporate or sputter deposition. Of course, the substrate also influences the copper metal by changes in surface composition and topography offered to the depositing copper atoms.

Various deposition techniques are known to produce different characteristics such as: 1. crain size, 2. preferred grain orientation, and 3. surface topography.[15] Common deposition techniques used in the electronics industry are: 1. electroless, 2. electroplate, 3. evaporate, and 4. sputter deposition.

In the electroless process, the films are deposited from the chemical reduction of a cupric compound in an aqueous bath on to an activated non-metallic substrate. A seed pattern is deposited to provide nucleation sites for the copper metallization before immersion of the substrate into the electroless bath. The films grow as nucleated islands which gradually coalesce conforming to the rough texture of the substrate surface. Grains can be random, twinned or columnar and are controlled by bath parameters. Large, thick substrates can be used in this technique, since the bath can be of any convenient size. The copper film grows from the seed which also forms an adhesive bond between the copper and the substrate so that the copper film will not separate from the substrate. As implied by

the name, "electroless," the deposition occurs without electrical contact so the substrate does not need to be conductive.

In the electroplating process, films are formed on substrates in electrolytes under the influence of an electric field. In copper deposition, cupric solutions are used and the ions are deposited on a metallic substrate which acts as a cathode. Hydrogen can be incorporated into the films during the plating process. The grains can be: 1. dendritic, plate-like, cubic, pyramidal, or polycrystalline; 2. fine and angular or in large clusters depending on bath parameters.

In the evaporation process, films are deposited in a high vacuum on to substrates which may be preheated or cooled during deposition. The copper source can be evaporated by electron beam bombardment, filament evaporation, or inductive heating. Films can be columnar or random, and are dependent on substrate and deposition conditions.

In the sputtering process, films are deposited in a high vacuum with an inert gas background (argon) and high (several kilovolts) potentials applied to the cathode (target). There is a possibility of argon being incorporated into the films during deposition. During sputter deposition, films are continually bombarded by ions and/or energetic neutrals which can cause film damage. The film damage at point defects will have higher

energy than the rest of the film. The point defects could etch faster than undamaged portions of the film. (The point defects would be anodic to the remainder of the film.) Films can be columnar or random dependent on substrate and deposition conditions.

Processing of the accumulated metal film depends to some extent on the deposition technique. In an additive process, electroless film deposition adds copper directly to the substrate in the desired conductive pattern. Electroplate, evaporate, and sputter deposits form a blanket metallization ready for subtractive processing. Subtractive processing removes a portion of the deposited film leaving a conductive pattern available for use as an electrical path to support electronic components. Each metallization technique must result in a uniform, well-defined, high purity copper line. Uniformity is required to insure desired electrical characteristics for the entire metal pattern. For example, non-uniform, higher resistance regions could result in thermal hot spots and current density changes causing either gradual or even catastrophic electronic and/or physical failure. Good pattern definition is needed for the metal path to be consistent throughout. The remaining metal must also be a replica of the designed pattern to allow for proper interconnection of each electrical component being supported. High purity metal is required to prevent introduction of mobile conductive impurities which might

migrate to other parts of the electrical circuit presenting future reliability problems. Obviously such high quality conductive paths require careful monitoring during both thin film formation and later circuit processing.

Specifically, subtractive processing of the blanket metallization to form the desired conductive pattern may consist of chemical etching around a mask to remove excess material. Consistent with the philosophy of interchangeability in mass production the same etchant would be used regardless of the copper's origin. However, the resultant pattern is not always optimum. Some metallization may be over etched causing undercutting into the remainder of the conductive path. Other metallization may under etch requiring more exposures to the etchant with the risk of undercutting or lifting of the mask to expose even more copper to the etchant, decreasing the line width. This observed variation in etching has usually been attributed to changes in the etchant rather than correlated with the metallization.

The etching process may be compared to the widely studied process of copper corrosion. A few of the most recent papers reporting corrosion characteristics include details of the copper sample's microstructure.[1] Studies which provide information relevant to the etching of microcircuit metallization were reviewed as an introduction to the current study.[2] Besides the ambient

cuprous oxide always present on the copper film, corrosion will also produce some cuprous oxide. Cuprous oxide growth during corrosion was reported to be influenced by illumination,[5,6] magnetic fields,[7] oxygen in the electrolyte,[1,8] copper and chloride ions,[9] hydroxide and hydrogen ions,[10] and other additives to the electrolyte.[11]

Oxidation in solution has been studied by many researchers because of the extensive use of copper and copper alloys in ships and in aqueous carrying plumbing. The corrosion of copper has been studied by measuring electrochemical changes in the solution during the corrosion process. Some initial reported efforts have shown: 1. that the preparation of the electrodes does influence the electrochemistry of the corrosion process,[12] and 2. the solution parameters such as temperature and concentration do influence the preferential attack of the microstructure of the electrode.[1]

North et al., for example, demonstrated that for free corrosion and corrosion with applied potential, water and/or chloride ions accelerate the growth of cuprous oxide on copper electrodes (microstructure not reported) by modifying the defect structure of the cuprous oxide to make it less protective.[9] The hydroxide ion adsorbs from neutral aqueous solutions on to the oxide surface and replaces oxygen ions in the oxide lattice. This substitution results in the creation of one additional cation vacancy for each hydroxide substitution,

thus making the oxide even more permeable to the outward diffusion of cations from the sample to the solution and therefore, less protective.

When chloride ions are present in the solution, North suggested that the chloride ion replaces some of the oxygen ions in the oxide lattice. To neutralize the charge imbalance, one cuprous ion passes into solution for each chloride ion substitution. Additional cation vacancies created by the charge neutralization allowed easier diffusion of cuprous ions away from the metal film.

In an attempt to study the dissolution of Analar copper foil in weakly acidic solutions of either perchloric or hydrochloric acid in the pH range 4.0 - 5.5, Read controlled P_{O2}, pH, $[Cu^{++}]$, and ionic strength while ignoring variation of rate with surface preparation.[10] Assuming the total reaction to be:

$$Cu + 2H^{+} + 1/2\ O_2 = Cu^{++} + H_2O$$

the copper dissolution was followed by measuring the change in proton concentration. Read's samples consisted of strips of copper foil (15 cm x 3 cm) which were corroded by a magnetically stirred solution contained in a cylindrical water-jacketed vessel. Several rate measurements were made on the same surface because of the difficulty of reproducing surface conditions. (Raicheva[12] later showed that surface preparation will influence reaction rates.) Read also did not remove the original oxide layer.[10]

The initial portions of the experiments were discarded by Read because of the suspected introduction of carbon dioxide into the etchant with the copper sample. Therefore, Read's conclusions are based on results obtained after one hour of sample exposure to the solution. An apparent activation energy for corrosion is reported as $50 kJ \cdot mol^{-1}$, with reservations that the sample surface changed at 25°C. Dissolution rates in the range of 5×10^{-9} $mol \cdot h^{-1} cm^{-2}$ at 25°C were reported.

A solid-state mechanism, proposed by Read, to explain the oxidation and dissolution of copper was presented in terms of the production of cation vacancies and positive holes at the Cu_2O-H_2O interface and their later destruction at the Cu-Cu_2O interface after migration across the oxide film. Assumptions required for this mechanism are: 1. in an aqueous environment dissolution opposes film growth; 2. rate of oxide growth equals the rate of dissolution for films of constant thickness; and 3. film thickness can be considered constant when steady-state rates are observed. However, the solid-state model did not fully explain the data; and the conclusion was presented "that the slow step is a slow cation vacancy migration which rests on the available evidence concerning the enthalpy of migration." The slow step is the rate limiting step.

A study by Miller and Lawless used transmission electron microscopy to investigate the formation of an oxide layer on copper single crystals immersed in an aqueous solution of copper sulfate. The authors compare the interference patterns produced by the exposure of single crystal copper to: 1. dry oxygen vapor (250°C) and 2. an aqueous solution of cupric sulfate at a known concentration (50 grams per liter distilled water), temperature (25°C), and pH (3.8). The interference pattern was formed by various crystal faces responding differently to their environment. As a result of this qualitative comparison, Miller concludes that the rate of oxidation was much faster for crystals immersed in cupric sulfate solutions than for crystal exposed to dry oxygen or to water containing oxygen at the same temperature (25°C). Even though the rates were visually different the interference pattern arrangement on the crystals was similar regardless of oxidation mechanism.

No quantitative interpretations of reaction rates were attempted due to the roughness of the oxide surface. No effort was made to interpret the observed pH change after copper exposure to the solution. In fact, the pH was only measured twice, before and after copper immersion in the cupric sulfate solution. The oxide growth patterns were interpreted using the electrochemical theory of corrosion and the dislocation theory of crystal growth.[3]

Oxidation of copper in atmosphere has always been of interest because of the extensive use of copper and brass in buildings and statues, for example. A study by Pinnel et al. concentrated on oxidation in the temperature range of 50 to 150°C using an air atmosphere with 50% humidity. A sequential oxide growth mechanism was postulated to explain the observed growth rates on bulk copper. The first process was an immediate growth of a 1nm layer of cuprous oxide. The second process was parabolic and occurred as a function of time and temperature. One can conclude from this study that the copper sample will have at least 1nm of cuprous oxide present, the thickness of which is independent of the film deposition technique.[4]

Studies of the reaction of chlorine gas with copper surfaces have just begun with the increasing interest in plasma-assisted etching of copper. Winters et al.[24-26] and others[27-30,32] have studied etching of metals in reactive gases. Winters studied the interaction of chlorine gas with a Cu(100) single crystal using temperature programmed desorption in the temperature range of 150 to 200°C. The kinetics were shown to be zero order.

Winters proposes that reactions similar to oxidation are involved in the halogenation (formation of halides) of metals. In the vapor phase, a major difference between oxidation and halogenation is that saturated halides are often volatile while most oxides are nonvolatile. However,

both halogen and oxygen atoms tend to form negative ions at the surface.

Sesselmann and Chuang investigated the chlorination of copper surfaces in the vapor phase from 10 to 10^{10}L ($1L=1\times10^{-6}$Torr·sec). Surface layer combinations of CuCl and $CuCl_2$, depending on the experimental chlorine vapor pressure, were reported. Penetration depths and diffusion coefficients were determined as a function of the gas pressure and the exposure time. A dependence on gas pressure was found to exist in the system. Chlorine was reported to penetrate and dissolve into the bulk of the copper metal at 25°C. The suggested mechanism is that of the Cabrera-Mott oxidation type which involves field-assisted diffusion and lattice exchange of ions in the CuCl lattice and at the Cu-Cl_2 interface. The Cabrera-Mott model assumes the adsorption of oxygen atoms on the oxide surface with later tunneling of ionic species rapidly through the oxide to create a steady-state condition between the adsorbed oxygen and the metal sample. During the transfer process anions form, creating an electric field, which aids in the transport of ions across the oxide film. For this model, the rate determining step is assumed to be the dissolution of cations at the metal-oxide interface or anions at the oxide-gas interface, not the movement of ions in the oxide itself. This oxidation model assumes that the oxide formation is uniform throughout. Of course, Sesselmann and Chuang use the

Cabrera-Mott oxidation model suggesting that halogenation of copper by chlorine is similar in mechanism to oxidation of copper by oxygen.

This preliminary vapor phase research has shown that the chlorination of copper is a complex mechanism and dependent on the chlorine gas pressure. The copper microstructure was virtually ignored except for the mention of film thickness and crystal orientation. Grain size of the copper polycrystalline films was not given, but the preferred orientation was dominantly a (111) orientation. Sesselmann also notes that limited studies on a Cu(111) single crystal exhibits diffusion behavior similar to the polycrystalline material.[32]

Detailed information is lacking about the actual copper microstructure used in the reported solution and vapor corrosion or etching studies. Characteristics of the etching solution and the sample surface layer have been reported with no mention of the microstructure of the copper sample except for a few cases where chemical purity[11] and electrode preparation are detailed.[12] Leidheiser has predicted that changes in copper microstructure will influence the etching characteristics of the copper sample by changing the ratio of anodic to cathodic regions.[13] From the literature, the variables include: 1. material characteristics, 2. solution conditions, and 3. material to solution relationships. Material characteristics include: grain size, surface

topography, oxides on surface (before and after exposure to etchant), and surface films (e.g. examination of test sample with polysulfide solution clock reaction[11]). Solution conditions include: pH,[11,12] concentration of ions in solution (copper and chloride), dissolved oxygen content, illumination and magnetic fields present, sample exposure time, and temperature. The third variable includes: sample to electrolyte volume ratio and time in solution.

With all the above variables contributing to the interaction of copper with its environment, the lack of a complete study to thoroughly characterize the copper/cupric chloride system is not surprising. Although Read addressed the problem of copper free corrosion in weakly acidic solutions, "no great importance was attached to the variation of rate with surface preparation."[10] Raicheva addressed the surface preparation problem showing that the rate does vary with preparation; the author did not address microstructure as influencing the reaction rate.[12] However, Leidheiser did address the influence of microstructure from a theoretical viewpoint; experimental verification is still needed.[13]

II. Objective of Research

The objective of this research is to study the dissolution of copper in a dilute aqueous cupric chloride solution to achieve an understanding of the role of microstructure in the dissolution process. Presently, the

dissolution process has been limited to studies with emphasis on: 1. electrochemistry processes, 2: corrosion film growth and how the film is affected by solution or environmental conditions, and 3. halogenation of copper by reactive gases. These studies contribute to the understanding of how copper responds to its environment; but they do not address the issue of how a reaction is influenced by the copper microstructure. Of particular interest are the microstructures intrinsic to copper films formed by current deposition techniques and how each microstructure would influence copper dissolution in an etchant presently used in the microelectronics industry. A multidisciplinary approach using the information available from electrochemistry, materials science, and chemical kinetics, reported in the introduction, is necessary to study this complex processing of copper films used in the electronics industry. One can speculate that the benefits of the described research would be to provide the initial information to begin a much needed, but as yet non-existent, data base for reliable copper processing for use as interconnects in microelectronic applications.

The samples for this study are thin copper films deposited using electroless plating, electroplating, and two vacuum techniques (evaporate and sputter deposition). The substrates were activated reinforced epoxy resin circuit board for electroless deposition, titanium for electroplating, and chromium over polyimide for vacuum

deposition. As discussed previously, the copper microstructure is influenced by deposition technique and by receiving substrate to form unique samples. Therefore, each copper microstructure and its interaction with the etchant must be known in order to determine the controlling mechanism.

The microstructure and etching characteristics of these four different copper samples have been investigated prior to chemical etching by: optical microscopy, x-ray diffraction (XRD), scanning electron microscopy (SEM), Auger electron spectroscopy (AES), and secondary ion mass spectroscopy (SIMS). All the techniques, except XRD, will also be used after chemical etching to evaluate the exposed surface.

This multidisciplinary approach is designed to: 1. investigate differences in the microstructure of copper films deposited by different techniques on to appropriate substrates now used in the microelectronics industry for production or research, 2. obtain correlations between microstructure differences and chemical etching of different copper films, and 3. monitor pH change during the etching process as a possible dynamic tracer for both dissolution and corrosion film formation. The use of pH as a dynamic tracer would be similar to Read's[10] approach enabling the researcher to follow free corrosion rather than corrosion during electrochemistry which requires an electrical potential to be applied to the electrode or

sample. The solution conditions (temperature, volume, etc.) have been kept constant for each set of experiments. Also, the sample volume was kept small compared to the etchant volume and the time in solution was monitored. Experimental procedures are described in the next section.

III. EXPERIMENTAL PROCEDURE

Despite the amount of reported research on copper corrosion there is no one set of experimental procedures to be followed for the investigation of either the metal/solution or the metal/vapor system. Also there is no reported work specifically addressing the free corrosion of polycrystalline copper by dilute aqueous solutions of cupric chloride. Therefore, initial systematic probing of the copper-cupric chloride system must be used to glean as much information as possible from each analysis. Colorimetric and gravimetric techniques are used to establish solution parameters essential to obtain measurable pH changes during the initial copper/solution reaction. These empirical results also provide the basis for specimen preparations in subsequent studies.

The original thin copper films are analyzed by XRD for preferred grain orientation. The copper surfaces are also characterized before and after different cupric chloride exposures using SEM, AES, and SIMS. After determining appropriate solution parameters, as discussed later, pH changes during etching are measured with

increasing exposure time. Then, after sample-cupric chloride interaction, Auger depth profiling (ADP) was performed on selected samples.

SAMPLE PREPARATION

As-Received

The electroless copper sample was deposited, as described in the introduction, on to a reinforced epoxy resin printed circuit board from a conventional copper sulfate - formaldehyde bath. Substrate activation was achieved with a Pd-Sn seed process developed at IBM.

The electroplate sample was deposited from a small experimental laboratory scale acidic copper sulfate bath. A titanium plate or mandrel is typically used as a substrate when the deposited film will be removed for mechanical testing. In this case, the copper film was removed prior to characterization and dissolution. Because of the thickness (50,800nm) of the copper, this copper film is self-supporting when removed from the substrate.

The evaporate copper sample was processed by a batch method. In this instance, the substrate consisted of a polyimide film with a thin chromium adhesive layer between the copper thin film (8,000nm) and the polyimide. This combination of thin chromium and flexible polyimide substrate was horizontally supported on a titanium frame. The evaporate films were formed using an electron beam technique in a chamber with a base vacuum of $2\text{-}6\times10^{-6}$ Torr. The substrates were preheated for 45 minutes at

200°C. After deposition, the samples were vacuum cooled for 30 minutes before backfilling the chamber with nitrogen gas.

The sputter films were deposited using a multiple (10) pass technique in a vacuum chamber with a base vacuum of 5×10^{-5} Torr, and then backfilled to 1×10^{-3} Torr with argon gas. The substrate is the same as described for evaporate samples. After sputter deposition, the samples were moved to an auxiliary chamber, and there brought to atmospheric pressure by backfilling with air.

SPECIMEN PREPARATION

COLORIMETRIC AND GRAVIMETRIC ANALYSES

Colorimetric and gravimetric analyses are carried out sequentially on the same set of as-received samples partitioned into one-quarter inch discs. Because of differences in film thickness and substrates of the plated and vacuum deposited films, as explained earlier, there are variations in the sample preparation prior to experimental work.

Electroless plated samples are punched directly from the as-received copper plated epoxy resin board which remained with the sample to support the thin copper film. Each sample disc is then mounted on individual strips of polypropylene adhesive tape, another strip of tape with a punched hole to expose the sample is placed adhesive side down to the original tape in order to prevent exposure of the adhesive to the solution during etching. The disc

edges are protected from the etch with acid resistant lacquer purchased from GC Electronics, Division of Hydrometals, Inc., Rockford, Illinois.

Electroplate copper sheets are removed from the titanium mandrel by carefully filing away the copper along the edges of the mandrel allowing separation of the remaining copper film. The remainder of the preparation is the same as that followed for the electroless samples.

Curling of the vacuum deposited films during preliminary sample preparation does indicate the presence of stress in these films. In order to prevent curling, and therefore stress relief in the samples to be etched, polypropylene adhesive tape is stretched across the polyimide side of the composite and cut to the inside dimension of the titanium frame. This support mechanism is the main difference between the preparation of the plated and vacuum deposited samples. The polypropylene tape adheres to the polyimide allowing the reinforced composite film to be removed from the frame without curling. The reinforced copper film is then partitioned into one-quarter inch diameter discs which are mounted on tape and the edges protected with acid resistant lacquer as for the electroless samples. The base weight is determined by averaging the original weight for the samples prior to reinforcement.

SPECIMEN PREPARATION

DISSOLUTION

For the film dissolution studies, specimen preparation is dependent on substrate properties and size of the as-received substrates. Both the electroless and electroplate samples are larger than the 44mm x 44mm square evaporate and sputter samples. Since the titanium frames have to be intact to hold the evaporate and sputter samples shape to prevent stress relief, the frame size is the limiting sample size for the dissolution studies. Therefore, to keep the sample sizes similar, the larger electroless and electroplate samples were cut into 44mm x 44mm square pieces. The cupric chloride concentration was increased to 0.01M to compensate for the increased sample size. To remove ambient oxide, the samples are immersed in dilute (1:1) sulfuric acid, rinsed in distilled water, and dried with nitrogen gas. The samples are immersed immediately in the 0.01M cupric chloride solutions minimizing the formation of oxides because of ambient exposure. As shown by Pinnel the ambient oxide layer grows to approximately 1nm thickness instantaneously with exposure to the atmosphere, and therefore certainly, before the sample can be submerged in the etchant.[4]

GRAVIMETRIC

Ten specimens of each deposition type are etched in 0.001, 0.01, 0.1, and 1M cupric chloride (Purum grade from

Fluka Corporation) for varying times. Each set of specimens is examined for color changes and the concentration (0.001M) with the widest color range (discussed later in section) chosen for the remainder of the colorimetric and gravimetric experiments.

Next, all specimens, regardless of deposition type are etched using the following procedure. The etching solution (150ml of 0.001M $CuCl_2$ in a polypropylene beaker) is brought to the selected temperature while being magnetically stirred. All specimens of one deposition type are immersed in the etchant at once. At predetermined intervals, one sample is removed from the cupric chloride solution, rinsed in distilled water, dried with kimwipes, and stored in a desiccator containing silica gel desiccant. After etching, all the specimen discs are removed from the polypropylene tape and the lacquer by soaking in acetone. The specimens are then rinsed in distilled water, dried, and stored in a desiccator with silica gel desiccant for at least 24 hours before the final weighing and optical photography. Weight change is calculated as the weight change per area ($mg \cdot cm^{-2}$). After this section of the experiment was performed it was found that Wilson reported that silica gel is not adequate for use as a desiccant, but that calcium chloride is acceptable.[16] Subsequent experiments use calcium chloride as the desiccant.

COLORIMETRIC

Colors develop as a surface film forms because of interference fringes produced by light rays reflecting from both the metal surface and the oxide layer. There is a path length difference for the light rays which depends on the film thickness. The path length difference for the reflected light rays is related to the oxide thickness by: $n\lambda/2 = 2ry$ where y = oxide thickness, λ = wavelength, r=refractive index, and n = odd integer.[34-39] Colorimetric observations are made with a Bausch and Lomb stereomicroscope (30x) using reflected light. The color variation is tabulated and compared to the interaction time with cupric chloride.

Photography of the specimens with a Nikon FG 35mm camera and microscope eyepiece-adapter on either a Reichert or Unitron Series N metallograph (75x) was used as a permanent record of the color changes across the specimen. The camera is set for automatic exposure (Kodak 400 film) while the actual focusing is accomplished with the microscope controls.

To select solution concentration for the following colorimetric and gravimetric experiments, different specimens are exposed to 0.0001, 0.001, 0.01, 0.1, and 1.0M $CuCl_2$ solutions, as described previously. The criteria for solution concentration for the next experiments was simply the speed of reaction. The desired rate would allow the reaction to occur so that a series of

data points could be accurately taken during the initial stages of dissolution.

BULK CHARACTERIZATIONS

XRD

A GE XRD6 diffractometer at 30KV and 22.5 mamps allows one to measure the reflected x-ray intensity at each Bragg angle. In this case, a continuous trace is obtained from which the integrated intensity, represented by the area under the trace for each reflection, could be calculated. Of particular interest are the integrated intensities for the 100 and 111 reflections so that the 100:111 integrated intensity ratio could be compared to the Powder Data File for determination of the presence of preferred orientation.

SURFACE CHARACTERIZATION

SEM,AES,SIMS

The Perkin-Elmer PHI600 Multiprobe with add-on SIMS is a versatile ultra-high vacuum spectrometer which has both electron and ion beam probes. A heated lanthanum hexaboride crystal supplies the electron beam for SEM and AES. An energized ion beam supplied by a duoplasmatron is used: 1. to clean the sample before analysis, 2. to depth profile, and 3. to perform SIMS. Instrumental parameters for each technique are listed in Table 1. Also, a comparison of pertinent information obtained from these surface characterization techniques is given in Table 2.

ADPs, Auger depth profiles, are obtained using the duoplasmatron ion beam to remove atomic surface layers of sample while monitoring the peak to peak height of selected elements determined by previous AES surveys. The purpose of an ADP is to detect changes in concentration of elements with increasing distance from the sample's surface.

DISSOLUTION

A Corning Model 145 pH meter with a temperature probe for automatic compensation for changes in the pH electrode response with temperature, a Corning thermal printer, Corning combination pH electrode, cupric chloride dihydrate (Purum grade) from Fluka Corporation, a gas dispersion tube, nitrogen gas, tempering beaker, and constant temperature baths (Cole-Palmer Model 1267-60 and Forma Scientific Model 2095) are used in the dissolution study. The meter is standardized with pH 4 and 6 buffers. During actual dissolution experiments, the temperature probe is inserted into the constant temperature bath because the cupric chloride solution etches the stainless steel temperature probe.

All samples regardless of deposition type are etched using the following procedure: 1. temperature (3, 10, 20, or 45°C) and open (air) or closed (nitrogen cover gas) system are selected; 2. the etchant (250ml of 0.01M $CuCl_2$ in a Pyrex tempering beaker) is magnetically stirred. (If the experiment is in a closed system, the nitrogen gas is

bubbled through the solution with a gas dispersion tube while the etchant is cooled or heated to the selected temperature); 3. the copper sample is neither cleaned nor inserted into the etchant until both temperature and pH readings are stable. The pH probe is inserted at one side of the tempering beaker. The sample is held by a polypropylene tweezer at one edge and is totally immersed during the etching period. The pH is recorded automatically during etching, eliminating errors possible with manually recording data. After the pre-selected interval or after the pH remained constant, the sample is removed from the etching solution, quenched in distilled water, dried with nitrogen gas, and stored in a desiccator with calcium chloride desiccant until surface characterization was performed in the scanning Auger multiprobe.

IV. RESULTS AND DISCUSSION

During this research, several experimental techniques are used to delve into the copper/cupric chloride system. In the interest of clarity and simplicity, results from each technique will be presented and discussed independent of each other. As data from each technique are reported, previously reported data will be appended to the discussion in order to maintain a current perspective of the reaction of copper with a dilute aqueous cupric chloride solution. This approach is especially useful for the gravimetric, colorimetric, and SIMS experimentation.

However, the SEM, AES and related techniques are so intertwined that to separate results from each other would add another level of difficulty to reaching the proper interpretation of the data. Therefore, SEM images and AES surveys, maps, and depth profiling will be presented together as necessary.

Sample preparation

As demonstrated by the curling of the evaporate and sputter samples subsequent to removal from the substrate, there is a residual stress present in the deposited film. In general, this stress suggests that the d-spacing of the planes is larger at the substrate-copper film interface than at the free copper surface for these samples. In particular, it is apparent that the internal energy of the sample changed through the sample depth. Leidheiser,[13] as previously discussed, suggested that differential strain in the sample would cause different areas on the sample to become anodic or cathodic with respect to each other resulting in the corrosion of the sample by allowing electrons to travel from one area to another. Knowledge of the differential strain present in each of the samples would be beneficial to understanding corrosion characteristics in this system. However, previous work done with similar copper samples has shown that one tool (XRD) for studying stress measures large general regions and the affect of smaller specific areas are "averaged out."[17] Another tool (TEM) does sample small regions, but

its results, because of sampling techniques and restrictions on sample size, cannot be correlated with dissolution rate measurements unless large areas of the sample are known to have the local microstructure. Furthermore, thinning required to reduce the sample thickness to less than 150nm before examination by TEM could add artifacts and/or remove information left by the original exposure to cupric chloride and, therefore, TEM is not a viable tool in this study.

In order to study dissolution of the as-deposited samples, obviously the sample preparation must not alter the original microstructure by inadvertently allowing stress relief to occur. Thus, to retain the original sample stresses for colorimetric and gravimetric studies, a thick polypropylene adhesive tape was stretched across the polyimide side of the samples preventing stress relief of the vacuum deposited samples when removed from the titanium frame. This sample reinforcement sufficed for the preliminary gravimetric and colorimetric studies.

However, for the study of dissolution using pH changes, samples were left intact on the frames so that artifacts were not added to the study by sample preparation. Even though the stresses could not be measured, for reasons discussed above, care was taken to retain the stresses in the sample where they could continue to influence the sample's interaction with the

cupric chloride solution and contribute to variations in the measured corrosion characteristics.

GRAVIMETRIC

Figures 1 and 2 are the plots of weight change per unit area($mgm \cdot cm^{-2}$) versus time for samples etched in 0.001M $CuCl_2$ at room and ice bath temperatures, respectively. One sample was exposed to the cupric chloride until all copper was removed to establish that both copper dissolution and corrosion film growth occurred.

Electroless, electroplate, evaporate, and sputter samples etched at room temperature (Figure 1) showed similar weight changes, albeit they were all small. Moreover, an attempt to calculate a reaction rate for the electroplate sample which would not be affected by a substrate resulted in a reaction rate of $5 \times 10^{-7} mol \cdot h^{-1} cm^{-2}$. (The correlation factor was very low.)

The weight changes in 0.001M $CuCl_2$ at ice bath temperature are shown in Figure 2. The electroless, evaporate and sputter samples follow similar trends - very flat lines indicating little change in weight.

The electroplate sample exhibits an erratic weight change of both positive and negative excursions. The final sample removed from the electrolyte had a weight loss of $10 mgm \cdot cm^{-2}$ and a reaction rate of $3 \times 10^{-3} mol \cdot h^{-1} cm^{-2}$ with a very low correlation factor. This substantial increase in reaction rate with decreasing temperature is certainly an

indication that the gravimetric method will not suffice for quantitative information in this instance.

Sample size, substrate composition, and substrate interactions with the etchant all prohibit the use of gravimetric analysis to monitor etching. One problem is that the small samples which were used to limit the amount of substrate exposed to the etch are not heavy enough for accurate weight measurements on the available equipment. A second problem is that the polyimide substrate for the vacuum deposited copper samples is known to absorb moisture. Larger samples would provide more polyimide for moisture absorption which was already high as shown by the control sample's weight gain of over 10% for vacuum deposited samples. An original assumption that the substrates were inert is not true as at least the polyimide acts as a desiccant and contributes to the samples' weight gain.[16]

Results from these gravimetric experiments emphasized that not only the copper sample but also the support system is important. Thus, planning of experiments must include substrate considerations to avoid experimental artifacts. This substrate-sample and -solution interaction led to unforeseen conflicts in the interpretation of data from the gravimetric studies.

COLORIMETRIC

Colorimetric results are summarized as color variation with time in Table 3. These results are for the

surfaces of the samples etched for varying amounts of time in 0.001M $CuCl_2$ at room temperature. The times at which different interference colors are observed as the oxide film thickness changes may be traced through the table of results.

Optical photographs of the original copper samples were taken before exposure of the sample to the 0.001M $CuCl_2$ solution for 1.8 hours at room temperature. Photographs of the original and exposed samples could then be compared.

Optical micrographs are shown in Figures 3 and 4 for electroless original copper and electroless after 1.8 hours exposure to 0.001M $CuCl_2$ at room temperature, respectively. The original and etched electroless samples are highly reflective. The etched sample shows some light reddish areas across the sample.

Electroplate original and etched samples are shown in Figures 5 and 6, respectively. Color changes in the etched sample are observed to range from brownish areas to greenish areas.

Evaporate original and etched sample micrographs are presented in Figures 7 and 8. In Figure 7 the roll lines from the original stainless steel substrate are visible. In Figure 8, wide variations in the color of the corrosion film can be readily observed. The roll lines are not visible because of the thickness to the corrosion film.

Sputter original and etched sample micrographs are shown in Figures 9 and 10, respectively. In Figure 9, the roll lines are visible. The corrosion film can be observed to occur in patches of different colors and shapes. There are areas which appear to be unetched. Some of the roll lines are still visible through the corrosion film.

Attempts to correlate colors and thicknesses becomes very difficult. The decision to call red either red brown or red involves a thickness range of almost 100nm. Qualitative results may be obtained by observing, as a function of time, the changes in color as the oxide thickness changes as listed in Table 4.[39]

Using these color-thickness correlations with experimental time, relative reaction rates were calculated from these preliminary experiments. To avoid the ambiguity which seems to occur with increasing experimental times, the reaction rates were calculated with the maximum oxide thicknesses determined at 290 seconds. For electroless, electroplate, evaporate, and sputter samples the reaction rates are 2.6×10^{-5}, 2.6×10^{-5}, 1.1×10^{-5}, and 2.0×10^{-5} $mol\cdot h^{-1}cm^{-2}$, respectively. These rates are comparable but seemingly insensitive to the differences in surface structure known to exist between samples. Of course, the distinction must be made that these rates are calculated for oxide film growth and would presumably correlate with dissolution rates only for a system at steady-state. A system, by Read's definition, would be at

steady-state when the surface film grows at the same rate as the copper sample dissolves, then and only then could the film growth and dissolution rates possibly, but not necessarily, be equal.

Experimental rates from the colorimetric data are larger than Read's reaction rates. However, there are differences in the experiments, for example, Read waited for 20 to 30 minutes, after sample introduction, before taking any measurements; whereas the present data represents the initial copper dissolution beginning with sample introduction to the solution. Also, the question remains as to whether Read measured: 1. oxide film growth and copper dissolution or 2. oxide film growth and oxide film dissolution. One must speculate as to whether the film dissolution equals the copper dissolution even at constant oxide film thickness or steady state conditions as assumed by Read.

This study has shown that the interference colors which develop because of oxide layer formation on the copper samples can be a qualitative method for assessing the rate of oxide formation. This technique could be used to compare samples in order to set up initial etching parameters, i.e., contact time, temperature, or concentration of etchant so that the colors develop slowly enough for observation. Then these same parameters could be used for more extensive dissolution studies including pH measurement as an indication of solution changes.

However, the interference color thickness technique is too subjective for quantitative studies of this system. Also, the final goal is to look at the initial copper dissolution which does not necessarily occur only with oxidation; hydrolysis and chlorination being other possibilities for dissolution mechanisms.

AS- RECEIVED SAMPLES

XRD

Tables 5 through 8 are XRD data for electroless, electroplate, evaporate, and sputter samples.

XRD results show that the samples do have different preferred orientations. In XRD of thin polycrystalline samples the integrated intensity obtained for each hkl reflection is proportional to the volume of all grains having these particular {hkl} planes lying parallel to the sample's surface. Differences between experimental values and the Powder Data File, of randomly oriented samples indicate a preferred orientation.[33] The Powder Data File ratio of the integrated intensity for the 100 reflection with the 111 reflection is 46 for a randomly oriented, powder copper sample.

The integrated intensity ratio for the 100 reflection with the 111 reflection for electroless, electroplate, evaporate, and sputter samples is 137, 52, 33, and 3, respectively. Therefore, the electroless and electroplate samples with a higher 100 reflection to 111 reflection ratio than the Powder Data File value have more {100}

planes parallel to the sample's surface than a randomly oriented sample. Evaporate and sputter samples with a lower 100 reflection to 111 reflection ratio than the Powder Data File value have more {111} planes parallel to the samples surface than a randomly oriented sample.

These are semi-quantitative results which show differences in the microstructure of the as-received samples and suggest that differences may exist in the etching characteristics of the samples, especially since it is known that the {100} planes oxidize faster than the {111} planes. The preferred orientation for each sample agrees with those reported by other researchers[15] for similar samples.

SEM

Figures 11 through 15 are SEM images of the original surface of electroless, electroplate, evaporate, and sputter samples, respectively. The micrographs demonstrate the differences in the surface topography with deposition technique. SEM results are summarized in Table 9 with deposition method, preferred orientation, and thickness.

Figures 16 through 19 are SEM images of the ion beam etched surface after argon sputter for electroless, electroplate, evaporate, and sputter samples, respectively. SEM micrographs of the original samples reveal a variety of surface topographies.

The electroless sample (Figure 11) is rough with many sharp facets and an average grain size of 2.6μm. A SEM micrograph (Figure 16) of the electroless samples after exposure to the ion beam etch (1.5 minute sputter ≈2nm material removed) shows that the surface remains rough and still exhibits well developed facets.

The electroplate sample (Figure 12) is fine-grained (0.5μm) with no sharp facets or microscopically apparent orientation noted. This grain size is comparable to the 0.3μm measured at IBM using TEM.[18] The electroplate sample (Figure 17, 30 minute sputter etch ≈60nm material removed) shows a roughening of the surface features and an increase in the grain size to 1.8μm.

The evaporate sample (Figure 13) has an average grain size of 1.8μm. The surface retains the impressions of the polyimide substrate. The evaporate sample (Figure 18, 78 minutes sputter etch ≈156nm material removed) shows a roughening of the surface. The size of the surface grains remains at 1.8μm.

The sputter sample (Figure 14) at 1000x looks uniform. The particle size averages 1μm. IBM reported a non-uniform grain size ranging from 1-5μm.[18] At 5000x (Figure 15), the sputter sample has areas of roughly 0.2μm size which appear dark in the SEM image, an indication that they are small holes. The sputter samples (Figure 19, 34 minutes sputter etch ≈68nm material removed) develop cones which are an indication of preferential etching at

the grain boundaries. Cone development would suggest the sputter sample has a columnar structure (i.e., elongated grains grew from the substrate inclined to the substrate surface). This columnar structure was later confirmed by IBM.[18]

AES

Figures 20 through 23 are AES surveys of original electroless, electroplate, evaporate, and sputter samples, respectively. Numbers next to the positive excursion of peaks are elemental concentrations in atomic per cent.

AES results for the as-received samples show a variation in oxygen, chlorine, and carbon elemental compositions. The electroless and electroplate samples have trace quantities of chlorine on the surface. AES surveys show different elemental concentrations in atomic percent for the original samples. The elemental concentrations are calculated semi-quantitatively using peak-to-peak heights and beam sensitivities for each element.[85] The electroless samples show a surface composition of 49, 17, 34, and 0.3 atomic percent of copper, oxygen, carbon, and chlorine, respectively. The electroplate surface layers contain 63, 17, 20, and 0.3 atomic percent copper, oxygen, carbon, and chlorine, respectively. The evaporate samples show 57, 18, and 24 atomic percent of copper, oxygen, and carbon, respectively. The sputter sample has 57, 20, and 23 atomic percent of copper, oxygen, and carbon, respectively.

Figures 24 through 29 are AES surveys of the as-deposited samples after Ar^+ exposure. AES of the as-received samples did show chlorine, carbon, and oxygen contaminates on the sample. After cleaning the sample with the ion beam for two minutes or less, the AES revealed only copper (<1% impurities) for all the samples.

Sputter samples are deposited in a high vacuum with an inert gas (argon) background and high (several kilovolts) potential applied to the cathode (target). Although, there is a possibility that argon could be incorporated into the sample, no argon was found during AES.

The contaminates found on the sample surfaces were only those which one would expect to see after exposure to the atmosphere; especially the carbon and oxygen. The chlorine is not unusual for the samples deposited from a solution.

SIMS

Figures 30 through 33 are SIMS spectra for original electroless, electroplate, evaporate, and sputter samples, respectively. Figure 34 is a bar graph for comparison of the SIMS data for the original, unetched copper samples.

The SIMS surveys of as-received samples shows that ion clusters of hydrogen, lithium, fluorine, carbon, oxygen, sodium, magnesium, aluminum, silicon, chlorine, potassium, calcium, titanium, and phosphorous are found in some or all the original samples. These contaminants can

be attributed to instrumental background and can be detected because of the increased sensitivity of the SIMS technique over AES. One source of contamination is a system memory of previous work in the chamber and will not be reported for the rest of the samples.

For this study, the Cu_2^+/Cu_3^+ ratio is of interest as a measure of surface atomic grouping on the sample. The Cu_2^+/Cu_3^+ ratios are 1.60, 1.20, 0.87, and 2.33 for the electroless, electroplate, evaporate, and sputter samples, respectively. The sputter deposited sample has the highest Cu_2^+/Cu_3^+ ratio of the experimental samples. Considering that its closest packed, {111} planes, are parallel to the sample surface this result is surprising. One would expect a lower Cu_2^+/Cu_3^+ ratio than for the more open 100 structure. This high ratio could be an indication of the columnar structure and defects observed on the sputter sample's surface. Therefore, the ratio of roughly one for the other three samples represents more perfect samples rather than differences in grain orientation within the samples.

DISSOLUTION

An oxide film is known to grow on the sample, so one needs to determine what if any pH change is produced by this extraneous oxide film growth. Thus, in order to determine any interference which might occur from the distilled water reacting with the copper sample or from interaction of the cupric chloride with either air or

nitrogen to cause spurious pH changes, three types of blanks were run (Figures 35 - 39). The first type used evaporate copper samples in distilled water at 45°C for open or closed systems. The evaporate copper in an open system shows no pH change until the second hour, after which the pH gradually rose a total of 0.02 pH unit. The evaporate copper in distilled, deionized water and a closed system gradually increased the pH by 0.2 pH unit during the first hour staying level for the remainder of the ten hours. Therefore, neither instance should pose a problem for measuring pH during copper exposure to cupric chloride in distilled, deionized water.

The second blank was distilled water at 45°C with no copper sample and a closed system. The pH decreased by 0.2 pH unit. Again, the presence of water as a solvent for the cupric chloride should not present a problem to the planned experimentation.

The third set of blanks investigated the reaction of the etchant, 0.01M $CuCl_2$ at 45°C with no sample in a closed and an open system. The blank in a closed system (Figure 38) showed an increase in pH but quickly dropped to 1.6 pH units below the original value during the first two hours. To avoid interference with this initial reaction, solutions to be used in a closed system experiment were purged with nitrogen for at least two hours to allow the etchant to stabilize before sample introduction to the solution. The blank (Figure 39) in the open system showed that the pH decreased initially and

then remained constant at 0.1 pH unit below the original value.

Figures 40 through 58 are plots of pH change versus exposure time to dilute (0.01M) aqueous cupric chloride solutions for different temperatures, deposition samples, open and closed systems as labelled. For example, changes in the pH with time of the electrolyte in contact with electroless copper are shown in Figures 40 through 44. The specific shape of the resulting curves change as the etch parameters (temperature and atmosphere) are varied but general features remain as demonstrated in the following descriptions of the experimental data. The decision to plot pH change rather than pH itself was governed by the necessity to compare solutions at different temperatures and perhaps sightly different initial pH values. Comparison of pH change provides an immediate indication of different magnitudes of pH change by looking at the presented graph.

Figure 40 shows pH change with time for electroless copper in 0.01M $CuCl_2$ at 45°C in a closed system. The pH shows an initial sharp rise and then a gradual decrease during the first two hours of etching. The pH decreased until gradually reaching a plateau roughly 0.9 pH unit above the initial pH of the solution.

Figure 41 shows the pH change with time for electroless copper in 0.01M $CuCl_2$ at 45°C in an open system, to have a more gradual initial increase and fall

to a plateau value leaving a final positive pH change. The maximum pH change is 1.0 pH unit.

Figure 42 shows the pH change versus time for electroless copper in 0.01M $CuCl_2$ at 20°C in a closed system. The pH change rises to a plateau, then begins a gradual descent to rise and fall twice more before it finally, after roughly six hours of etching, reaches a plateau. The maximum pH change is 1.4 pH units.

Figure 43 shows the pH change versus time for electroless copper in 0.01M $CuCl_2$ at 10°C in an open system. The pH change increases rapidly and levels off to a positive plateau value. The maximum pH change is 1.1 pH units.

Figure 44 shows the pH change versus time for electroless copper in 0.01M $CuCl_2$ at 3°C in a closed system. The pH change rises to a maximum, then gradually decreases for two hours after which the fall becomes steeper and finally reaches a plateau after six hours of etching. The maximum pH change is 2.3 pH units.

The remaining Figures (45 to 58) show similar trends for the electroplate, evaporate, and sputter samples. Although the time to maximum pH change may change and the descent slope varies, the curves are similar for each type of sample. Also Figure 52, shows the evaporate etched at 45°C, closed system with no light exhibiting oscillations similar to those seen in an evaporate sample etched under the same conditions except with light

present. This experiment demonstrated that the presence or absence of light did not affect the dissolution results or result in oscillations. Table 10 summarizes the characteristics of the pH change versus time curve during extensive etching at 45°C for copper samples in 0.01M $CuCl_2$ in an open system.

In analyzing the dissolution of the copper samples it is important to note that after the initial well-behaved pH change with sample exposure time some erratic pH changes are observed. These erratic changes or oscillations have been attributed by other researchers to the changes from corrosion film formation to corrosion film dissolution.[19-21] In other words, the oscillations are an indication that the initial linear reaction has changed to a non-steady state behavior of the system which involves corrosion film formation.

In confirmation of the corrosion film break-up causing the pH oscillations, some green solids are found on the sample and the beaker at the end of the experiments which were allowed to continue beyond the initial linear region. This solid analyzed by energy dispersive spectroscopy is found to contain copper, chlorine, iron, and titanium. Of course, the copper is from either the sample or the solution. However, the most likely source is the sample, since the solubility products for CuCl and Cu_2O are not exceeded in the solution as would be required to remove copper from the solution as a precipitate. The

iron most likely comes from the temperature probe which after the first experiment is inserted in the constant temperature bath rather than the etch solution to eliminate etching of both the probe and the intended sample. The titanium frame would be the most likely source of titanium. This corrosion product is found on the sample and beaker after, but not during, the linear region of pH change indicating that the linear region involves more than corrosion film formation.

In this study, the computer program "Microql," by J. C. Westall and E. M. Perdue was used in order to determine the ionic species present in dilute aqueous cupric chloride solutions. The use of Microql assumes that the reaction occurring at a particular time can be analyzed by using a known component concentration (in this case pH is measured) to calculate the reaction species present in the solution. This assumption is used in both catalysis and environmental water studies when the reaction equations and equilibrium constants are well known. Microql is used during this research to determine the amount of each species present as the solution pH changes during copper dissolution. In order to study the initial copper reaction, computer modeling was limited to the linear region of the pH change versus time for the copper/cupric chloride system. The reactions of copper in solution have been investigated by many researchers. Hence, chemical equations and equilibrium constants are

available for use with computer modeling (Table 11). Using the chemical equations, one can first determine possible input components to be $Cu^{++}_{(aqueous)}$, $Cl^{-}_{(aqueous)}$, $H^{+}_{(aqueous)}$, $Cu_{(s)}$ a solid from both sample and reaction product, $CuO_{(s)}$ a solid as a possible reaction product, $CuCl_{(s)}$ a solid as a possible reaction product, and $Cu_2O_{(s)}$ a solid as a possible reaction product. Second, the initial aqueous concentrations are determined from the original solution concentration {$[Cu^{++}]$=0.01M; $[Cl^{-1}]$=0.02M} and the measured pH. The Cu^{++} and Cl^{-} "free" concentrations are determined from the original values by the model, while the H^{+} "free" concentration is held constant at the value determined experimentally at that time to simulate solution conditions. Solid components are assigned an activity of one by the program. Third, the species matrix is determined by the appropriate chemical reactions. Because of the dilute solution used during the experiments, chloride complexes with copper need not be considered.[40]

The first equation (see Table 11) is neglected since it is known that cuprous oxide forms even though cupric oxide is the thermodynamically preferred compound. Therefore, use of equation 1 (Table 11) in the Microql modeling would introduce errors not agreeing with facts.

The remaining chemical equations must be rearranged to conform to the rules for Microql which require that: 1. all solids must be entered as components, and 2. there can

be only one product species for each equation. Naturally, each equation must be modified following appropriate manipulation rules. For example, equations 2, 3, and 4 can be rewritten as:

$$\text{(2a)} \quad Cu^{++} + H_2O - H^+ = Cu(OH)^+$$

$$\text{(3a)} \quad 2Cu^{++} + 2H_2O - 2H^+ = Cu_2(OH)_2^{++}$$

$$\text{(4a)} \quad Cu^{++} + 3H_2O - 3H^+ = Cu(OH)_3^-$$

The equilibrium constants are not affected by the subtraction of H^+ from each side of the equation.

Equations 5, 6, and 7 are combined to meet the Microql requirements to give another equation (9):

$$2Cu_{(s)} + 2Cu^{++} + H_2O + Cl^- - 2H^+ - Cu_2O_{(s)} - CuCl_{(s)} = Cu^+;$$

log K = -13.53, which may be used in the Microql matrix.

The Microql matrix (Table 12, Open System and Table 13, Closed System) is formed by using equations: 2a, 3a, 4a, 5, 7, and 9. Equation 7 is included since Microql assumes an aqueous environment for the reactions. The open system also includes the equations for the interaction of water and carbon dioxide. The time and pH are fixed by experimental measurements while the remainder of the species are calculated using a Newton-Raphson multiple regression. The total copper concentration in the solution at a particular data point equals the sum of all the copper species in solution. Computer modeling allows for the determination of the concentration for each thermodynamically possible species and/or components which

are used to determine reaction rates and activation energies.

The equilibrium constants are available for reactions occurring at 25°C. In order to compensate for change with temperature, the equation: $\ln K = - G^{o}/RT$ is used to calculate equilibrium constants at each experimental temperature. The calculation is valid if G^{o} (change in free energy) varies only slightly with changes in temperature[22]. The equilibrium constants for the formation of each species at the experimental temperature are reported in Table 14. Table 15 is a representative Microql output which reports the copper ion speciation at each measured pH data point.

The total copper ions in solution are observed to increase as the pH increases (Table 15). However, the total copper change is so small (10^{-7} to 10^{-12} moles per liter) that it is swamped by the original 0.01M cupric ion in the solution. Therefore, rate calculations are made using the total of copper ions in solution minus the original cupric ion concentration in solution to circumvent this swamping effect. These reaction rates compare favorably to those reported by Read which were of the order $5 \times 10^{-9} mol \cdot h^{-1} cm^{-2}$ at 25°C. The reaction rates for all of the samples are reported in Table 16.

In two cases, the Arrhenius equation was solved to determine an activation energy for the initial copper/cupric chloride reaction. Since the reaction rates

were zero-order with respect to time, the reaction rate could be used as the rate constant (k) in the Arrhenius equation. The activation energy (see Table 17) for the dissolution of the strongly (100) oriented electroless samples using the nitrogen (closed system) data is $48 kJ \cdot mol^{-1}$ corresponding to Read's reported value of $50 kJ \cdot mol^{-1}$. The slightly (111) oriented evaporate sample has an activation energy of $85 kJ \cdot mol^{-1}$ for dissolution in a closed system. This activation energy is higher than Read's reported value and remains to be explained.

While these systems are not the same, it is also interesting to compare the present data with the extensive and well documented copper/chlorine vapor phase work by Sesselmann. In order to compare the present data with that obtained by Sesselmann, the reaction rates and activation energies must be calculated from the Sesselmann diffusion coefficients. Using D_o equal to $2 \times 10^{15} A^2 sec^{-1}$ in the equation; $D=D_o exp(-E/RT)$ it is possible to calculate activation energies at different chlorine pressures (Table 18). $D_o=2 \times 10^{15} A^2/sec$ is the value for the diffusion coefficient of copper in copper.[23] This choice of D_o is justified because the copper is more mobile than the chloride ion. The diffusion coefficient for the chlorine is much smaller than that of copper especially at low experimental temperatures. The calculated reaction rates for Sesselmann's data are of the same magnitude as the

experimental rates determined in this research and are reported in Table 18.

Sesselmann separates his data into two pressure dependent regions (Table 19); the first, with lower activation energies (45-75kJ·mol^{-1}) and higher reaction rates (6×10^{-12} to 6×10^{-7}mol·h^{-1}cm^{-2}), is designated as grain boundary diffusion. The second, with higher activation energies (54-82kJ·mol^{-1}) and lower reaction rates (4×10^{-13} to 4×10^{-8}mol·h^{-1}cm^{-2}), is designated as bulk diffusion for Sesselmann's predominately (111) oriented thin film samples. Accordingly, the electroless (48kJ·mol^{-1}, closed system) sample dissolution was controlled by grain boundary diffusion as evaluated by higher chlorine concentrations. In like manner, the evaporate sample (79kJ·mol^{-1}, closed system) would be in the range of bulk diffusion for a low chlorine pressure according to Sesselmann.

Similarly, if one labels Sesselmann's reaction rates according to diffusion type; bulk diffusion rates would lie between 10^{-13} and 6×10^{-12}mol·h^{-1}cm^{-2}, mixed grain boundary and bulk diffusion would lie between 6×10^{-13} and 4×10^{-8}mol·h^{-1}cm^{-2}, and grain boundary controlled diffusion between 2×10^{-8} and 6×10^{-7}mol·h^{-1}cm^{-2}. It is interesting to note that of all the calculated reaction rates only the (111) oriented evaporate sample dissolved in a closed system at 3°C had a reaction rate in the range for bulk diffusion. Whereas, the (100) oriented electroplate sample

dissolved in an open system at 45°C had a reaction rate in the region controlled by grain boundary diffusion. The remainder of the samples' reaction rates are in the range of mixed grain boundary and bulk diffusion control. One can speculate that both microstructure and environment can change control of a sample's dissolution characteristics from that of bulk diffusion to a mixture of grain boundary and bulk diffusion as shown by the evaporate sample; or from grain boundary to mixed control as shown by the electroplate system. Both of these samples are of slight preferred orientation; and perhaps more easily influenced by their surroundings than are the more strongly oriented electroless and sputter samples. This comparison of the two completely different systems serves a dual purpose: 1. even though the systems are different they both show diffusion of chlorine into the copper and 2. the activation energies are in the same range indicating that these experimental activation energies are reasonable.

Furthermore, comparison of the activation energies and preferred orientation (Table 20) of the copper samples suggests that there is a correlation between the activation energies and the preferred orientation of the thin samples. In single crystals, the {100} face oxidizes faster than the {111} face. In the polycrystalline samples studied, the {100} oriented electroless samples had a lower activation energy than did the {111} oriented evaporate samples. The theory

behind more rapid growth of {100} planes versus {111} planes is based on the number of available nucleation sites for each orientation. The {100} and the {111} planes provide four (4) and two (2) nucleation sites, respectively. Since correlation was found between preferred orientation and etching rate, these nucleation sites might also contribute to the dissolution of polycrystalline copper samples by providing active sites for the halogenation of the copper sample.

Furthermore, it is interesting to note that comparison of grain size and activation energy (Table 21) should also indicate a possible correlation of the two properties. The electroless has a larger grain size of 2.62μm and a smaller activation energy of $48 kJ \cdot mol^{-1}$ than the evaporate sample of 1.8μm grain size and an activation energy of $89 kJ \cdot mol^{-1}$. One could speculate that the larger grains of the (100) oriented electroless sample provides more nucleation sites and a more open structure for reactant penetration and a lower activation energy for dissolution of the sample than that required for a smaller grained more tightly packed structure as represented by the evaporate sample.

CHARACTERIZATION OF SAMPLES EXPOSED TO CUPRIC CHLORIDE

Linear region of pH change

SEM

Figures 59 through 63 are SEM images of electroless, electroplate, and evaporate samples after similar exposure to the etchant at 45°C an open system (short etch).

Figure 63 is a SEM image of an electroless short etch sample in the same area shown with AES elemental mapping. Figures 64 to 66 are AES elemental maps of an area on the electroless sample exposed to the short etch for chlorine, copper, and oxygen, respectively. Definite areas of chlorine and oxygen segregation are observed. This segregation supports the theory of oxygen and chlorine competition for the available nucleation sites and the sample's surface.

Figure 67 is a SEM image of the AES element mapped area for electroplate sample exposed to the short etch sequence. Figures 68 through 71 are chlorine, copper, oxygen, and carbon AES elemental maps, respectively. Definite outlines are apparent demonstrating that there are concentrated, complementary areas of each element.

Figure 62 is the SEM image for the AES map of the evaporate sample exposed to the short etch sequence. Figures 72 through 74 are the chlorine, copper, and oxygen elemental maps, respectively. Definite outlines are apparent for each element's area of concentration.

Especially note that the chlorine and oxygen do not co-exist in the same areas.

AES

Figures 75 through 77 are AES surveys of electroless, electroplate, and evaporate samples which had been exposed to the short etch sequence.

AES results for the short etch (8 minutes in 0.01M $CuCl_2$ at 45°C in an open system) sample show variation in the composition of the surface layer. Addition of the atomic percentage of oxygen, carbon, and chlorine present on the surface provides the total percentage of surface contamination for each sample. The total surface contamination is 37, 62, and 51 for electroless, electroplate, and evaporate samples, respectively.

The ADP shown in Figure 78 is for electroless copper after 8 minute exposure to cupric chloride at 45°C. The ADP traces the change in elemental concentration from the surface to the bulk sample revealing that the chlorine penetrated the copper sample. In this case, there is an actual chlorine-oxygen interface. This chlorine distribution through the copper sample shows that the chlorine is not an inert solution component as Microql suggests. This consideration and others will be discussed in a later section.

SIMS

Figures 79 through 81 are the SIMS spectra for electroless, electroplate, and evaporate samples exposed to the short etch sequence, respectively. Figure 82 is a bar graph comparison of SIMS data for the copper samples from the short etch.

The ratios of the ion clusters after etch are the same regardless of deposition type. However, the evaporate sample showed the largest change and the highest activation energy of the three measured samples.

SAMPLES EXPOSED TO CUPRIC CHLORIDE SOLUTION at 45°C

equilibrium pH region

SEM

Figures 83 through 88 are representative SEM images of the electroless, electroplate, evaporate, and sputter long etch samples. The samples were exposed to cupric chloride in the open system. Table 22 summarizes the SEM data for all the samples.

Figures 89 and 90 are the SEM images and accompanying AES spectra, respectively, of a faceted particle (pyramid) on the electroless sample exposed to the long etch sequence. Figure 91 is the SEM image showing location of points 1 and 2 on the surface for the acquisition of AES spectra in Figures 92 and 93, respectively. Figure 94 is the AES summary of the area shown in Figure 91.

Figure 95 is the SEM image of a representative area on an electroplate sample exposed to the long etch sequence. Figure 96 is the AES spectra of the area shown in Figure 95 and Figures 97-101 are the AES spectrum acquired at points 1-5, and the center of the area, respectively.

Samples exposed to the long etch sequence show distinct differences from the short etch samples and from each other. Although the surface differences are interesting, the examined surfaces are corrosion films and not the copper sample. However, certain observations relevant to the etching characteristics of the copper samples are possible. The pyramids are characteristic of grains with a (111) orientation which are growing even on the electroless and electroplate samples which have a (100) orientation.

AES

Figures 102 and 103 are AES surveys of evaporate and sputter samples which had been exposed to the long, open system etch sequence.

Figures 104 to 106 are the AES spectrum for the electroplate long etch sample, after argon ion beam sputter for 0.5, 1.0, and 1.5 minutes, respectively.

Figures 107 to 109 are the AES spectrum for random points across the evaporate sample exposed to the long etch sequence as shown in the SEM image of Figure 86.

Figures 110 to 115 are the AES spectrum for the points 1 through 6, respectively, of Figure 88 for the sputter sample exposed to the long etch sequence. The AES spectrum show large shifts in kinetic energy for the chlorine, oxygen, and copper AES peaks. These chemical shifts are generally attributed to the formation of compounds which affect the core energies of the reacting elements. The AES elemental maps in Figure 116 to 118 reveal the areas of copper, chlorine, and oxygen which are chemically bound to each other. Figure 119 is the AES carbon elemental map for the same area.

AES results for long exposure to the etchant reveal total surface contamination is 42, 73, 45, and 57 atomic percent for electroless, electroplate, evaporate, and sputter samples respectively. AES results are presented in Table 23. AES elemental maps for electroless, electroplate, and evaporate long etch samples were attempted. The elements are evenly distributed across the sample surface. There is no change in the signal intensity across the maps.

The AES elemental maps for the sputter sample after long etch show definite areas lacking in any copper or chlorine. Areas of copper and chlorine concentration coincided with large faceted particles. AES surveys indicated shifts of several electron volts in the AES peaks for copper, oxygen, and chlorine. Again, an indication of compound formation.

In summary, the surface analysis of the samples after interaction indicates the presence of CuCl and Cu_2O, agreeing with Bonhoeffer, on samples etched in either a closed or an open system.[21] Surface examination shows well developed cuprous oxide grains. Pyramidal grains on samples exposed to the etch for a long time are indicative of a growth with 111 orientation. Chlorine, which must come from the solution, is also found on the surface of each etched sample. Most noticeable is that for the electroplate sample, the surface chlorine atomic concentration (AES) decreases from 23% for the short etch sample to 1% for the long etch sample. One could speculate that this decrease in chlorine surface concentration is due to diffusion of the chloride ion into the bulk of the sample. This possibility will be discussed in a later section.

ADP

ADP for evaporate copper etched at 45°C in a closed system is shown in Figure 120. The ADP for evaporate copper exposed to cupric chloride at 45°C in a closed system for 28 hours shows a definite chloride-oxide interface. Previously reported research leads one to believe that the chlorine would either: 1. remain in solution or 2. penetrate the oxide layer to form a defect oxide structure destroying the samples' oxide passivity and allowing the copper to dissolve.[9] Penetration of the chlorine into the copper metallization could be because

of: 1. the ion beam pushing the chlorine in front of it (an artifact), 2. actual diffusion of the chlorine into the metal structure, or 3. migration of the chlorine along the grain boundaries. Examination of only the surface could lead to the erroneous conclusion that the chloride ion has penetrated only the cuprous oxide layer.

Figure 121 is an AES line survey taken across a fracture cross-section and shows chlorine through the copper with the oxygen concentration decreasing with increasing distance from the surface or depth into the copper. This sample had not been ion beam etched, so the chlorine was not driven into the copper sample by the ion beam. Of course, just the ability to fracture the normally ductile copper sample is an indication of microstructure changes to the copper sample.

The ADP also shows clearly that the oxygen is on the samples's surface while the chlorine has penetrated the bulk copper by some yet to be determined mechanism. A sharp CuCl-Cu interface is not expected, and is not observed, since the growth of the chlorinated surface layer is most likely not a simple layer by layer growth of stoichiometric CuCl. Therefore, the ADPs show that the chlorine extends for long distances (several thousand Angstroms) into the bulk copper agreeing with experiments by Sesselmann.[32] The ADP of electroless copper exposed to cupric chloride for 8 minutes at 45°C shows the chloride ion penetrating deep into the copper sample. This profile

is a section of a longer 60 minute profile with no change after the initial time.

The presence of cuprous chloride can be explained by halogenation of the copper. Halogenation has been documented in vapor phase reactions where halogens are used as reactive gases in laser and plasma etching of copper metallization for microelectronic circuits. A chlorine layer adsorbs on the copper surface, dissociates, and the chloride ion diffuses into the copper or the copper ion diffuses outward to the surface. Sesselmann observes chlorine penetration and dissolution into the bulk copper even at 25°C.[32] The activation energy from the current study is higher for some samples than the bulk diffusion activation energy calculated from Sesselmann's data as discussed earlier. During the bulk diffusion process (as defined by Sesselmann), the rate limiting steps are the chlorine adsorption and incorporation into the subsurface region. In the present study, parallel rate limiting steps can be defined as the separation of the chlorine from the solution, adsorption onto the surface, and then incorporation of chlorine into the subsurface region. Also, since the present experiment supplies the chloride ions from solution rather than chlorine gas, dissociation of the chlorine gas is not necessary. However, the chloride ion must lose its hydrated shell, adsorb, penetrate, and disperse through the copper sample.

Insertion of a copper sample into a solution causes the copper surface to become positive and act as cathode which should aid in attracting the chloride ion with a negative charge.[36] Once on the surface, the chloride ion can penetrate the sample at least via the grain boundaries and perhaps via the grains by bulk diffusion. The chloride ion most likely initially penetrates the sample via grain boundaries so that the chloride surface concentration is less at the grain boundaries. As chloride ions penetrate the grain boundaries, it is possible that the grains become oxidation sites for the formation of Cu_2O. It would then be expected that, as CuCl formation is indicated by AES, some chloride ion would remain on the grains to be incorporated in to the oxide structure explaining why other researchers report the role of the chloride ions to be that of breaking down the expected passive oxide, exposing the bare copper sample surface to the etchant.[9]

SIMS

Figures 122 through 125 are the SIMS spectra for electroless, electroplate, evaporate, and sputter samples exposed to the long etch sequence, respectively. Figure 126 is a comparison of the samples exposed to the long etching.

Figures 127 through 129 are bar graphs for comparison of SIMS data for original, short etched, and long etched samples for electroless, electroplate, and evaporate samples, respectively. Figure 130 is a bar graph for

comparison of SIMS data for original and long etched sputter samples.

For the long etch samples, the ratios of Cu_2^+/Cu_3^+ are 2.40, 2.50, 1.44, and 1.49 for the electroless, electroplate, evaporate, and sputter samples, respectively. It is interesting to note that comparing the Cu_2^+/Cu_3^+ ratios for the (100) oriented films before and after cupric chloride exposure, one observes that the Cu_3^+ clusters decrease relative to the Cu_2^+ clusters. One could speculate that this decrease indicates a disruption in the long-range order of the surface copper ions, perhaps caused by chloride ions penetrating the more open (100) structure. On the other hand, the (111) oriented evaporate sample consistently maintains a high Cu_3^+ cluster value and the sputter sample Cu_3^+ cluster value increases from the lowest initial value to a high value of Cu_3^+ clusters after long exposure to the cupric chloride solution. This trend towards higher Cu_3^+ cluster concentration could indicate that defects speculated to cause the Cu_3^+ cluster value for the original sputter sample to be low were removed during the initial copper dissolution to expose a more ordered copper surface which was less permeable to the chloride ion than the (100) structure and, thus a higher Cu_3^+ value was obtained for the (111) oriented sputter sample.

It is also interesting to note that the SIMS analysis confirms the presence of chlorine and its decrease in surface concentration especially for the electroplate long etch sample. This evidence agrees with the ADP data. Table 24 is a summary of the Cu_2^+/Cu_3^+ ratios for all samples.

V. SUMMARY

The objective of this research was to study the dissolution of copper in a dilute aqueous cupric chloride solution to achieve an understanding of the role that microstructure plays in the dissolution process. Of particular interest were the microstructures intrinsic to copper films formed by current deposition techniques and how each microstructure influences copper dissolution in a commercially used etchant. A multidisciplinary approach was used. Gravimetric analysis, colorimetric analysis as well as solution and sample characterization by XRD, dissolution, SEM, AES, and SIMS were the techniques employed.

The samples chosen for this study are directly relevant to those metallizations used in the microelectronics industry. Two deposition types of copper (electroless and evaporate) were from working production processes; the other two (electroplate and sputter) were from processes under evaluation for future use. Residual stresses were suspected to be present in all the films, and specifically found in the vacuum deposited films. The

decision was made to retain the stresses in the films by leaving the films on their respective substrates so that etching characteristics measured in the laboratory could be directly related to and compared with those found during commercial processing.

It was found that gravimetric analysis to obtain reaction rates was not feasible . The measured rates were erratic and unreliable and this was attributed to the polyimide backing adsorbing water during storage in a desiccator.[16]

Analysis of the interference colors due to corrosion film thickness changes was attempted to determine reaction rates. The procedure was expected to be a qualitative technique at best. On the other hand, the information obtained from the colorimetric analysis could be used to determine cupric chloride concentrations which would etch samples slowly enough for several data points to be taken during solution phase experiments. A concentration of 0.01M cupric chloride was used for the dissolution studies.

Dissolution of the films was studied by measuring pH changes with increasing exposure time of copper samples to cupric chloride solutions at different temperatures. Experiments were performed in closed and open systems. Computer modeling with the program "Microql" provided the speciation information required for reaction rate and activation energy determinations. The reaction rates and

activation energies compared well with the prior work done by Read[10] in solution and Sesselmann[32] in chlorine vapor and show a correlation with microstructural differences.

XRD results demonstrated that differently deposited samples had a variation in preferred grain orientation ranging from strong (111) to strong (100). The activation energy for dissolution of the strongly (100) oriented electroless samples using the closed system data is $48 kJ \cdot mol^{-1}$ corresponding to Read's value of $50 kJ \cdot mol^{-1}$. The slightly (111) oriented evaporate sample has an activation energy of $79 kJ \cdot mol^{-1}$ for dissolution in a closed system. The activation energy is the lowest for the (100) preferred orientation and highest for the (111) preferred orientation. This agrees well with the results found for the oxidation of single crystals and suggests that chloride uses four nucleation sites available from the (100) orientation as proposed from the results of the oxidation studies. These results are also consistent with the fact that the {100} planes have a more open atomic arrangement than the close-packed {111} planes, so that less energy would be required to move an atom or an ion through the (100) structure than the (111) structure.

The grain size, determined using SEM photos (and confirmed by TEM at IBM), was found to lie in the range from 0.5 to 2.6 μm depending on the film deposition technique. The activation energy increases with decreasing average grain size. This was not expected because

processes controlled by grain boundary diffusion are generally less activated than those controlled by bulk diffusion. A correlation with increasing number of grain boundaries could be interpreted by the reasoning that as the grain size decreases the number of available nucleation sites from the preferred orientation decreases. Thus preferred orientation appears to be the dominant microstructural parameter that determined dissolution rates. This phenomenon is not observed in an open system. One could speculate that the presence of oxygen in the open system masks the influence of the nucleation sites on the grain boundaries by providing competition with the chloride ion for these areas. Therefore, a variation in rate with microstructural change would not be observed when oxygen dominates the system.

AES and ADP were used to determine the composition of the surface film resulting from the exposure of copper to the cupric chloride solution. The surface film on each sample was found to contain copper, chlorine, and oxygen, but not necessarily in the same relative concentrations from sample to sample. ADP revealed that chloride deeply penetrated the copper sample while the oxide concentration decreased with increasing distance from the sample's surface. A line profile across a fracture surface also showed that the chlorine continued into the sample even after oxygen concentration ceased.

The Cu_2^+/Cu_3^+ cluster ratios were determined for the as-received and etched samples using SIMS. A low cluster ratio indicates more long-range order while a high cluster ratio indicates less long-range order. The slightly (111) oriented evaporate film had the lowest cluster ratio while the (100) oriented films, with a more open structure, had ratios between the columnar sputter film and the evaporate film cluster ratio values. The activation energies measured for these two samples increased with increasing degree of (111) orientation. SIMS results further confirm the importance of crystallographic orientation on the dissolution kinetics of copper samples in dilute copper chloride electrolytes.

VI. CONCLUSIONS AND RECOMMENDATIONS

The copper/copper chloride system is indeed complex and its complete evaluation presents a challenge. This research has provided initial information for a long needed data base which will aid the microelectronics industry in defining those properties requiring control for the mass production of reliable copper interconnects.

An important general conclusion drawn from this research is that the etching characteristics of polycrystalline thin copper films are dependent on the film's microstructure. The activation energies and reaction rates determined by this investigation are applicable to the intrinsic microstructures of the present

samples. These values are dependent on the sample's microstructure, especially the structure of the surface initially exposed to the etchant. For dissolution and corrosion investigations to contribute meaningful information to a universal data base, knowledge of the microstructure is essential. An experimental procedure is recommended as a method to insure that the information required to relate etching kinetics to microstructure is obtained during an investigation.

This procedure includes:

1. characterization of the as-received samples using XRD for preferred orientation, SEM for grain size, AES for surface composition, and SIMS for local surface structure
2. characterization of the dissolution rate of a particular sample using pH change and computer modeling to calculate speciation changes
3. characterization of surface changes caused by sample exposure to the solution using AES for chemical composition changes, ADP for distribution of elements into sample, and SIMS for local surface structural changes.

MODE	PARAMETERS		
	Sample tilt degrees	electron beam	ion beam
SEM	30	5 or 10kV, 1nA	
AES	30	5 kV, 100nA	
SIMS	60		7 kV

base vacuum = $3\text{-}5 \times 10^{-10}$ Torr

Table 1: PHI 600 MULTIPROBE PARAMETERS

MODE	
SEM	1. secondary electrons emitted from sample (affected by surface topography) 2. grain size
AES	1. Auger electrons which are characteristic of surface chemical compositional 2. Auger maps to show chemical composition variations across surface 3. Auger point spectra for identification of unusual surface features 4. elemental concentrations calculated from peak-to-peak height and sensitivity factors 5. Auger depth profiling- duoplasmatron is used to slowly etch through the film thickness while Auger electrons from predetermined elements are sequentially monitored 6. limit of detection of 0.1 atomic percent
SIMS	1. sputtered atoms are analyzed by an energy-filtered quadrupole mass spectrometer 2. sensitive to surface composition and atom clustering 3. limit of detection is in the parts per billion

Table 2: Surface Techniques

Time (sec)	electroless strong(100)	electroplate slight(100)	evaporate slight(111)	sputter strong(111)
5	reddish edge blue with brown area	blue edge blue with red	clear edge bluish tint bluish with brown areas	uniform bluish tint
10	clear edge bluish with darker regions	clear edge light with red areas	clear edge blue blue/red	uniform bluish/ brown tint
106	reddish edge blue shades of	clear edge light with dark red	uniform bluish surface	uniform bluish- brown tint
290	clear edge blue red,orange, red with blue	clear edge blue red/orange/ light blue	clear edge uniform blue surface	uniform bluish brown tint
390	reddish edge light blue purple & dark blue	clear edge blue region red/orange/ dark blue	blue edge red	clear edge blue/orange
800	reddish edge blue/red	red edge patchy blue	blue edge blue/red	bluish matrix red patchy area
1625	reddish edge dark red/ blue	red edge blue/ greenish	clear area blue/red	bluish areas reddish areas
3180	brown to blue to dark red to blue	red area green/blue/ dark blue	clear edge light & dark blue	reddish edge bluish/orange/ red
6400	patchy patterns reddish/ greenish/brown	red edge patchy green	blue edge light & dark blue	blue/red areas of copper color

Table 3: Colorimetric results

color	oxide thickness(nm)
brown	38-42
purple	45
violet	48
blue(either light or dark)	50
green	83-97
yellow	98-111
orange	120
red	126

Table 4: Qualitative correlation of color change and oxide thickness

Measured d-spacing (Angstroms)	reflection	radiation
2.13	Cu_{111}	CuKß
2.088	Cu_{111}	FeKα
2.08	Cu_{111}	$WL\alpha_1$
2.077	Cu_{111}	CuKα
1.80	Cu_{200}	CuKß
1.805	Cu_{200}	$WL\alpha_1$
1.81	Cu_{200}	CuKα
1.81	Cu_{200}	FeKß
1.78	Cu_{200}	FeKα
1.3	Cu_{220}	CuKß
1.27	Cu_{220}	FeKα
1.23	Cu_{220}	CuKα
1.11	Cu_{311}	CuKα
1.09	Cu_{311}	CuKß
1.04	Cu_{222}	CuKα
0.91	Cu_{400}	CuKα

Table 5: XRD: original electroless

Measured d-spacing (Angstroms)	reflection	radiation
2.09	Cu_{111}	CuKß
2.08	Cu_{111}	CuKα
2.077	Cu_{111}	FeKα
1.99	Cu_{111}	$WL\alpha_1$
1.82	Cu_{200}	CuKß
1.80	Cu_{200}	$FeK\beta_1$
1.80	Cu_{200}	CuKα
1.79	Cu_{200}	$WL\alpha_1$
1.28	Cu_{220}	CuKß
1.27	Cu_{220}	$WL\alpha_1$
1.27	Cu_{220}	CuKα
1.12	Cu_{311}	$WL\beta_2$
1.09	Cu_{311}	CuKß
1.09	Cu_{311}	CuLα
1.04	Cu_{222}	CuKα
0.90	Cu_{400}	CuKα
0.83	Cu_{331}	CuKß
0.81	Cu_{420}	CuKß

Table 6: XRD: original electroplate

Measured d-spacing (Angstroms)	reflection	radiation
2.077	Cu_{111}	FeKα
2.073	Cu_{111}	FeKβ
2.073	Cu_{111}	WLα
2.07	Cu_{111}	CuKβ
2.071	Cu_{111}	CuKα
2.067	Cu_{111}	$WL\beta_1$
2.066	Cu_{111}	$WL\beta_2$
1.80	Cu_{200}	CuKβ
1.80	Cu_{200}	$WL\alpha_1$
1.796	Cu_{200}	CuKα
1.31	Cu_{220}	FeKβ
1.29	Cu_{220}	CuKβ
1.27	Cu_{220}	$WL\beta_2$
1.27	Cu_{220}	CuKα
1.09	Cu_{311}	CuKα
1.04	Cu_{222}	CuKα
0.90	Cu_{400}	CuKβ
0.90	Cu_{400}	CuKα
0.90	Cu_{400}	CuKα
0.82	Cu_{331}	CuKβ

Table 7: XRD: original evaporate

Measured d-spacing (Angstroms)	reflection	radiation
2.08	Cu_{111}	FeLα
2.07	Cu_{111}	FeKβ
2.073	Cu_{111}	$WL\beta_1$
2.07	Cu_{111}	CuKβ
2.07	Cu_{111}	$WL\alpha_1$
2.07	Cu_{111}	CuKα
2.06	Cu_{111}	$WL\beta_1$
1.83	Cu_{200}	$WL\alpha_1$
1.80	Cu_{200}	FeKα
1.80	Cu_{200}	CuKβ
1.80	Cu_{200}	CuKα
1.28	Cu_{220}	CuKα
1.08	Cu_{311}	$WL\alpha_1$
1.08	Cu_{311}	CuKβ
1.08	Cu_{311}	CuKα
1.04	Cu_{222}	CuKα
0.82	Cu_{331}	CuKβ

Table 8: XRD: original sputter

SAMPLE	
ELECTROLESS	DEPOSITION PARAMETERS copper sulfate-formaldehyde plating bath on to activated reinforce epoxy resin circuit board. FILM CHARACTERISTICS 8,000nm thick; average grain size = 2.6μm; strong 100 orientation
ELECTROPLATE	DEPOSITION PARAMETERS acidic copper sulfate bath; deposited on to titanium mandrel FILM CHARACTERISTICS 50,800nm thick; removed from substrate; average grain size = 0.5μm; slight 100 orientation
EVAPORATE	DEPOSITION PARAMETERS base vacuum 2 to 6×10^{-6}Torr; substrate-chromium on polyimide film stretched across a windowed titanium frame- preheated substrate for 45 minutes at 200°C; vacuum system cooled for 30 minutes before backfilling with nitrogen gas FILM CHARACTERISTICS 8,000nm thick; average grain size= 1.8-m; slight 111 orientation
SPUTTER	DEPOSITION PARAMETERS base vacuum- 5×10^{-5}Torr; backfilled to 1×10^{-3} Torr with Argon; substrate was the same as that evaporate sample; 10 passes under the cathode to build desired thickness; auxiliary chamber backfilled with air prior to sample removal FILM CHARACTERISTICS 8,000nm thick; average grain size = 1.0-m; strong 111 orientation

Table 9: Deposition parameters and film characteristics

Deposition Technique	Time (hours) to peak	equilibrium	total
Electroless	0.75	1.75	4.5
Electroplated	0.25	>10	20
Evaporated	0.75	5	28
Sputtered	0.5	8	20

Table 10: pH: summary of long etch results

(0.01M $CuCl_2$ at 45°C open system)

1. $Cu^{++} + H_2O = CuO_{(s)} + 2H^+$; $\log K_1 = -7.77$
2. $Cu^{++} + H_2O = Cu(OH)^+ + H^+$; $\log K_2 = -8.06$
3. $2Cu^{++} + 2H_2O = Cu_2(OH)_2^{++} + 2H^+$; $\log K_3 = -10.43$
4. $Cu^{++} + 3H_2O = Cu(OH)_3^- + 3H^+$; $\log K_4 = -27.6$
5. $2Cu_{(s)} + 2Cu^{++} + 2(OH)^- = 2Cu^+ + Cu_2O_{(s)} + H_2O$;
   $\log K_5 = 8.70$
6. $CuCl_{(s)} = Cu^+ + Cl^-$; $\log K_6 = -5.77$
7. $H_2O = H^+ + (OH)^-$; $\log K_7 = -14.00$

Table 11: Chemical equations and equilibrium constants at 25°C

COMPONENTS

SPECIES	Cu^{++}	Cl^{-}	H^{+}	CO_{2g}	Cu_s	$CuCl_s$	Cu_2O_s
$(CuOH)^{+}$	+1	0	-1	0	0	0	0
$Cu(OH)_3^{-}$	+1	0	-3	0	0	0	0
$Cu_2(OH)_2^{++}$	+2	0	-2	0	0	0	0
Cu^{+}	+2	+1	-2	0	+2	-1	-1
H_2CO_3	+2	+1	-2	0	+2	-1	-1
HCO_3^{-}	0	0	0	+1	0	0	0
CO_2^{-}	0	0	-2	+1	0	0	0
OH^{-}	0	0	-1	0	0	0	0

Table 12: Microql matrix for an open system

	COMPONENTS					
SPECIES	Cu^{++}	Cl^{-}	H^{+}	Cu_s	$CuCl_s$	Cu_2O_s
$(CuOH)^{+}$	+1	0	-1	0	0	0
$Cu(OH)_3^{-}$	+1	0	-3	0	0	0
$Cu_2(OH)_2^{++}$	+2	0	-2	0	0	0
Cu^{+}	+2	+1	-2	+2	-1	-1
OH^{-}	0	0	-1	0	0	0

Table 13: Microql matrix for a closed system

Log K

SPECIES	TEMPERATURE (°C) 3	10	20	45
$(CuOH)^+$	-8.63	-8.42	-8.06	-7.48
$Cu_2(OH)_2^{++}$	-11.70	-10.90	-10.43	-9.69
$Cu(OH)_3^-$	-29.56	-28.82	-27.60	-25.64
Cu^+	-13.82	-13.48	-12.90	-11.99
OH^-	-14.73	-14.53	-14.17	-13.40

Table 14: Equilibrium constants calculated for each experimental temperature

CONCENTRATION (M)

pH	Time (min)	Cu^{++}	$(CuOH)^{+}$ (10^{9})	$Cu(OH)_3^{-}$ (10^{28})	$Cu_2(OH)_2^{++}$ (10^{11})	Cu^{+} (10^{11})	$Cu_{tot}-Cu^{++}$ (10^{9})
3.67	0	0.01	0.14	0.18	3.72	3.72	0.25
3.66	10	0.01	0.15	0.22	4.26	4.28	0.26
4.17	20	0.01	0.49	7.40	4.47	4.48	1.83
4.34	30	0.01	0.72	24.00	9.77	9.80	3.66
4.42	40	0.01	0.87	41.70	14.1	14.20	5.11
4.47	50	0.01	1.00	58.90	17.8	17.80	6.32
4.51	60	0.01	1.07	77.60	21.4	21.40	7.49
4.56	70	0.01	1.20	110.00	26.9	27.00	9.28
4.59	80	0.01	1.29	135.00	30.9	31.00	10.60
4.58	90	0.01	1.26	126.00	29.5	29.60	10.10
4.60	100	0.01	1.32	144.00	32.4	32.40	11.00

Table 15: Microql output for copper species in the Electroless, 45°C, open system

SAMPLE	TEMPERATURE (°C)	RATE ($mol \cdot h^{-1} cm^{-2}$) SYSTEM CLOSED	OPEN
ELECTROLESS			
	45	$9X10^{-9}$	-------
	45	------	$1.9X10^{-10}$
	20	$7X10^{-11}$	-------
	10	-------	$1.5X10^{-10}$
	3	$8X10^{-10}$	-------
ELECTROPLATE			
	45	$6X10^{-10}$	-------
	45	-------	$1X10^{-7}$
	10	-------	$2X10^{-9}$
	3	$5X10^{-10}$	------
EVAPORATE			
	45	$5X10^{-10}$	-------
	45	-------	$2X10^{-8}$
	20	$4X10^{-9}$	-------
	10	------	$3X10^{-10}$
	3	$4X10^{-12}$	-------
SPUTTER			
	45	$6X10^{-9}$	-------
	45	------	$2X10^{-8}$
	10	------	$1X10^{-11}$

Table 16: Experimental reaction rates

SAMPLE	Activation energy ($kJ \cdot mol^{-1}$)
	CLOSED SYSTEM
ELECTROLESS	48
EVAPORATE	79

Table 17: Experimental activation energies

Pressure (Torr)	Reaction Rate ($mol \cdot hr^{-1}$)	Reaction rate ($mol \cdot hr^{-1}$)
	Diffusion Mechanism	
	grain boundary	bulk
10^{-3}	6×10^{-12}	4×10^{-13}
10^{-2}	3×10^{-8}	6×10^{-9}
0.1	2×10^{-7}	8×10^{-9}
0.5	4×10^{-7}	1×10^{-8}
1.0	6×10^{-7}	4×10^{-8}

Table 18: Reaction rates calculated from Sesselmann's experimental diffusion constants

Pressure (Torr)	Diffusion activation energy ($kJ\ mol^{-1}$)	
	grain boundary	bulk
10^{-3}	75	82
10^{-2}	54	58
0.1	50	58
0.5	48	56
1.0	47	54

Table 19: Activation energies calculated from Sesselmann's experimental diffusion constants

SAMPLE	ACTIVATION ENERGY($kJ \cdot mol^{-1}$)	PREFERRED ORIENTATION ratio
electroless	48 closed	137 (100)
evaporate	79 closed	33 (111)

Table 20: Activation energy versus preferred orientation ratio

SAMPLE	ACTIVATION ENERGY ($kJ \cdot mol^{-1}$)	FILM THICKNESS/ GRAIN SIZE	GRAIN SIZE (μm)
electroless	48 closed	3.08	2.6
evaporate	79 closed	4.44	1.8

Table 21: Comparison of activation energy with film thickness/grain size and grain size

	GRAIN SIZE(μm)	COMMENTS
ELECTROLESS		
original	2.6	rough with many sharp facets
ion beam etch		remained rough with well developed facets
short etch	2.5	plate-like grains
long etch	10.0	pyramids with different orientations on fine-grained background (total time 4.5 hours).
ELECTROPLATE		
original	0.5	no sharp facets or apparent orientation noted
ion beam etch	1.6	roughening of surface features noted
short etch	4.0	plate-like grains present
long etch	1.4	randomly oriented large particles on a finer grained background (total time 20 hours).
EVAPORATE		
original	1.8	surface retained impressions of polyimide surface - grains were irregularly shaped and of random orientation
ion beam etch	1.8	roughening of surface apparent
short etch	1.4	plate-like grains
long etch	N/A	small and larger well defined particles - particles meshed together so that individual grains could not be distinguished (total time 28 hours).
SPUTTER		
original	1.0	uniform at 1000x, at 5000x - small pinholes (0.2μm) apparent. Grains were irregularly shaped and of random orientation
ion beam etch	N/A	cones developed- indication of preferential etching or columnar film structure
long etch	N/A	well defined pyramids on a background of smaller pyramids and irregularly shaped particles (total time 20 hours).

Table 22: SEM: SUMMARY

ELEMENTAL COMPOSITION
(atomic percent)

	COPPER	OXYGEN	CARBON	CHLORINE
ELECTROLESS				
original	49	17	34	0.3
short etch	62	14	13	10
long etch	57	24	6	12
ELECTROPLATE				
original	63	17	20	0.3
short etch	38	9	30	23
long etch	27	18	54	1
EVAPORATE				
original	57	19	24	0
short etch	49	14	32	5
long etch	54	10	7	28
SPUTTER				
original	57	20	23	0
long etch	43	24	20	13

Table 23: AES: SUMMARY

	Cu_2^+/Cu_3^+			
Sample	Electroless	Electroplate	Evaporate	Sputter
as-received	1.6	1.2	0.87	2.33
linear etch	2.4	2.2	2.1	------
equilibrium etch	2.4	2.5	1.44	1.49

Table 24: SIMS: SUMMARY

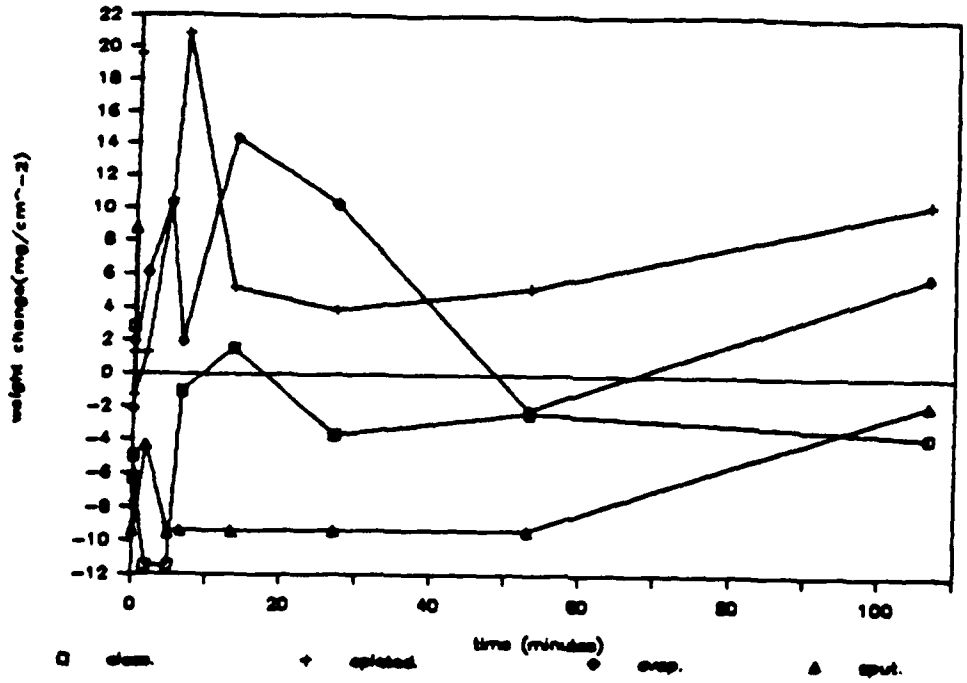

Figure 1: GRAVIMETRIC: room temperature

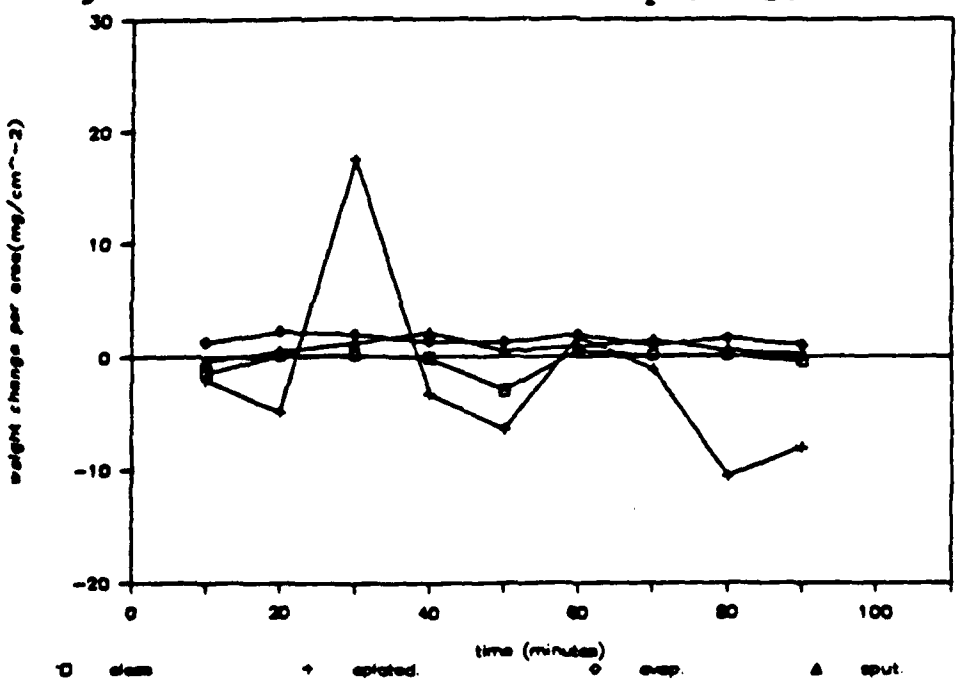

Figure 2: GRAVIMETRIC: ice bath

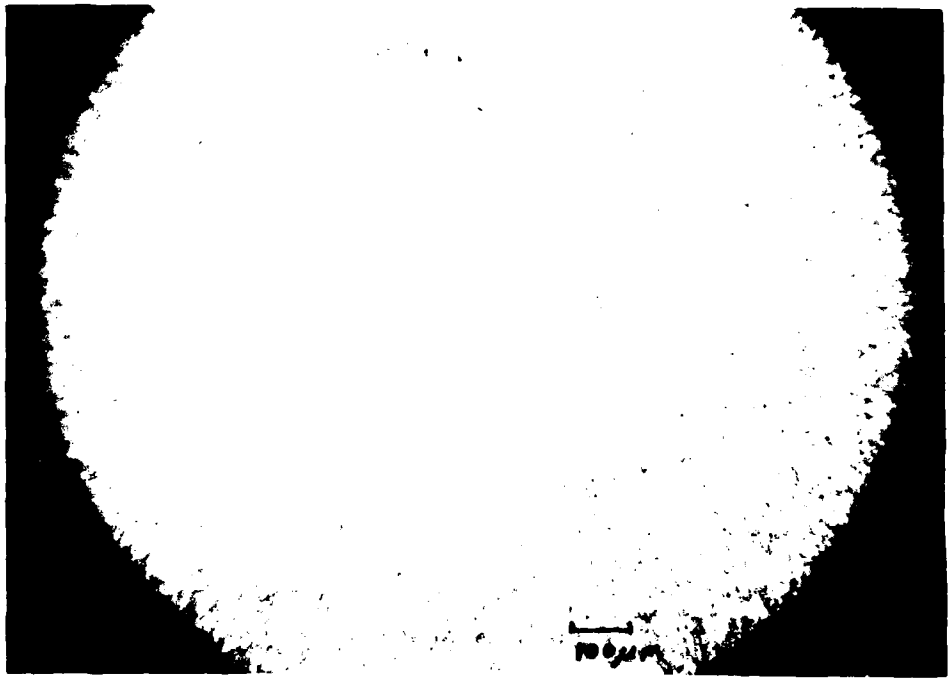

Figure 3: OPTICAL: original electroless

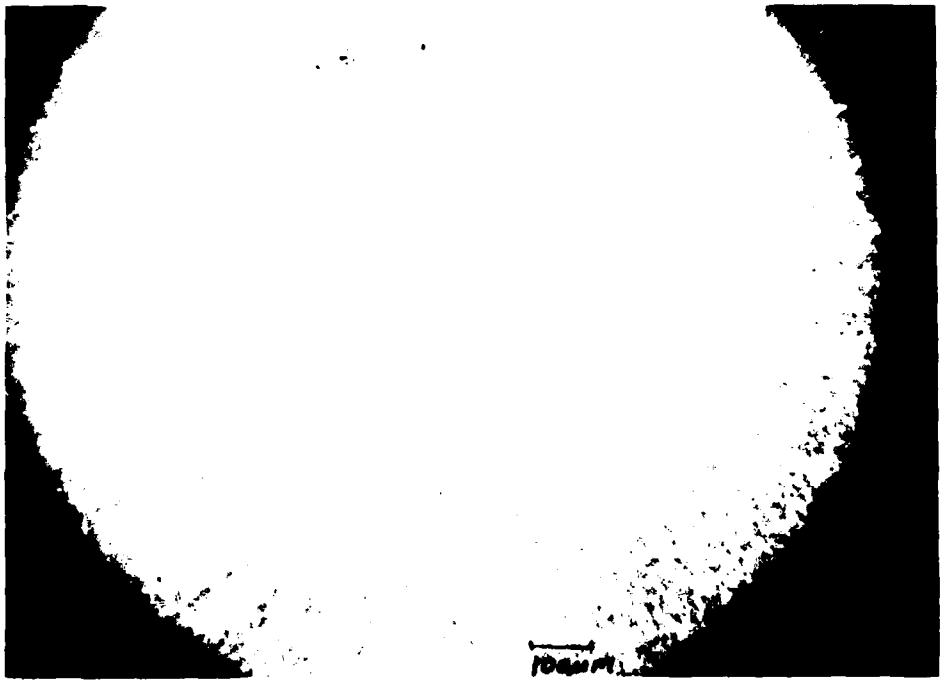

Figure 4: COLORIMETRIC: electroless after 1.8 hours exposure to 0.001M $CuCl_2$ at room temperature

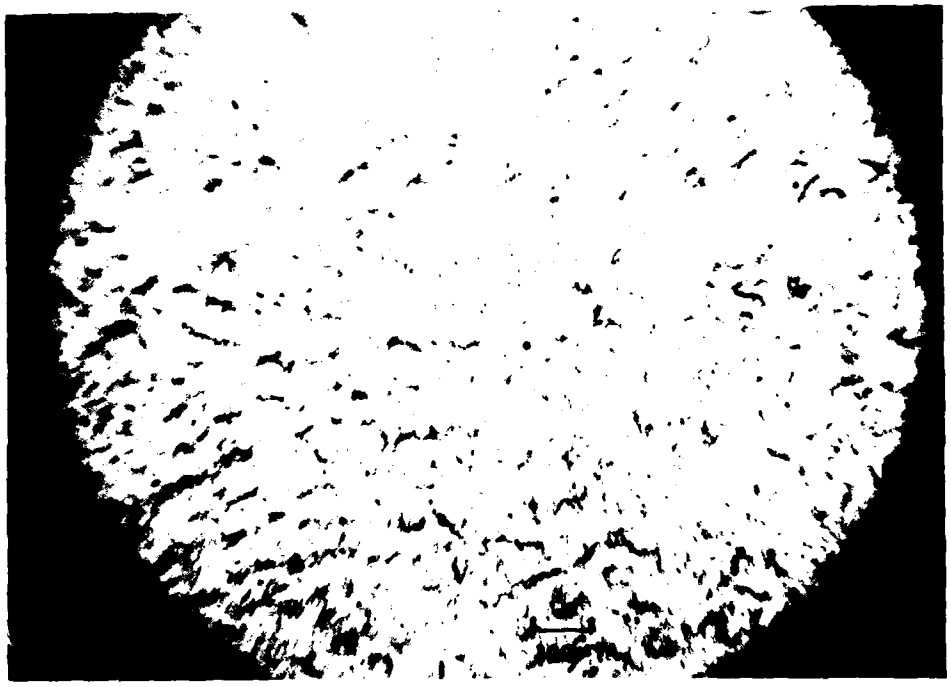

Figure 5: OPTICAL: original electroplate

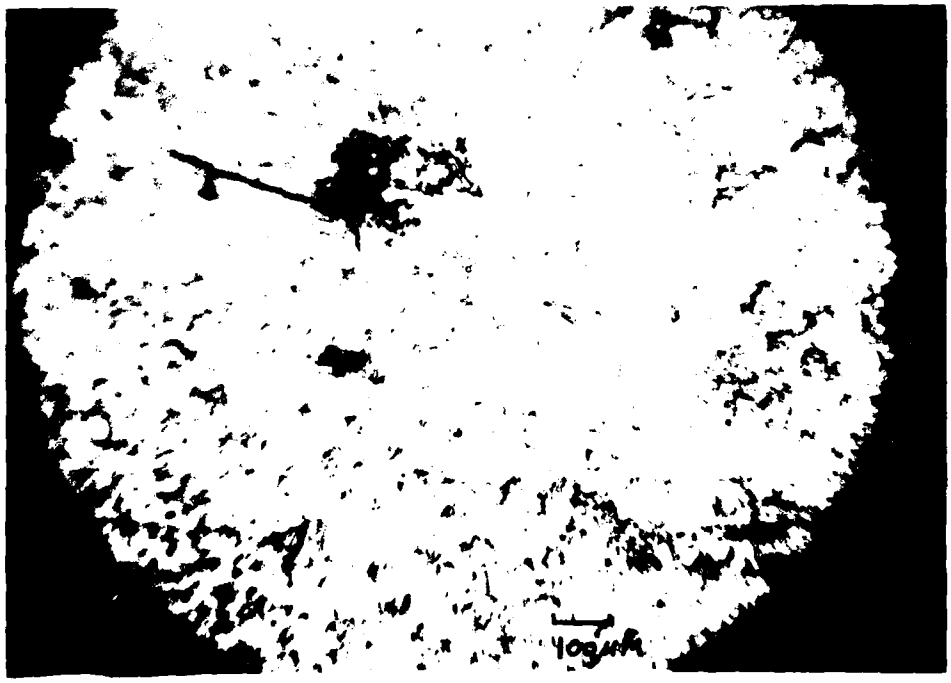

Figure 6: COLORIMETRIC: electroplate after 1.8 hours exposure to 0.001M $CuCl_2$ at room temperature

Figure 7: OPTICAL: original evaporate

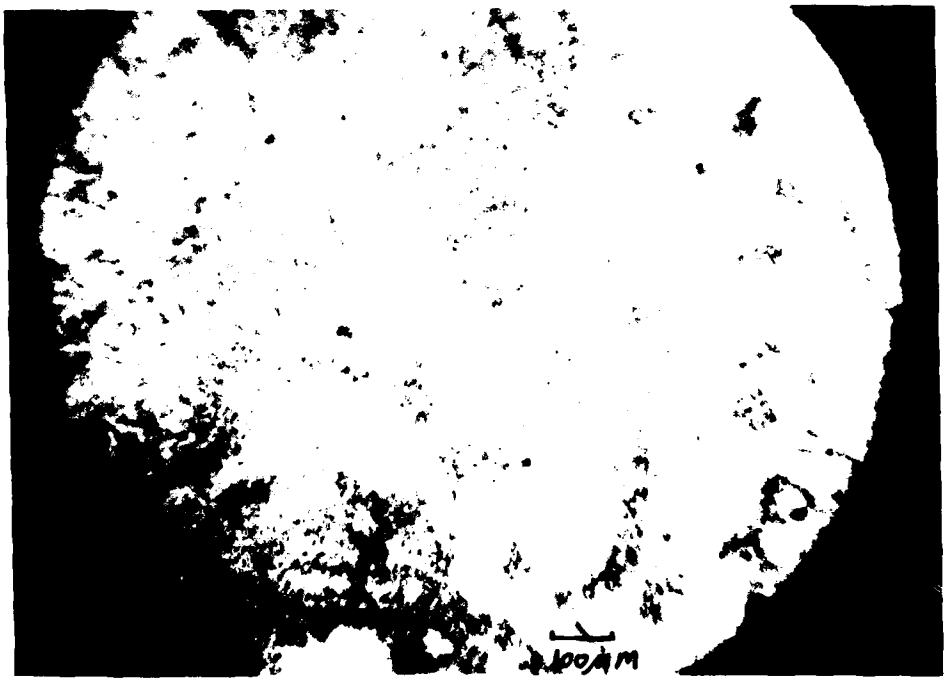

Figure 8: COLORIMETRIC: evaporate after 1.8 hours exposure to 0.001M $CuCl_2$ at room temperature

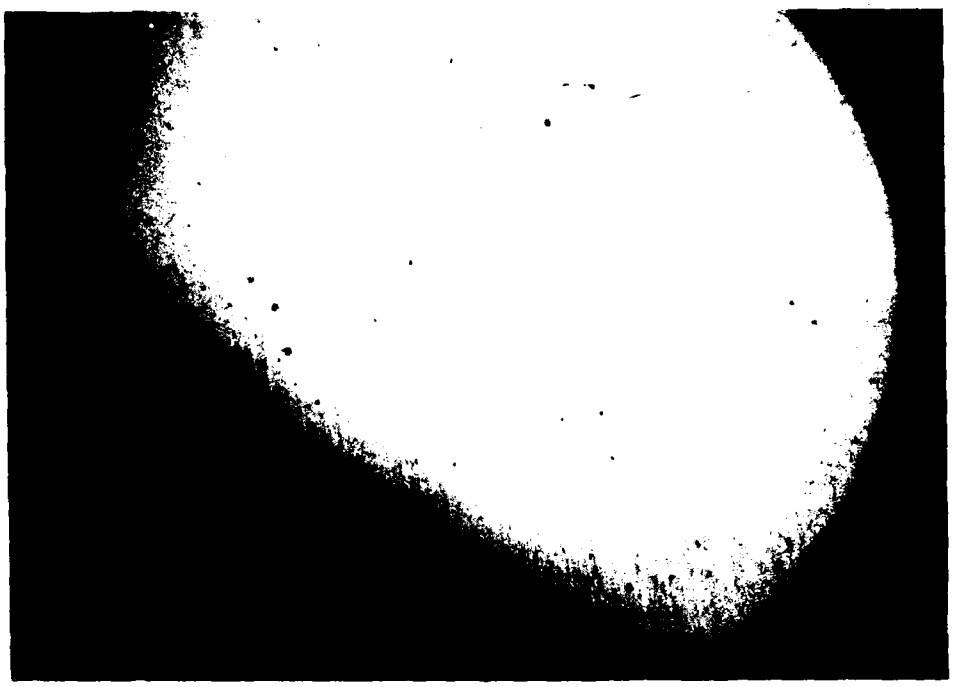

Figure 9: OPTICAL: sputter

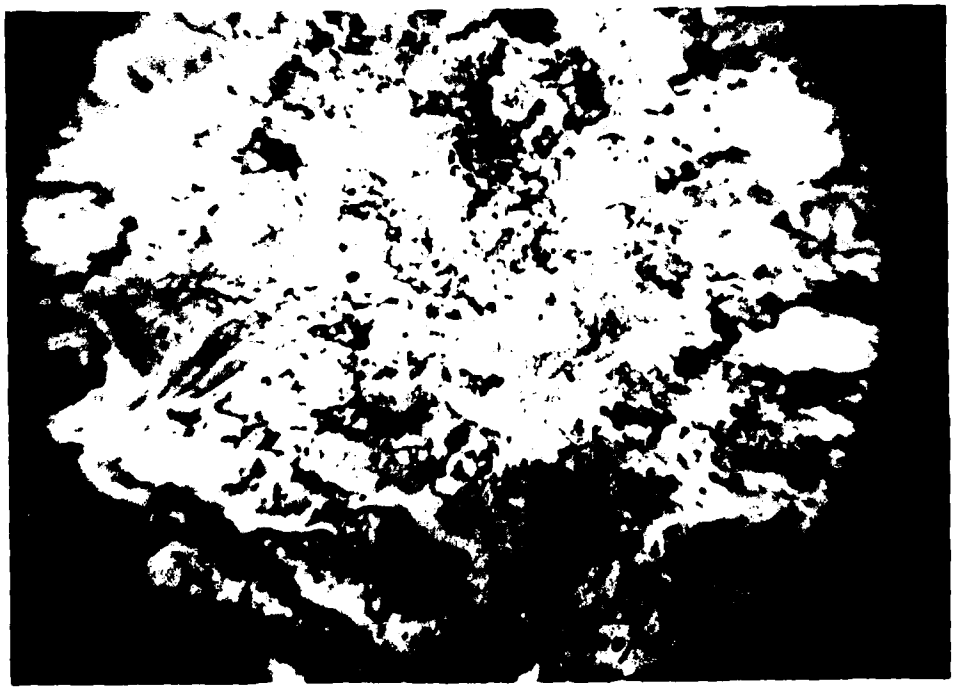

Figure 10: COLORIMETRIC: sputter after 1.8 hours exposure to 0.001M $CuCl_2$ at room temperature

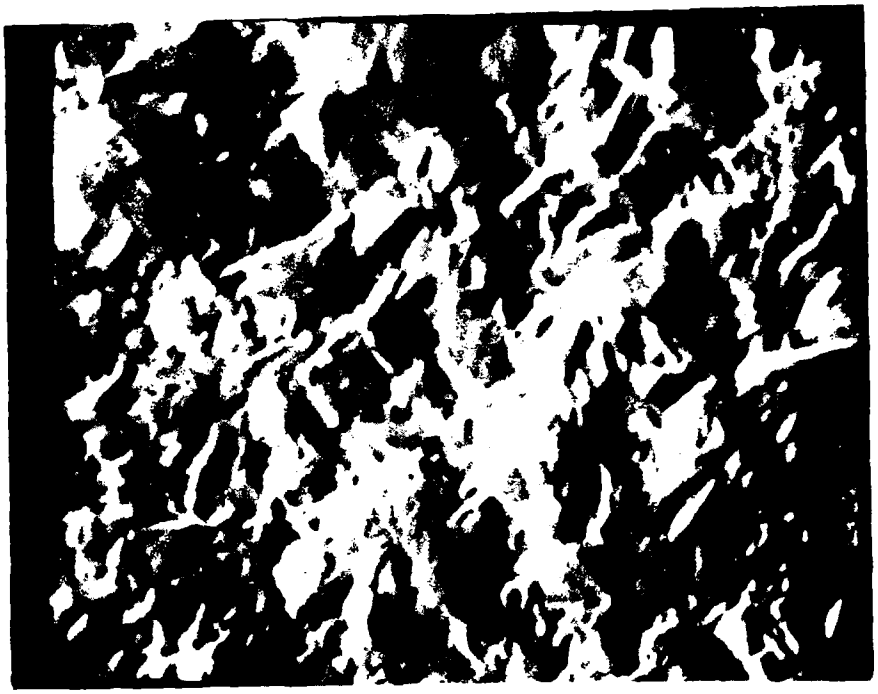

Figure 11: SEM: original electroless

Figure 12: SEM: original electroplate

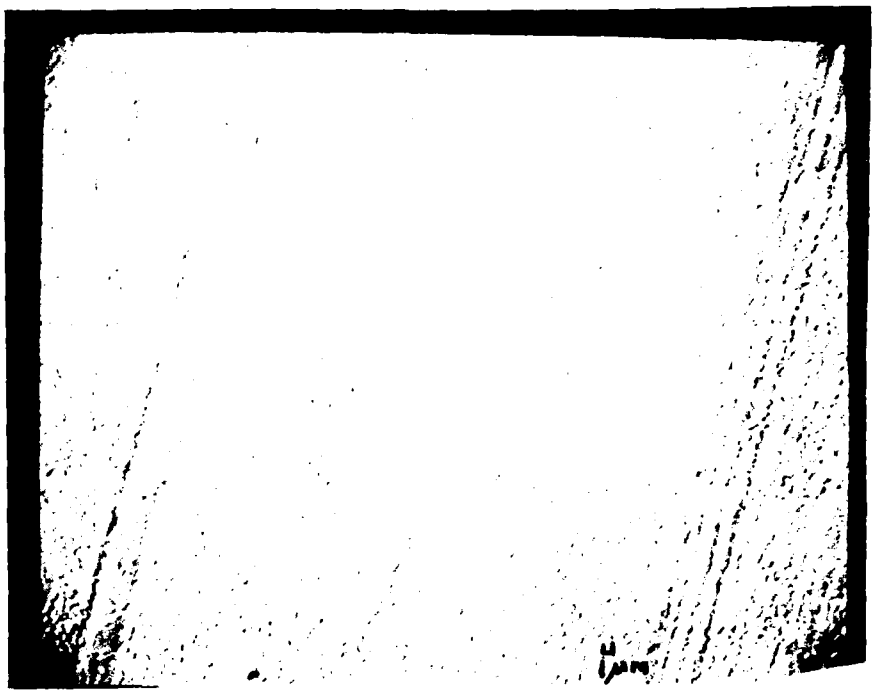

Figure 13: SEM: original evaporate

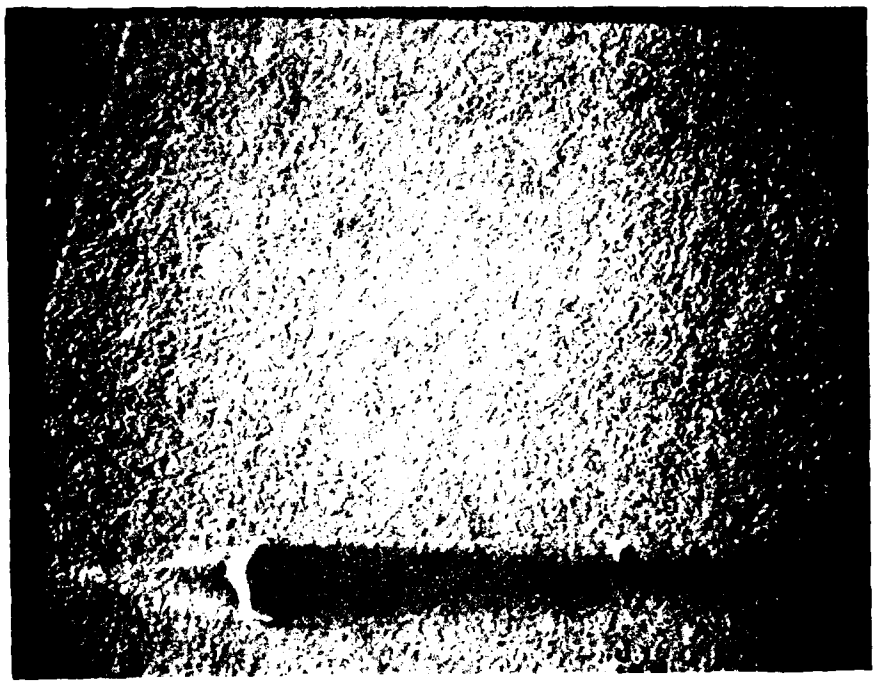

Figure 14: SEM: original sputter - 1000X

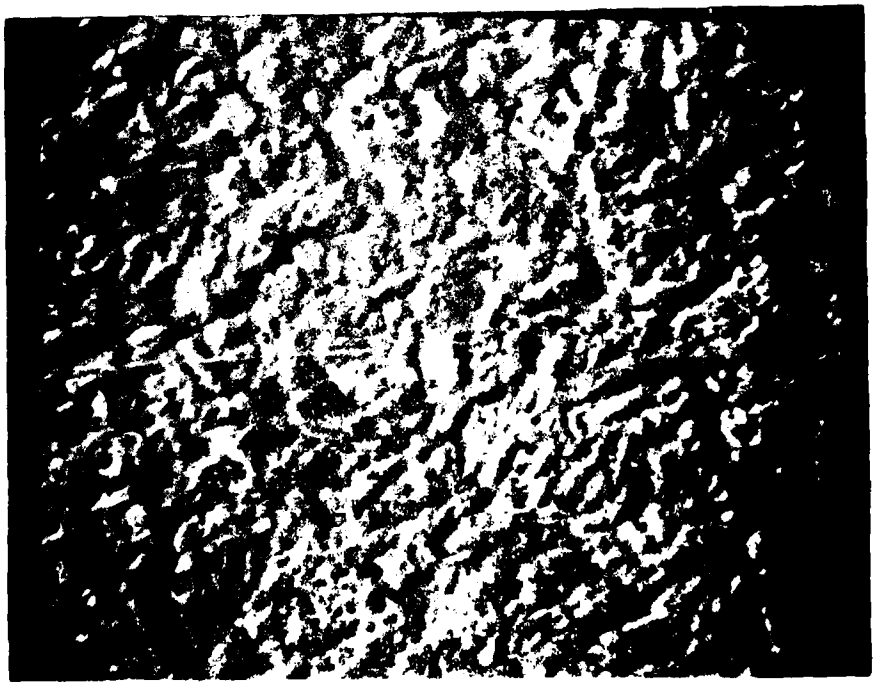

Figure 15: SEM: original sputter - 5000X

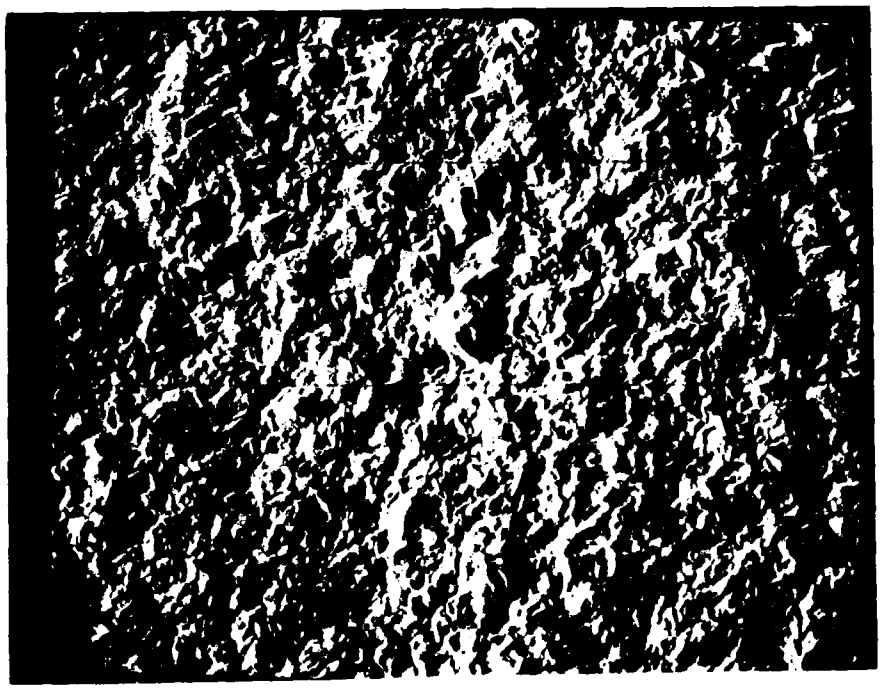

Figure 16: SEM: ion beam etch electroless 1.5 minute

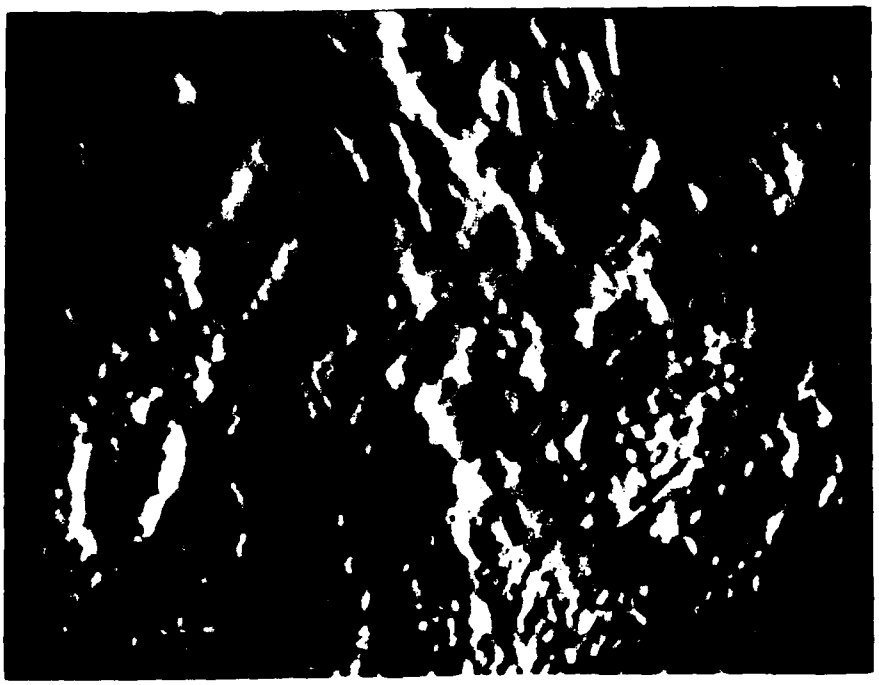

Figure 17: SEM: ion beam etch electroplate 30 minute

Figure 18: SEM: ion beam etch evaporate 78 minute

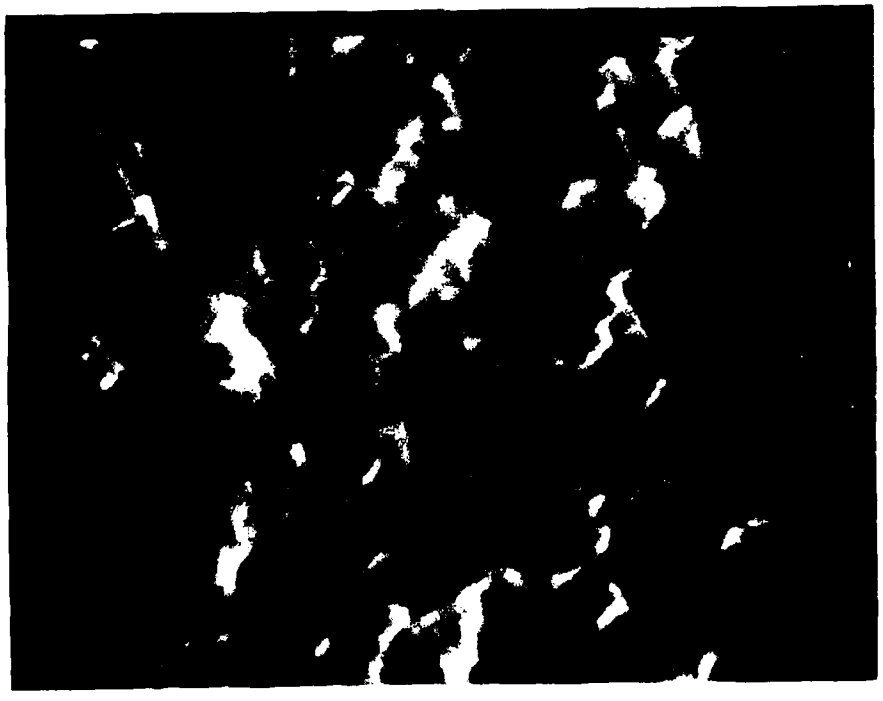

Figure 19: SEM: ion beam etch sputter 34 minute

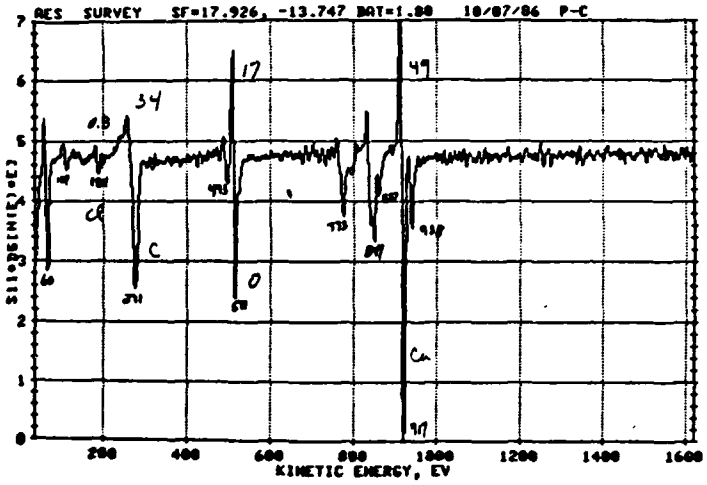

Figure 20: AES: original electroless

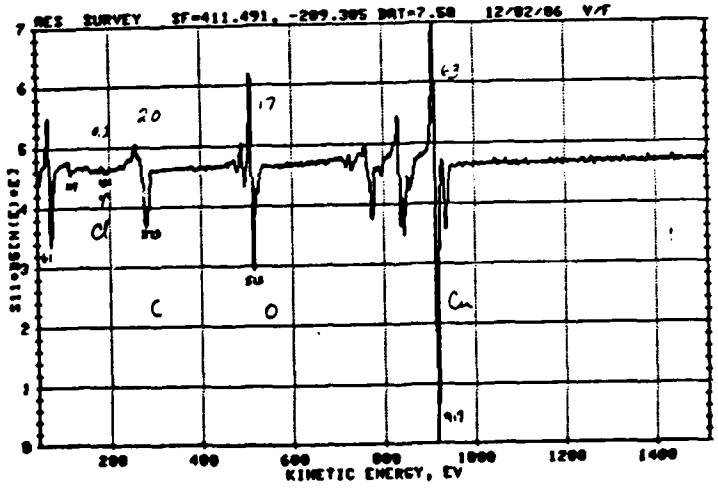

Figure 21: AES: original electroplate

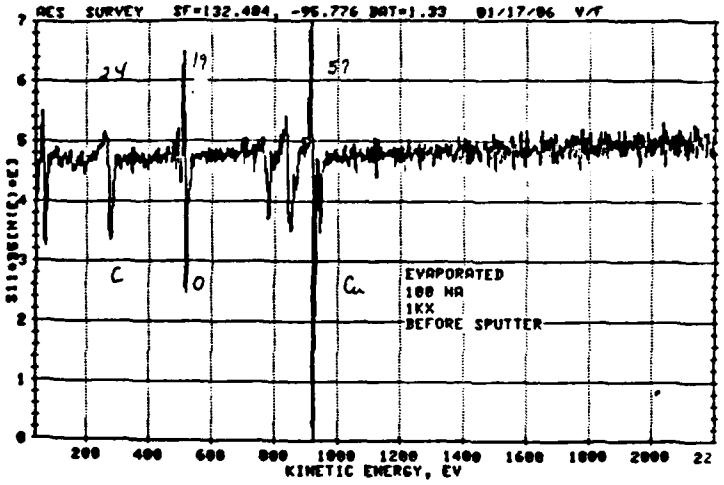

Figure 22: AES: original evaporate

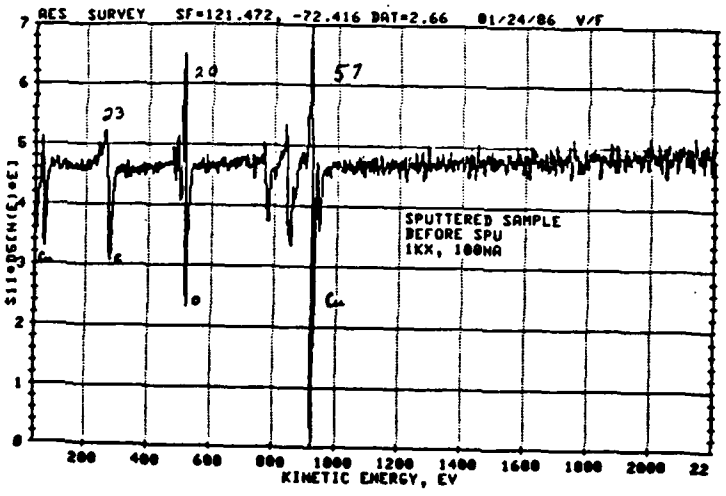

Figure 23: AES: original sputter

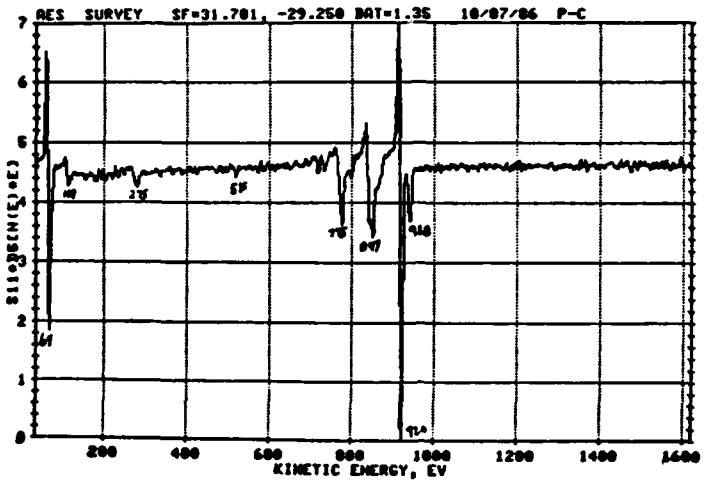

Figure 24: AES: electroless 1.0 min. ion beam etch

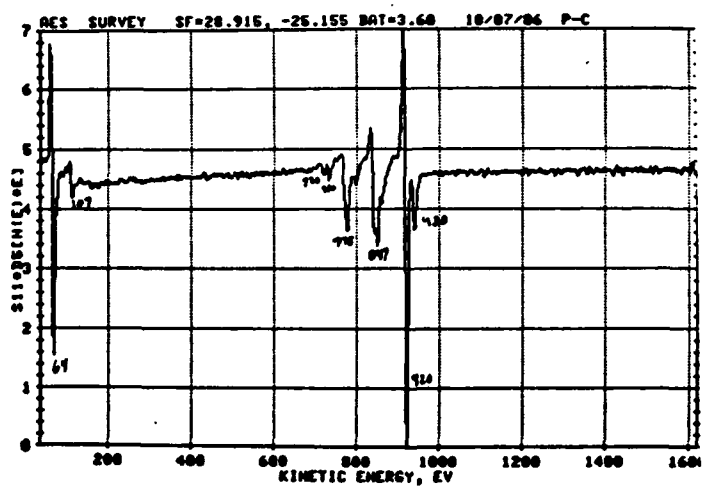

Figure 25: AES: electroless 1.5 min. ion beam etch

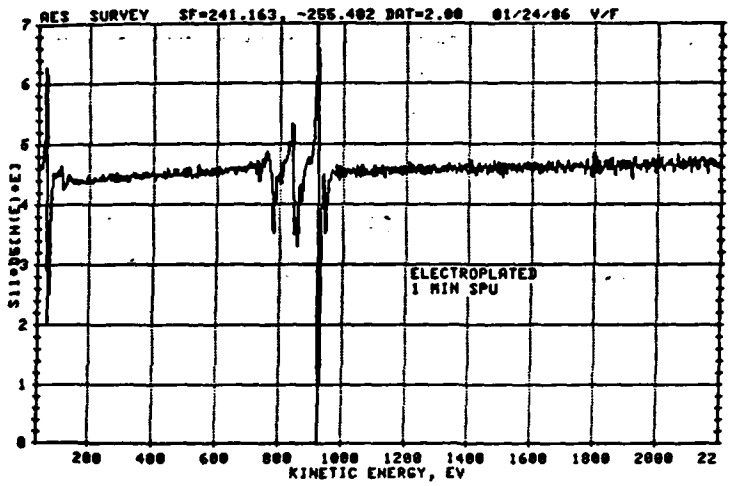

Figure 26: AES: electroplate 1.0 min. ion beam etch

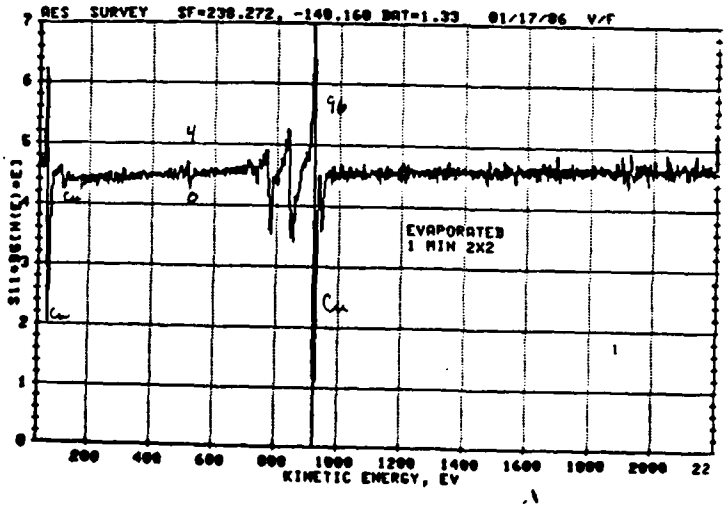

Figure 27: AES: evaporate 1.0 min. ion beam etch

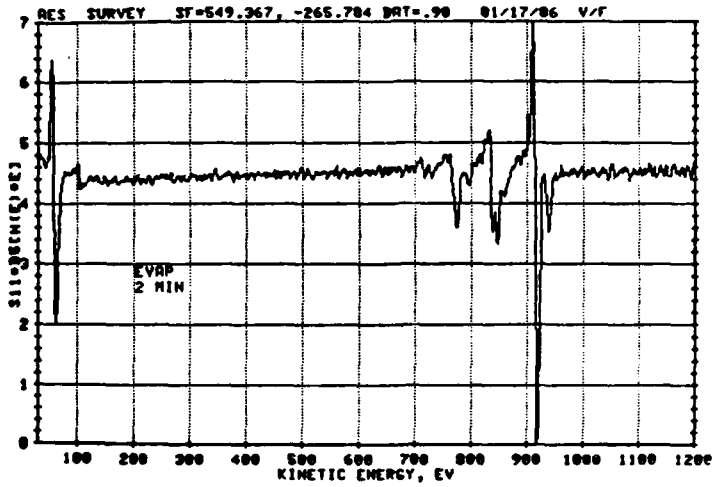

Figure 28: AES: evaporate 2.0 min. ion beam etch

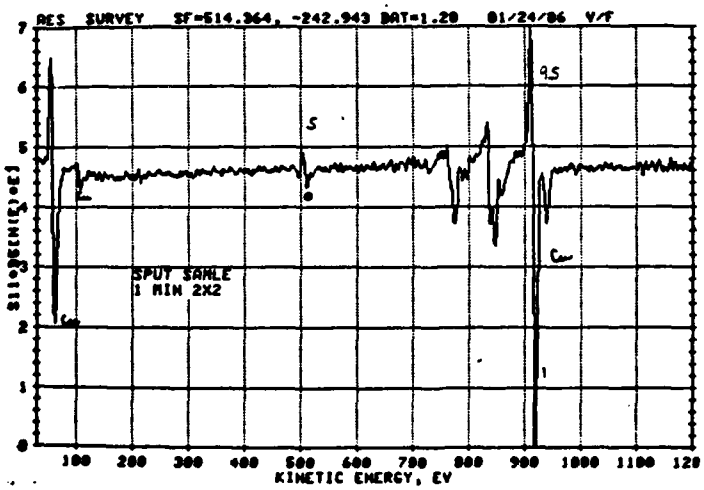

Figure 29: AES: sputter 1.0 min. ion beam etch

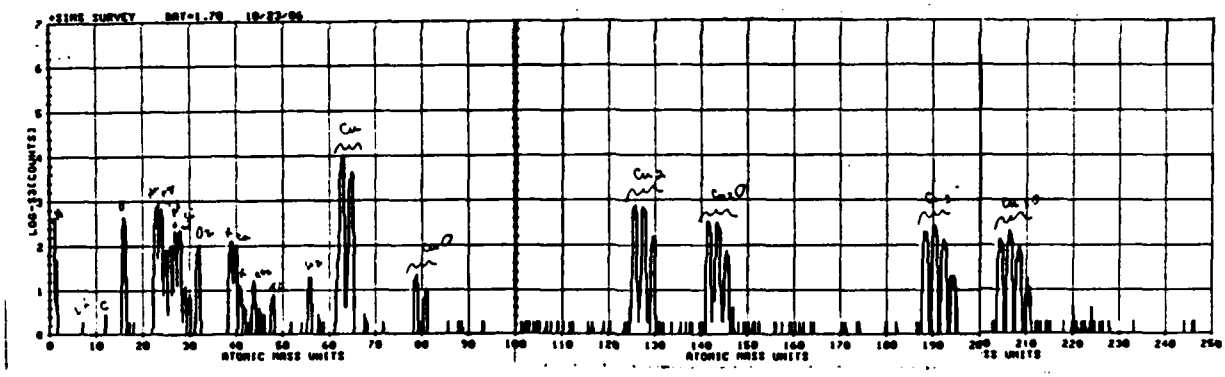

Figure 30: SIMS: original electroless

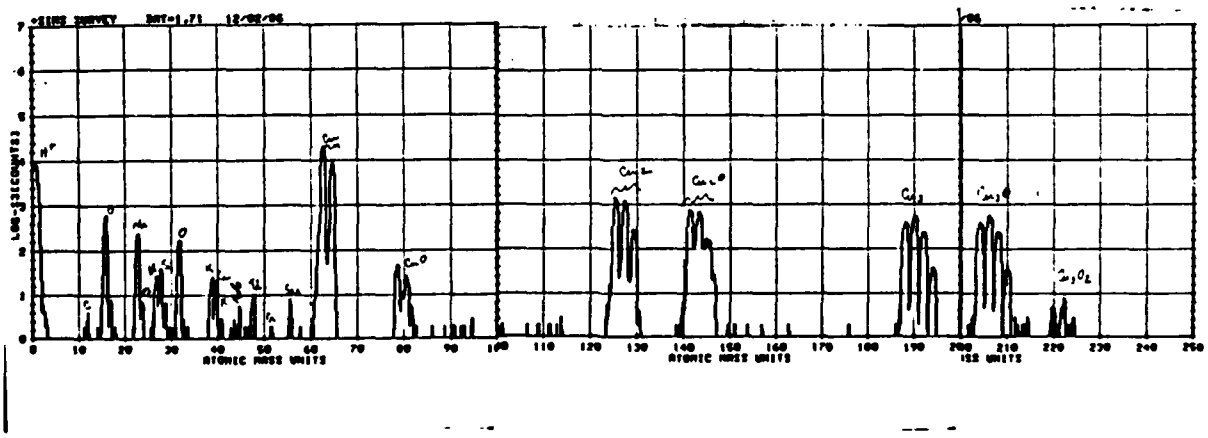

Figure 31: SIMS: original electroplate

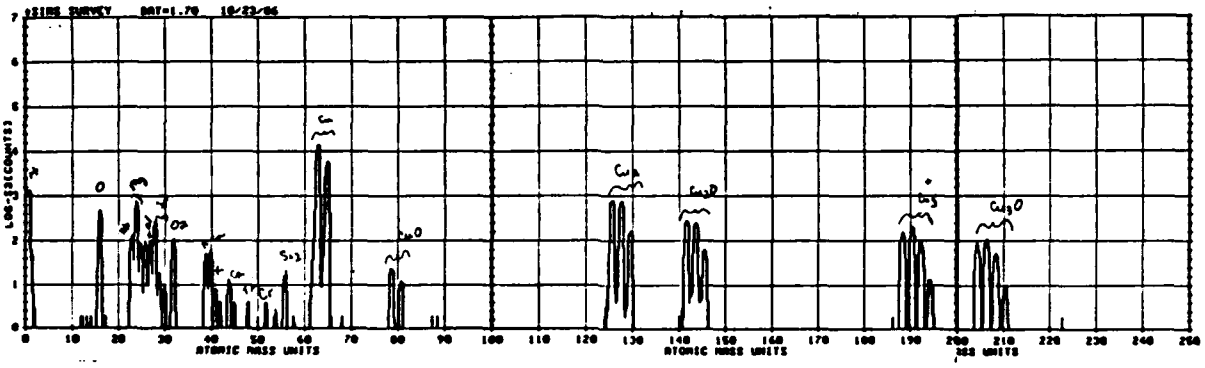

Figure 32: SIMS: original evaporate

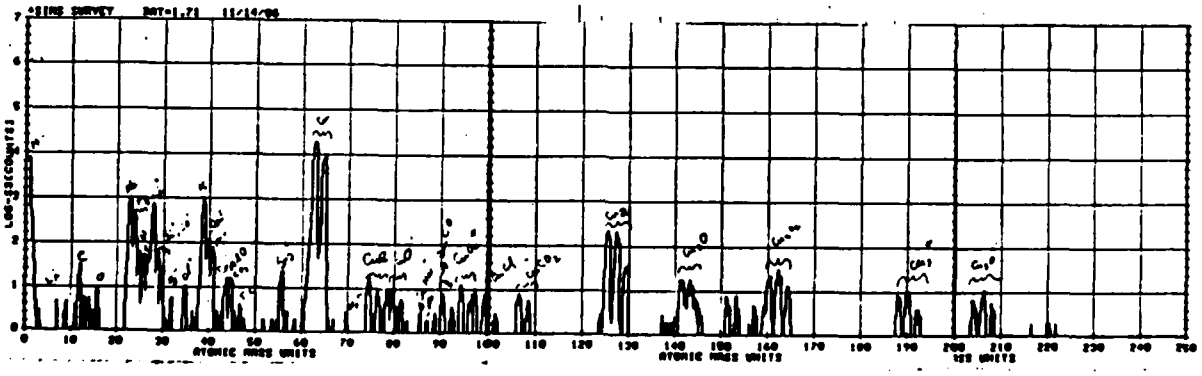

Figure 33: SIMS: original sputter

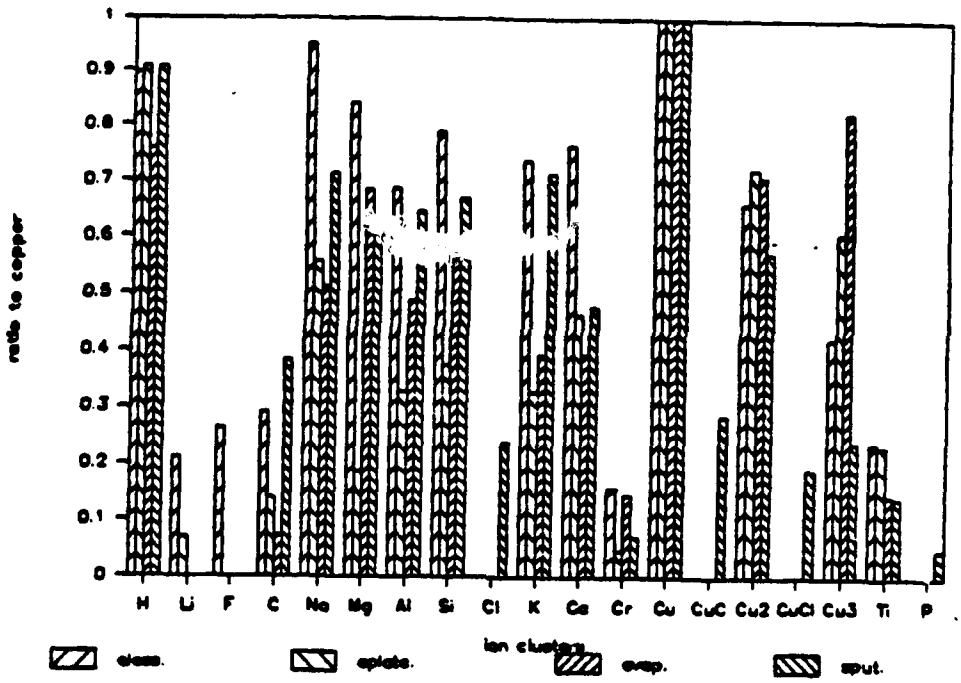

Figure 34: SIMS: comparison of original films

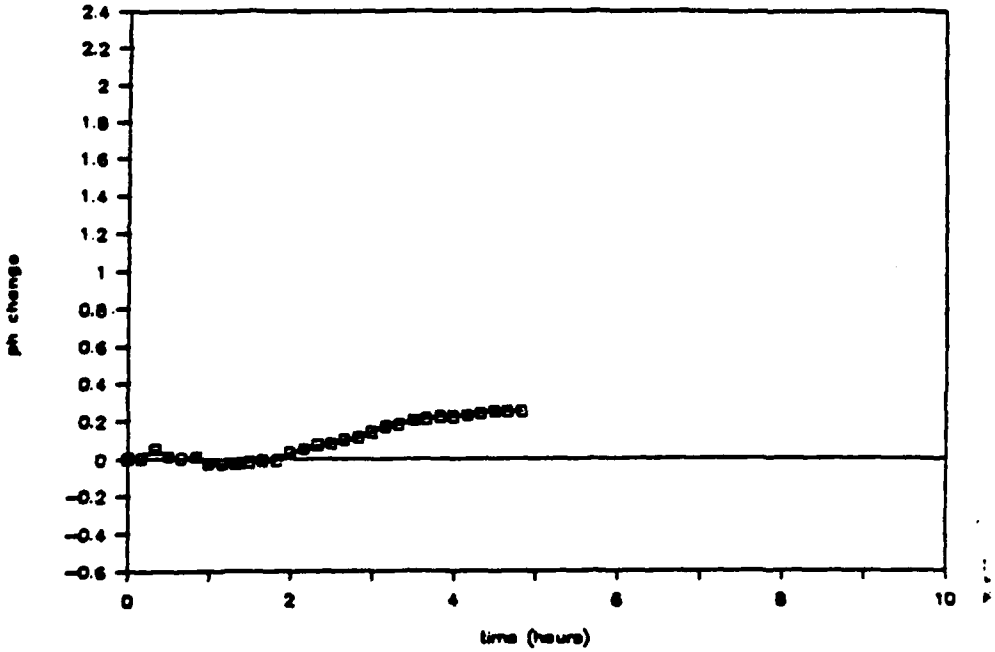

Figure 35: pH: blank 1

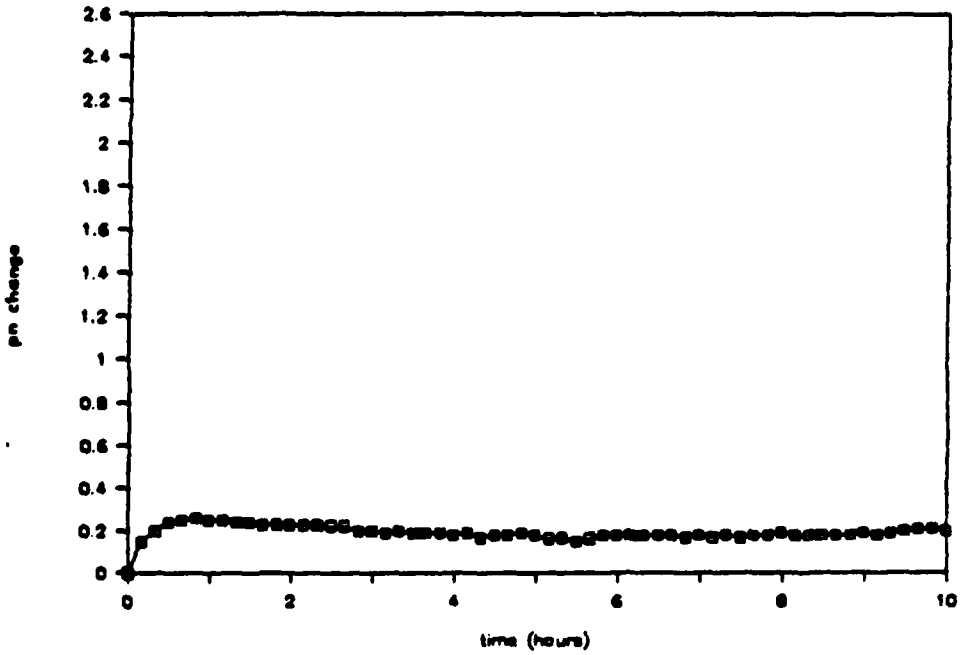

Figure 36: pH: blank 2

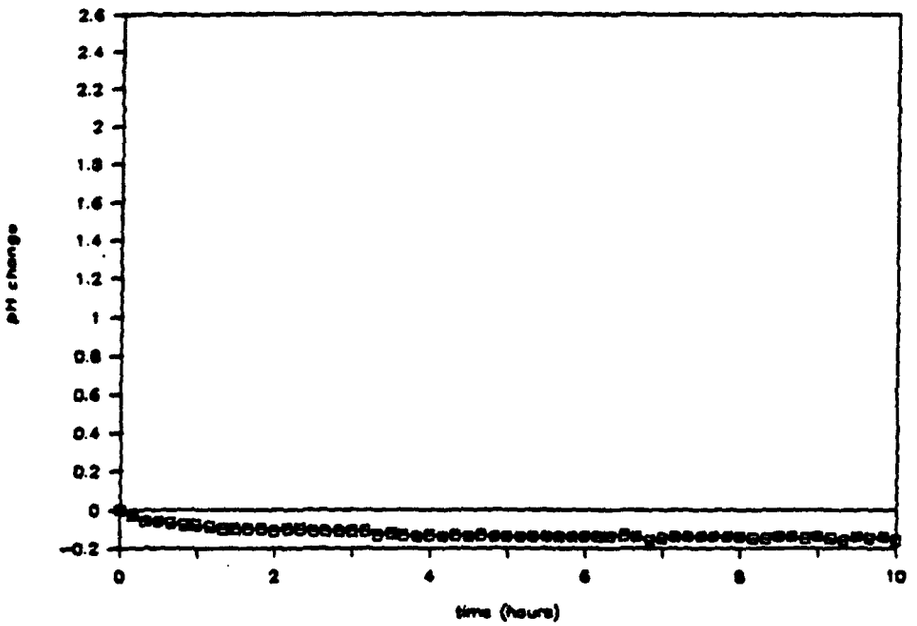

Figure 37: pH: blank 3

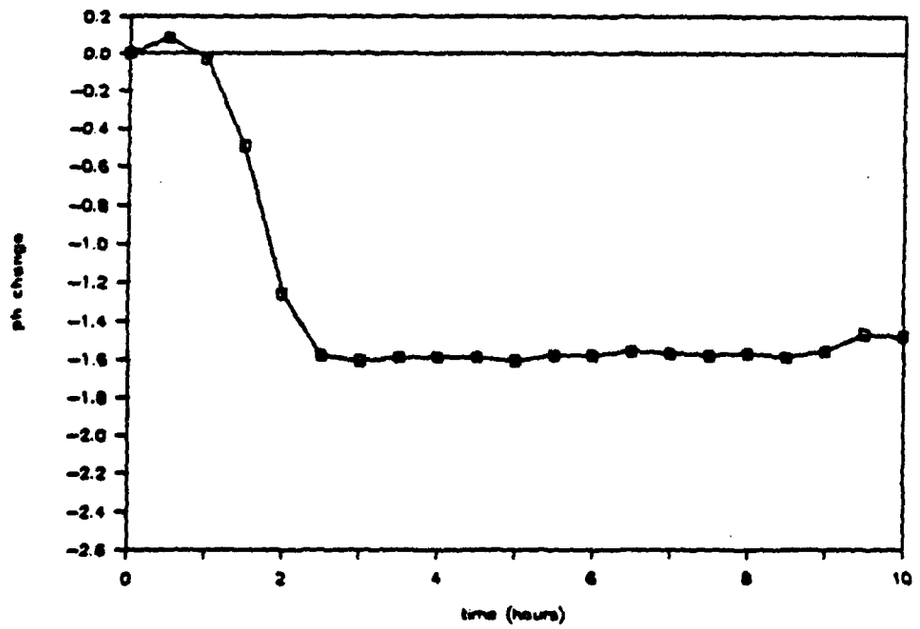

Figure 38: pH: blank 4

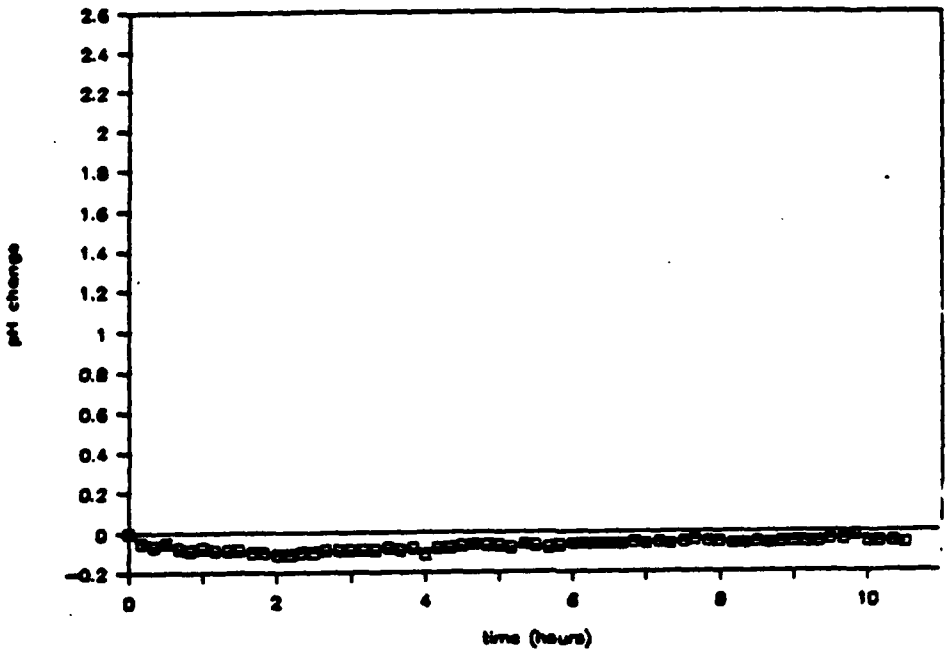

Figure 39: pH: blank 5

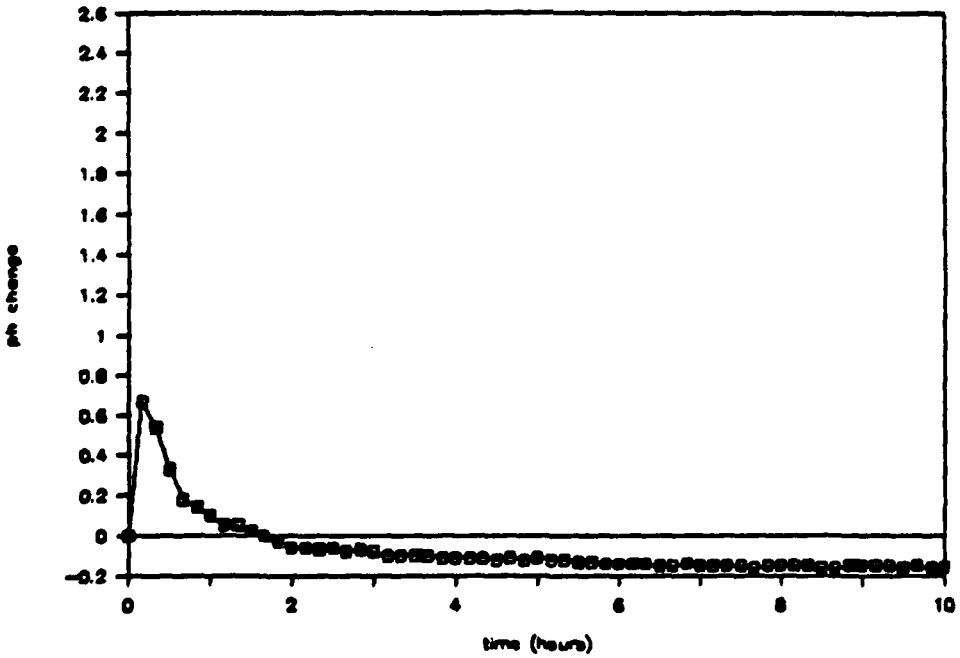

Figure 40: pH: electroless 45C closed

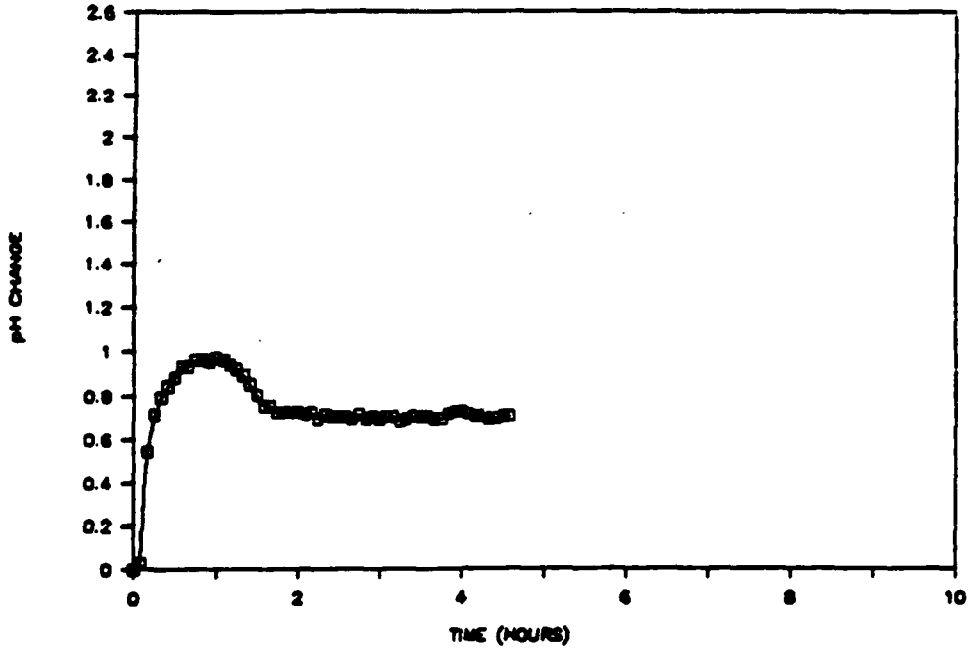

Figure 41: pH: electroless 45C open

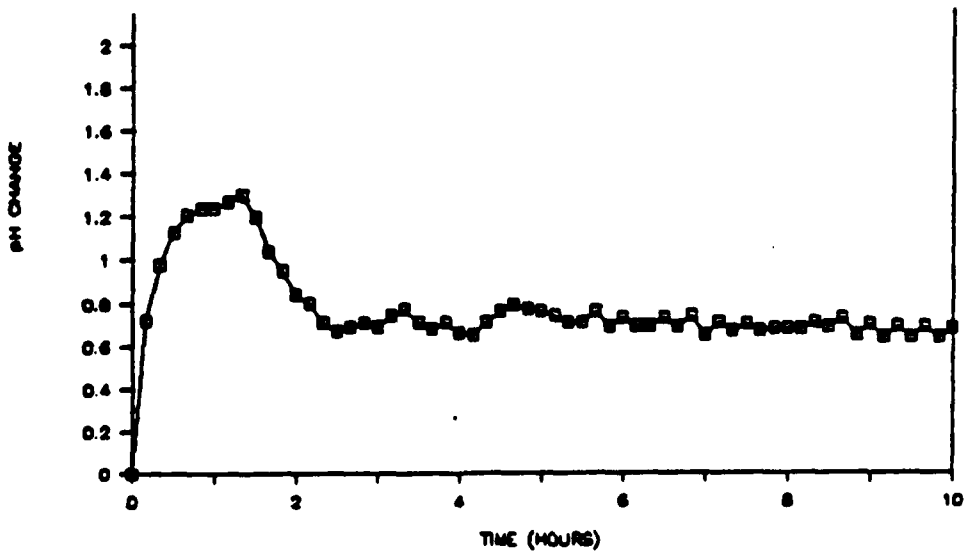

Figure 42: pH: electroless 20C closed

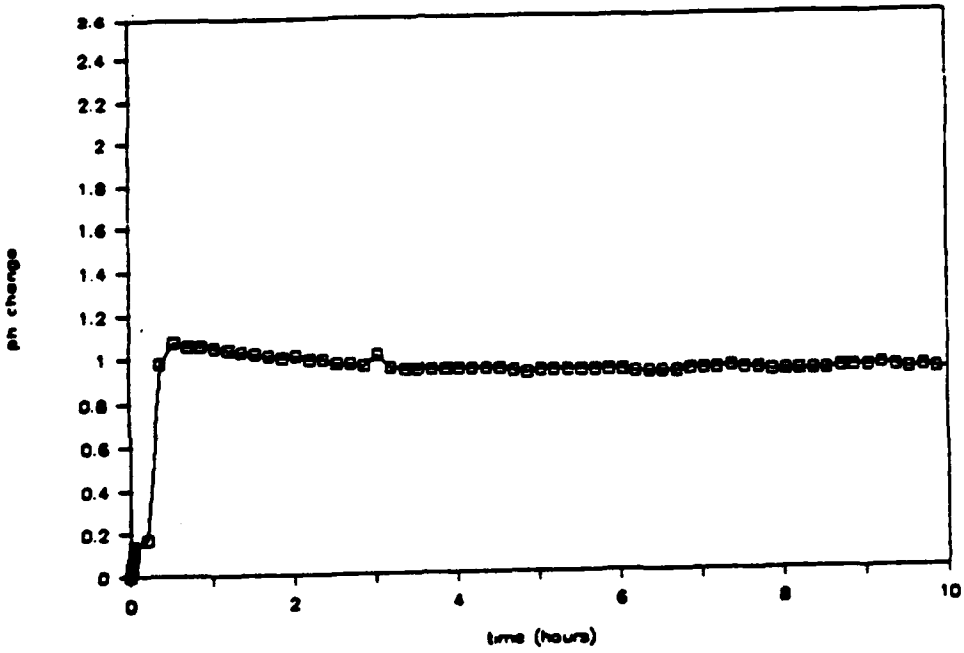

Figure 43: pH: electroless 10C open

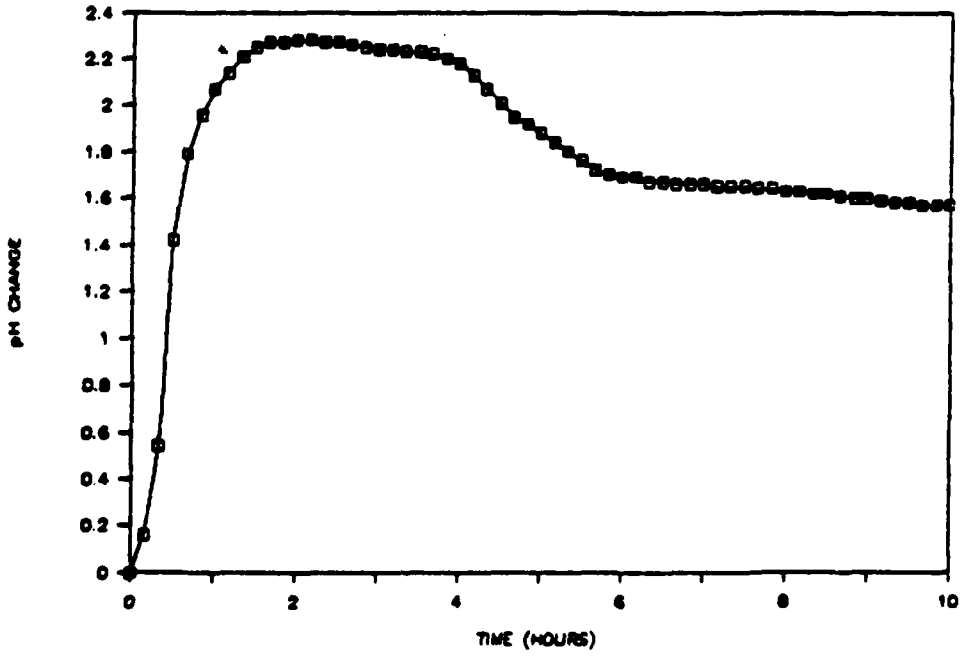

Figure 44: pH: electroless 3C closed

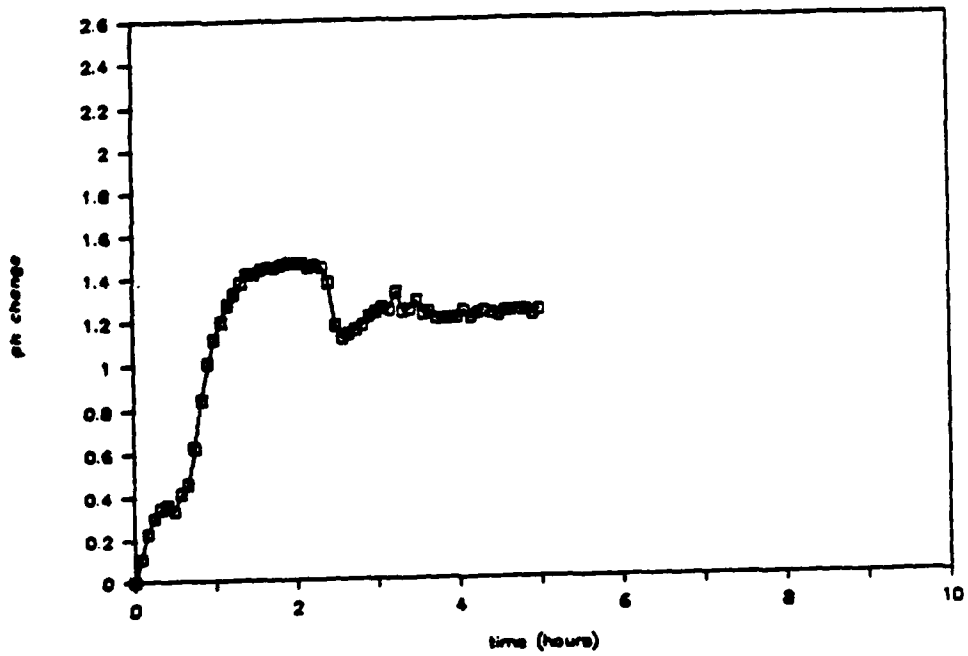

Figure 45: pH: electroplate 45C closed

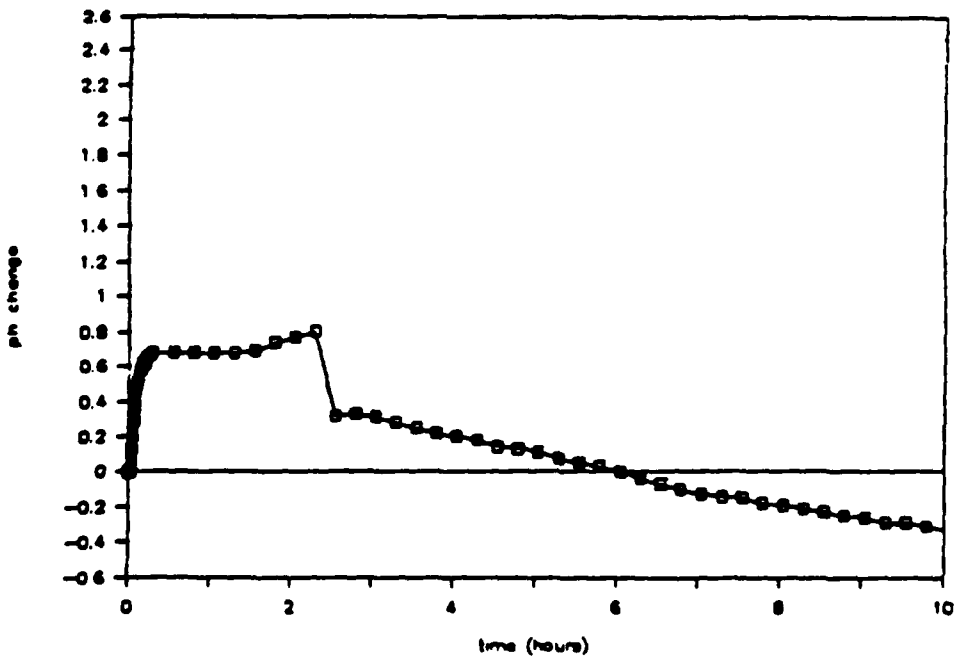

Figure 46: pH: electroplate 45C open

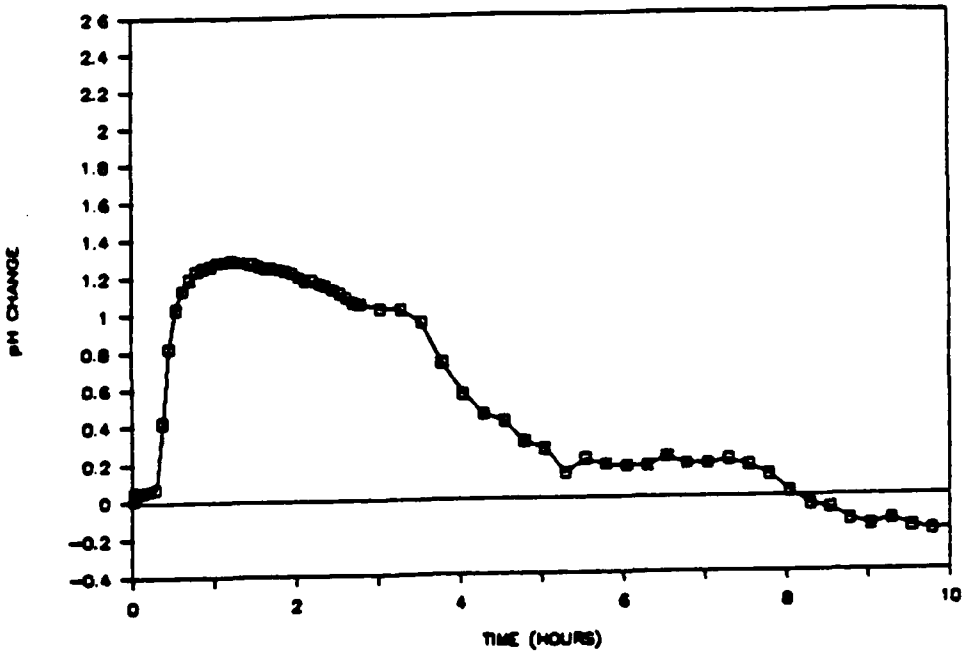

Figure 47: pH: electroplate 10C open

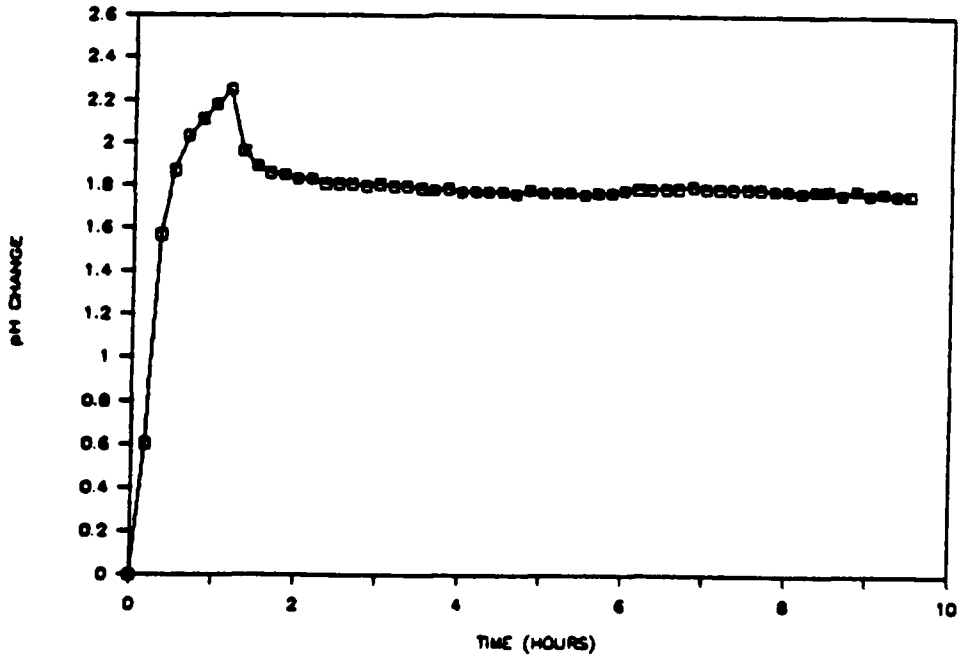

Figure 48: pH: electroplate 3C closed

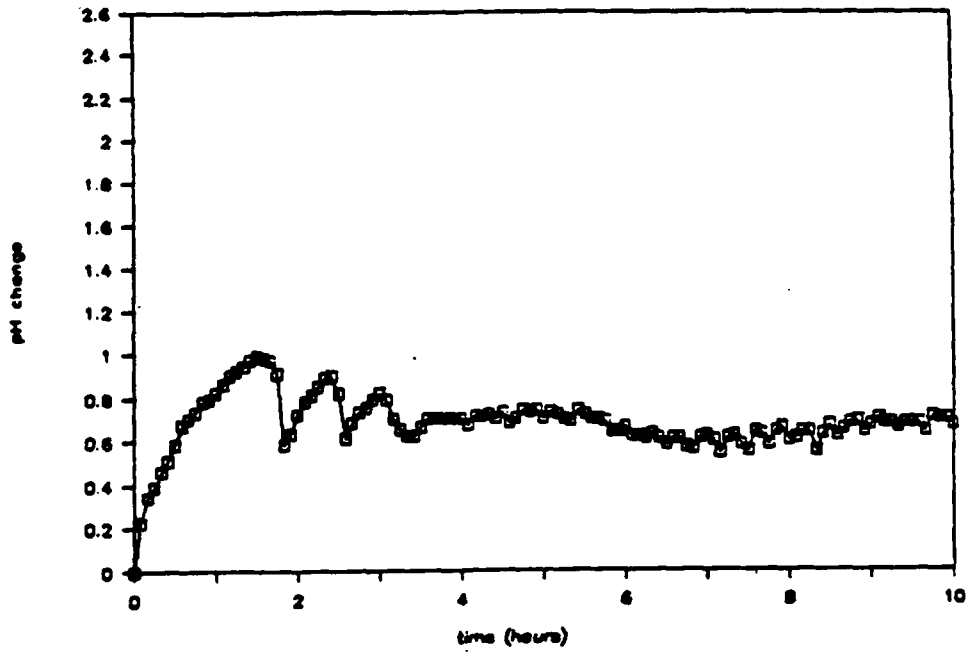

Figure 49: pH: evaporate 45C closed

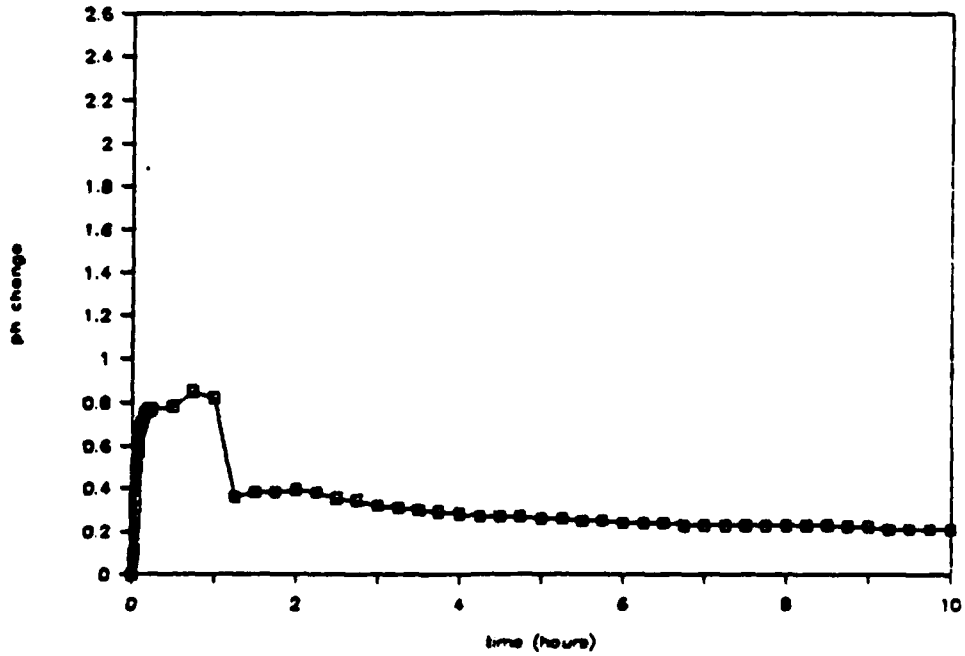

Figure 50: pH: evaporate 45C open

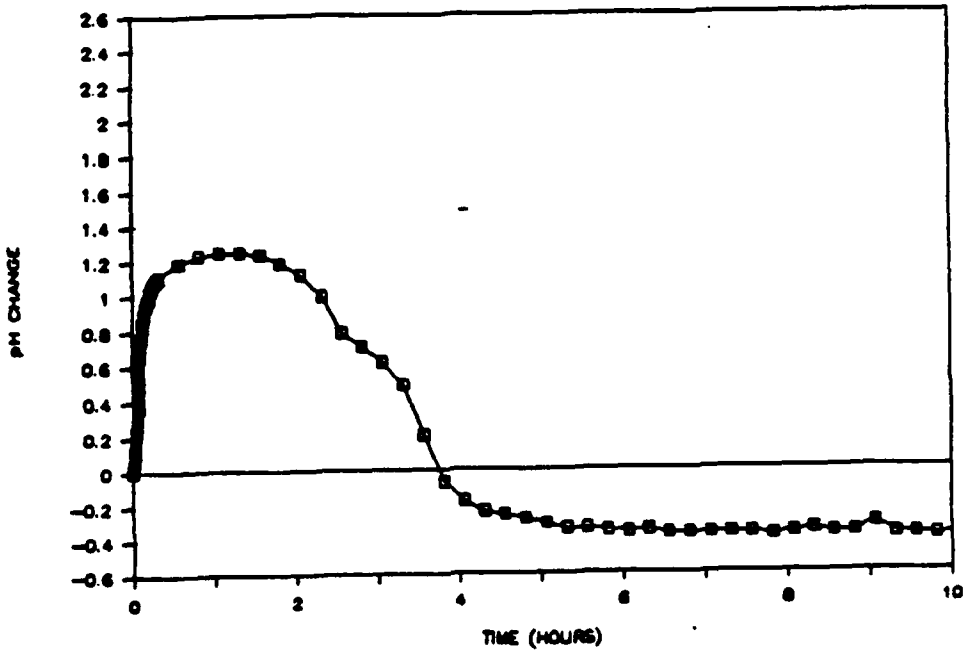

Figure 51: pH: evaporate 10C open

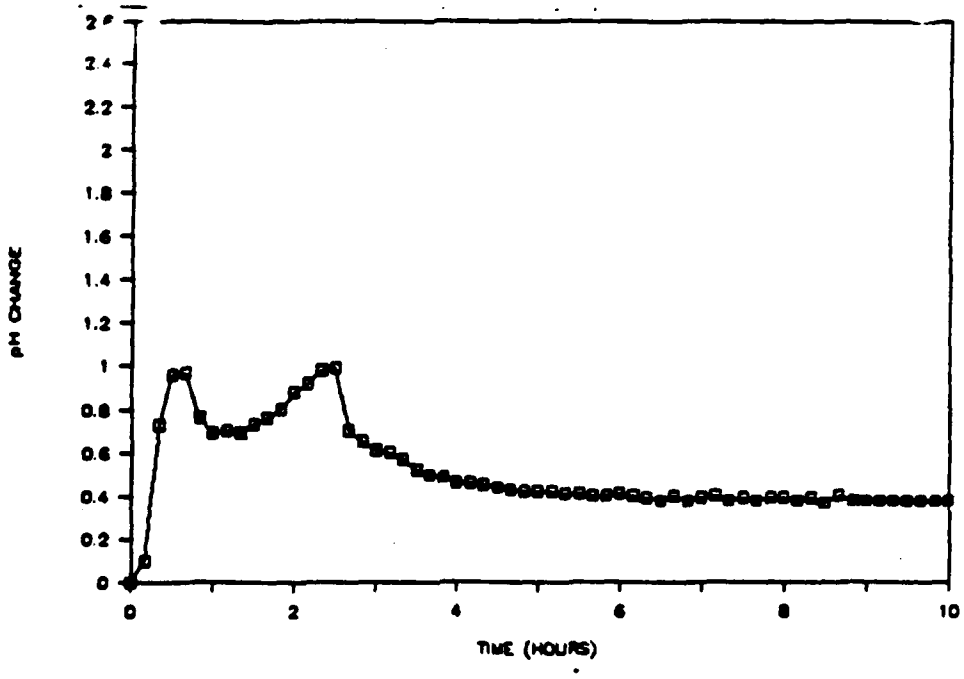

Figure 52: pH: evaporate 45C closed no light

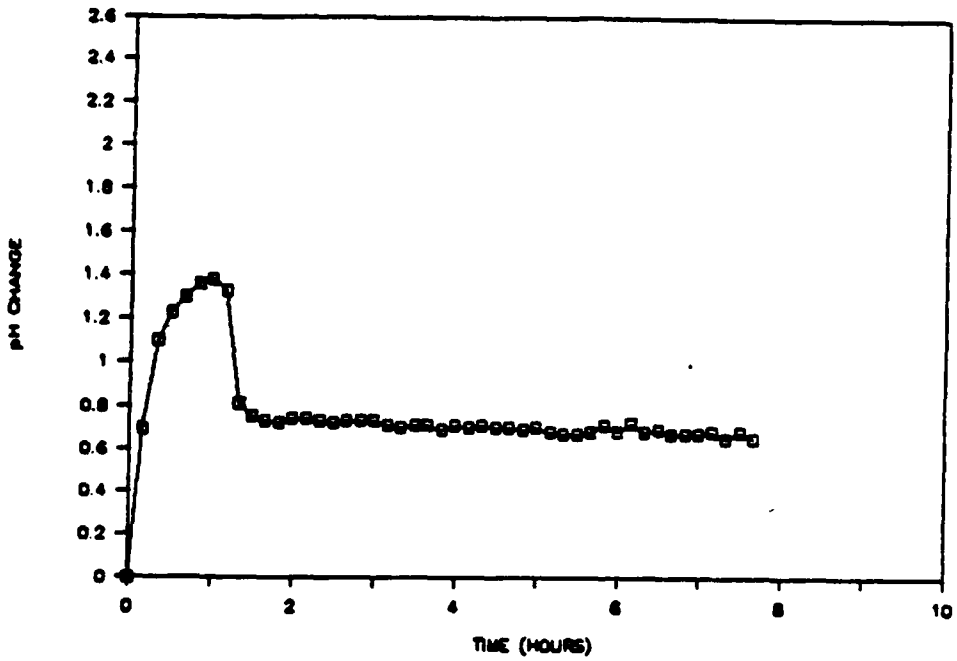

Figure 53: pH: evaporate 20C closed

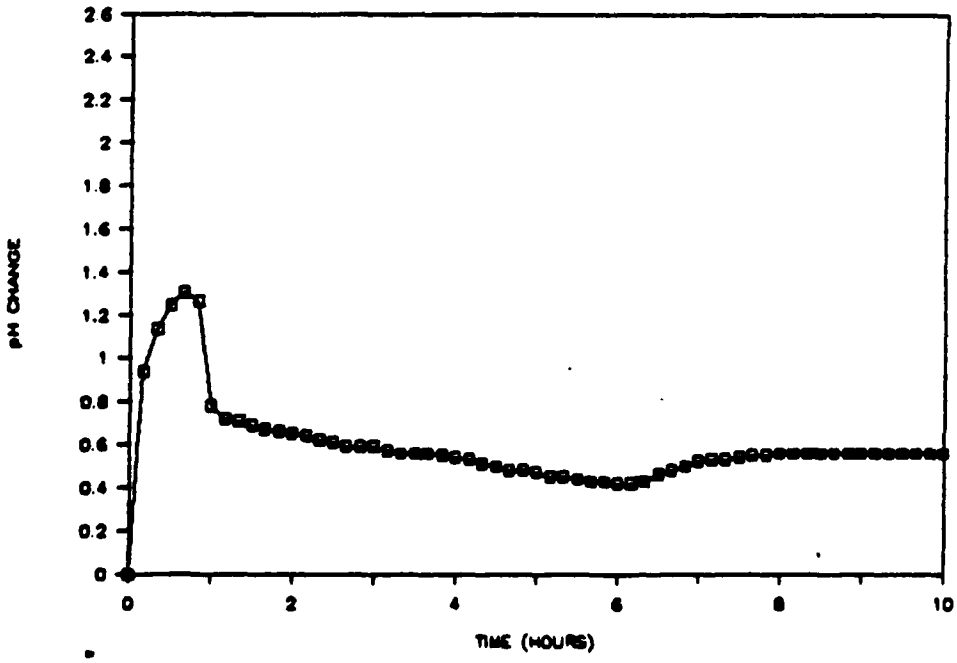

Figure 54: pH: evaporate 20C open

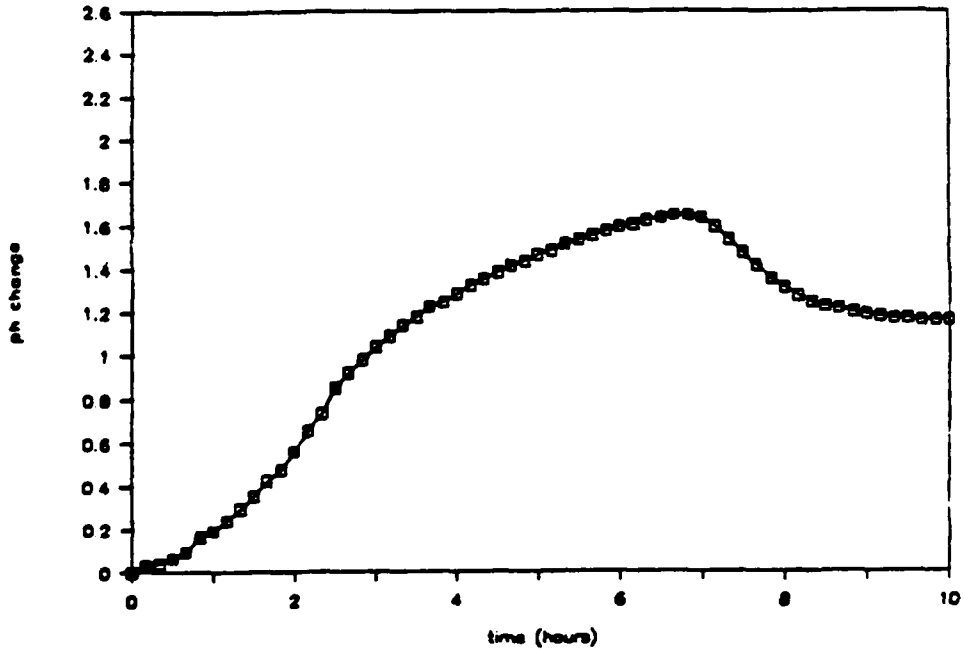

Figure 55: pH: evaporate 3C closed

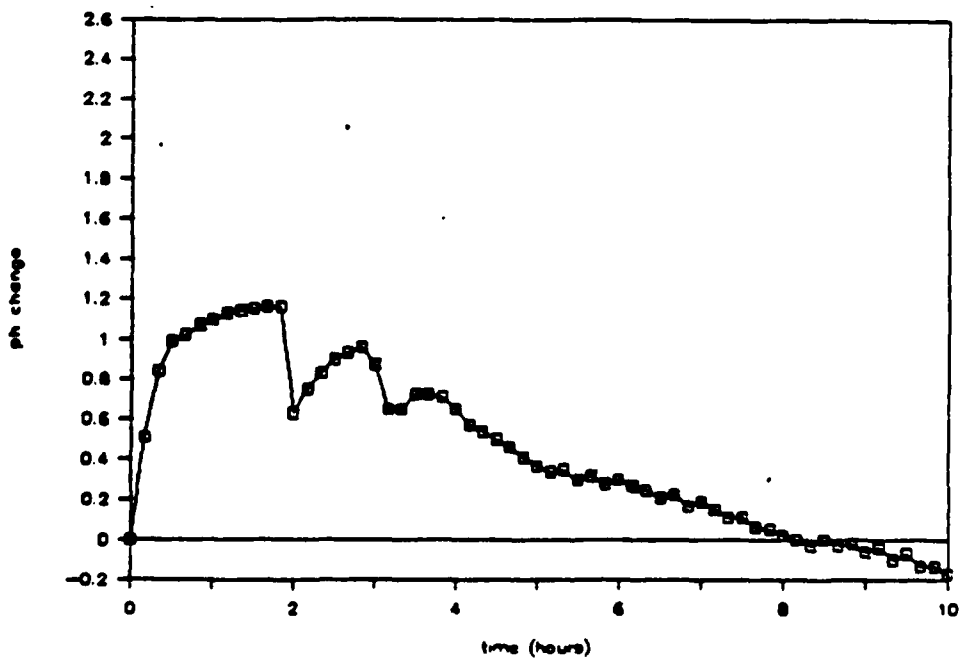

Figure 56: pH: sputter 45C closed

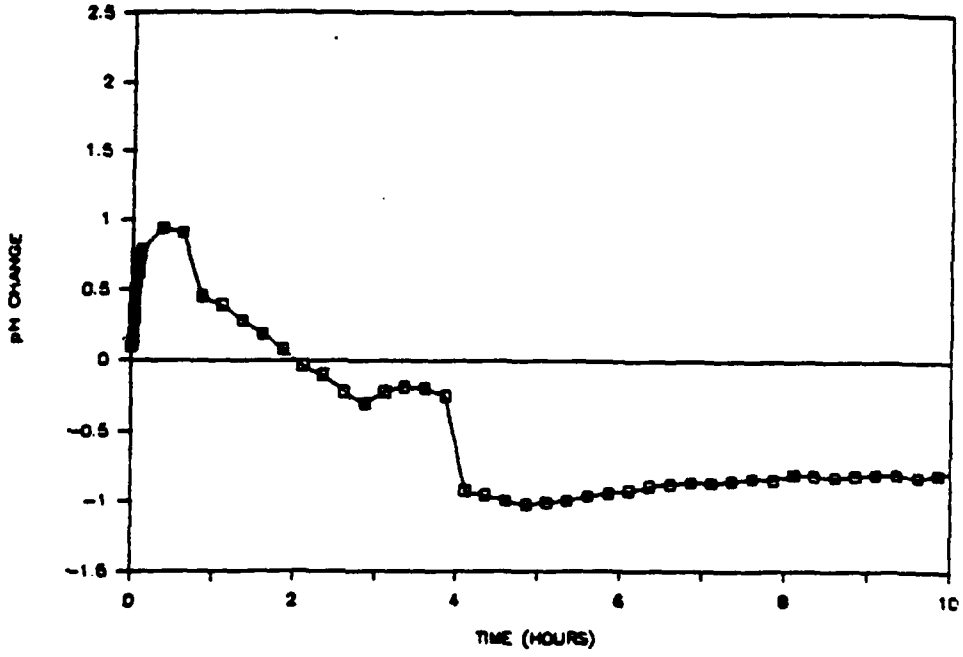

Figure 57: pH: sputter 45C open

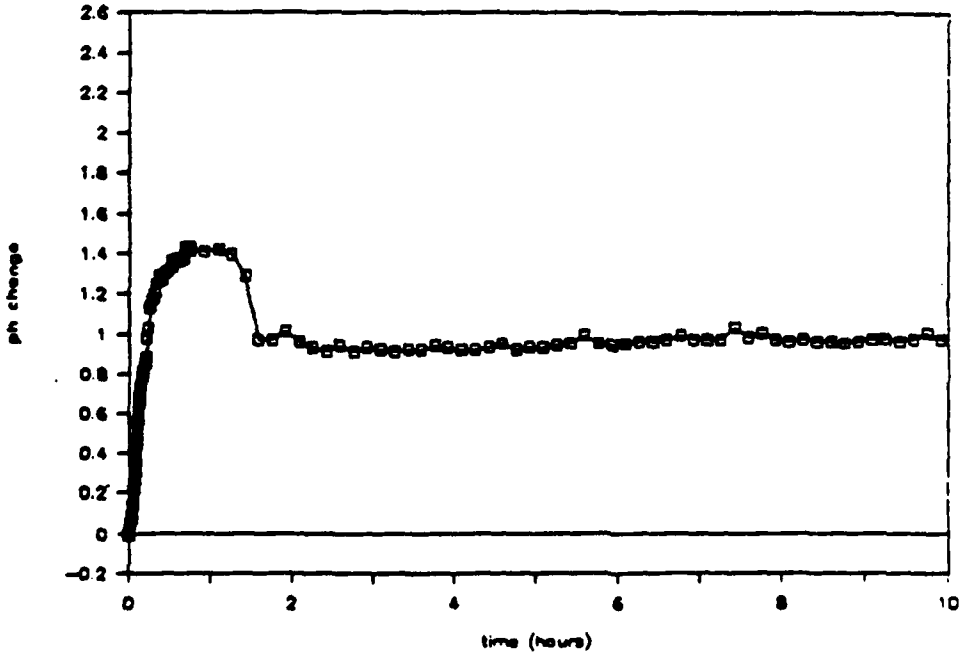

Figure 58: pH: sputter 10C open

Figure 59: SEM: electroless short etch

Figure 60: SEM: electroplate short etch

Figure 61: SEM: evaporate short etch

Figure 62: SEM: evaporate short etch

Figure 63: SEM: electroless short etch

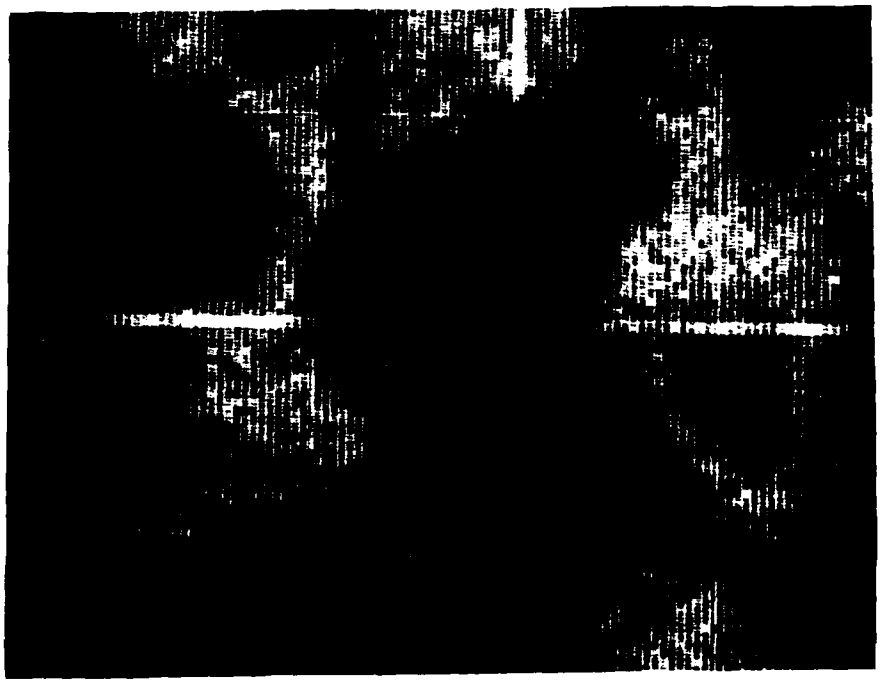

Figure 64: AES MAP: electroless short etch - chlorine

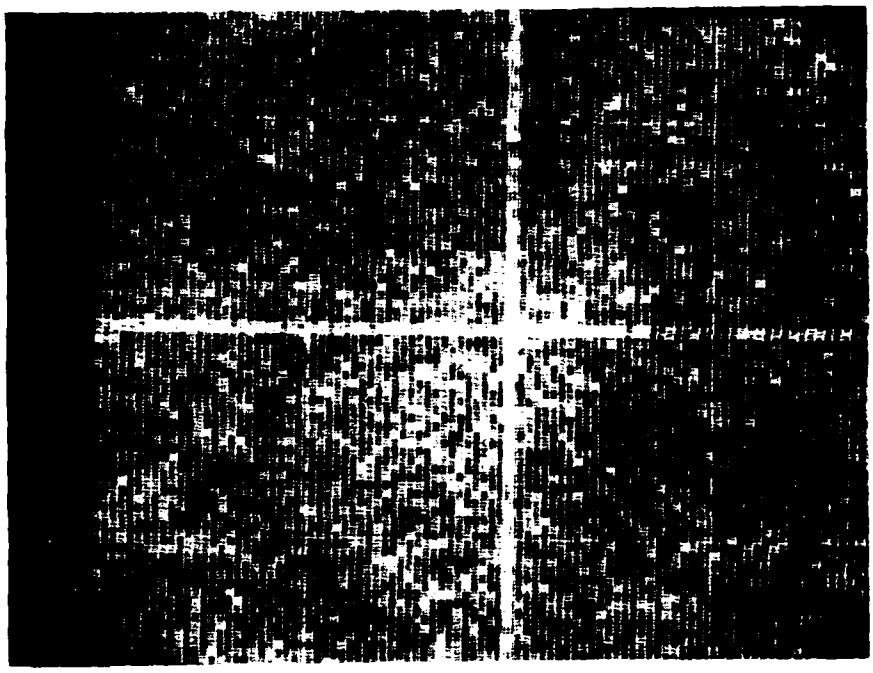

Figure 65: AES MAP: electroless short etch - copper

Figure 66: AES MAP: electroless short etch - oxygen

Figure 67: SEM: electroplate short etch

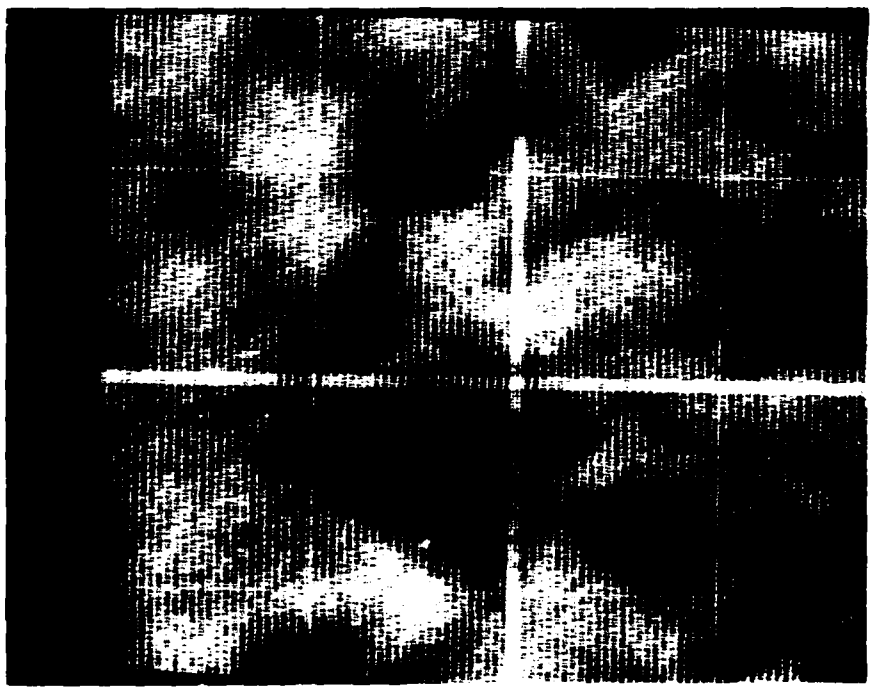

Figure 68: AES MAP: electroplate short etch - chlorine

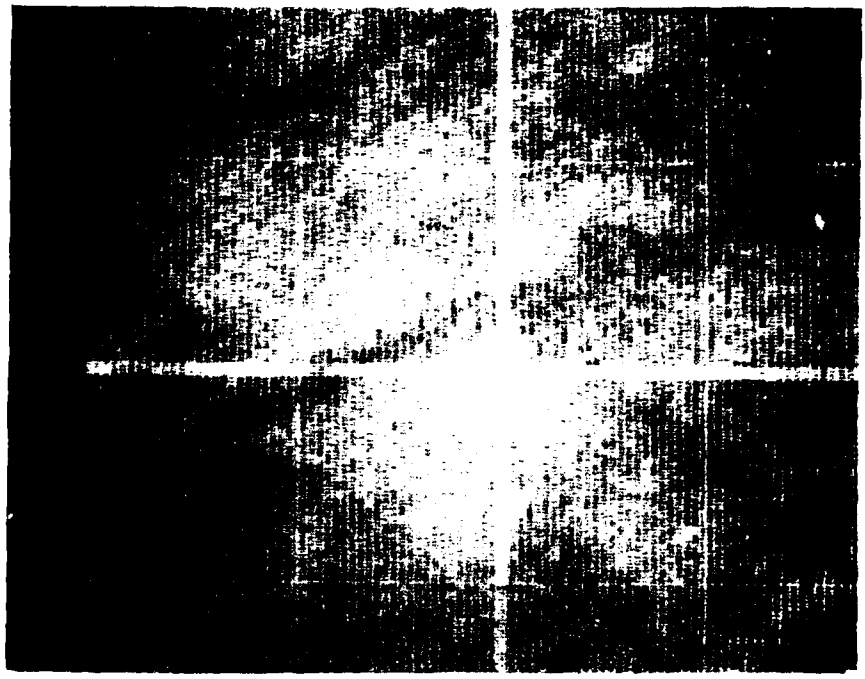

Figure 69: AES MAP: electroplate short etch - copper

Figure 70: AES MAP: electroplate short etch - oxygen

Figure 71: AES MAP: electroplate short etch - carbon

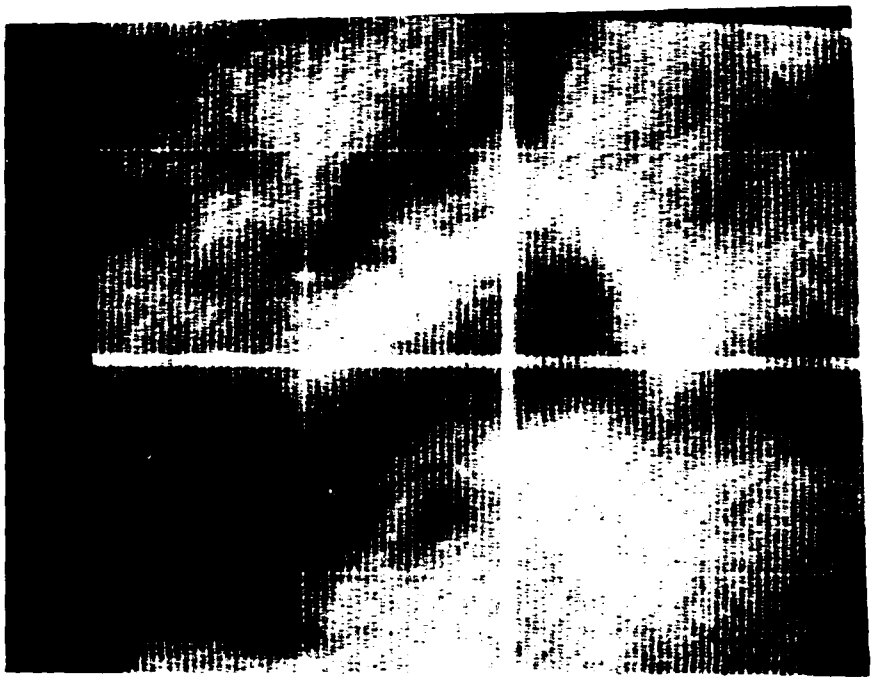

Figure 72: AES MAP: evaporate short etch - chlorine

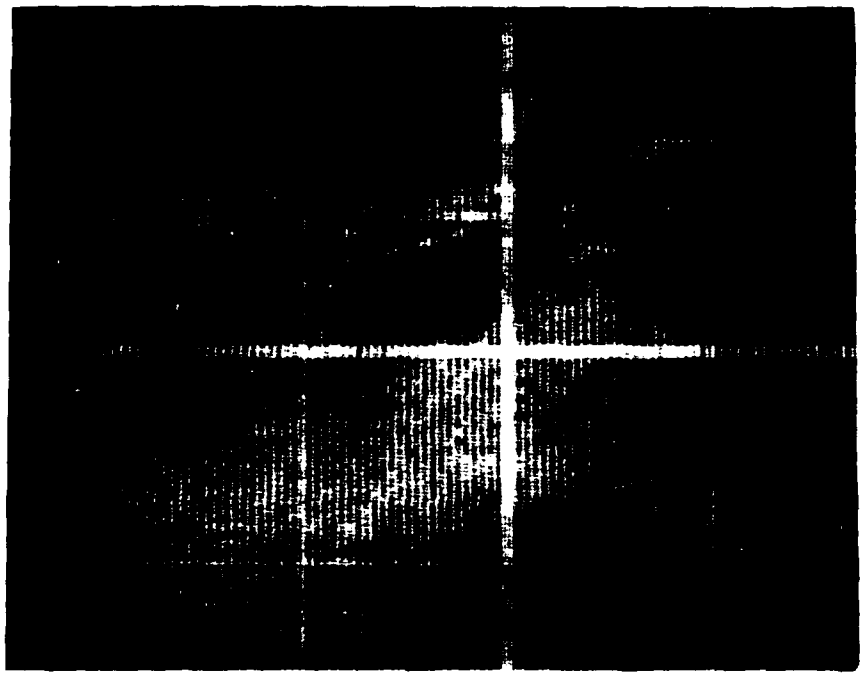

Figure 73: AES MAP: evaporate short etch - copper

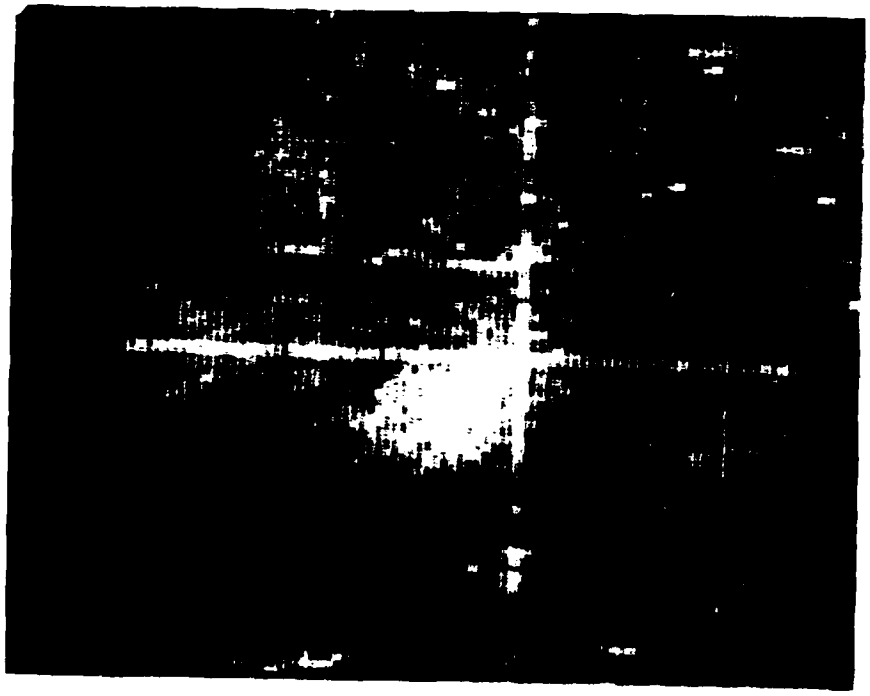

Figure 74: AES MAP: evaporate short etch - oxygen

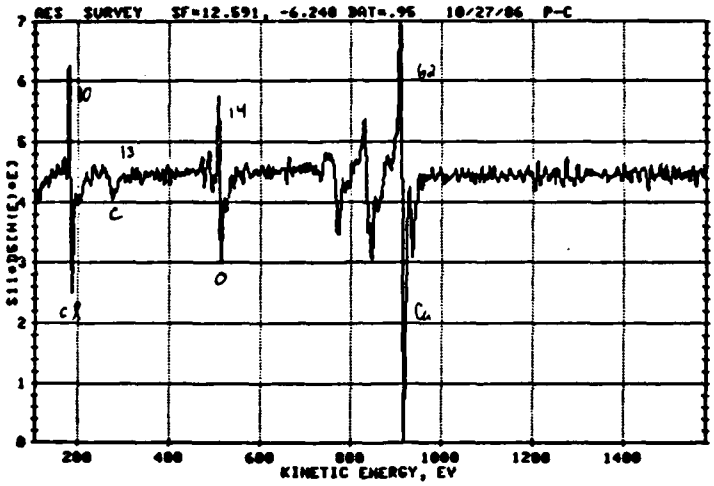

Figure 75: AES: electroless short etch

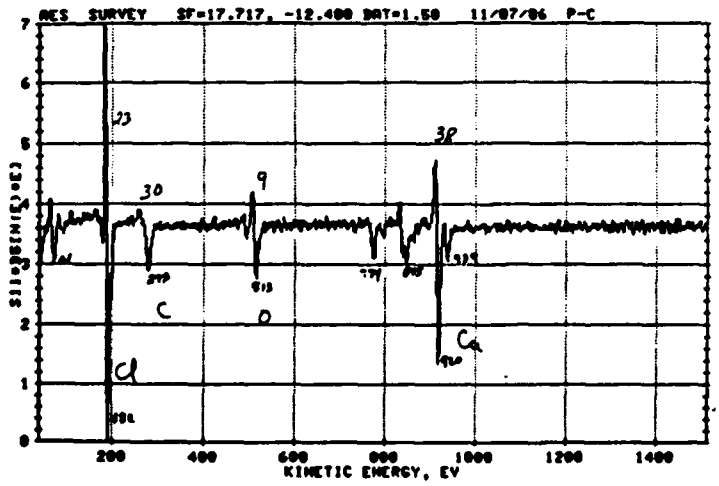

Figure 76: AES: electroplate short etch

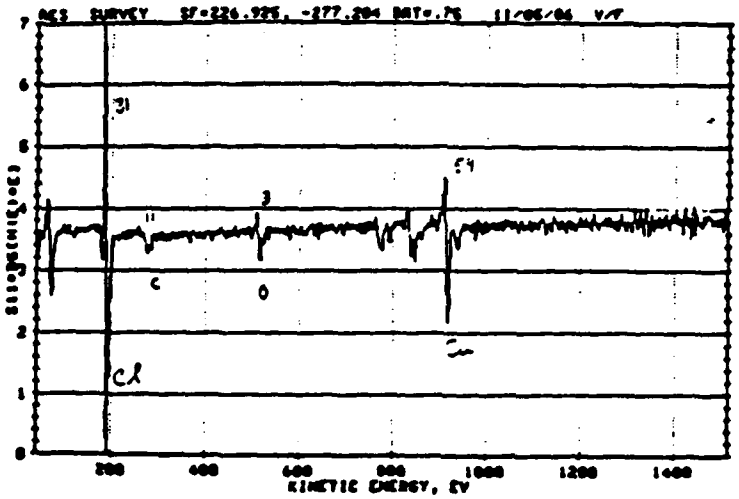

Figure 77: AES: evaporate short etch

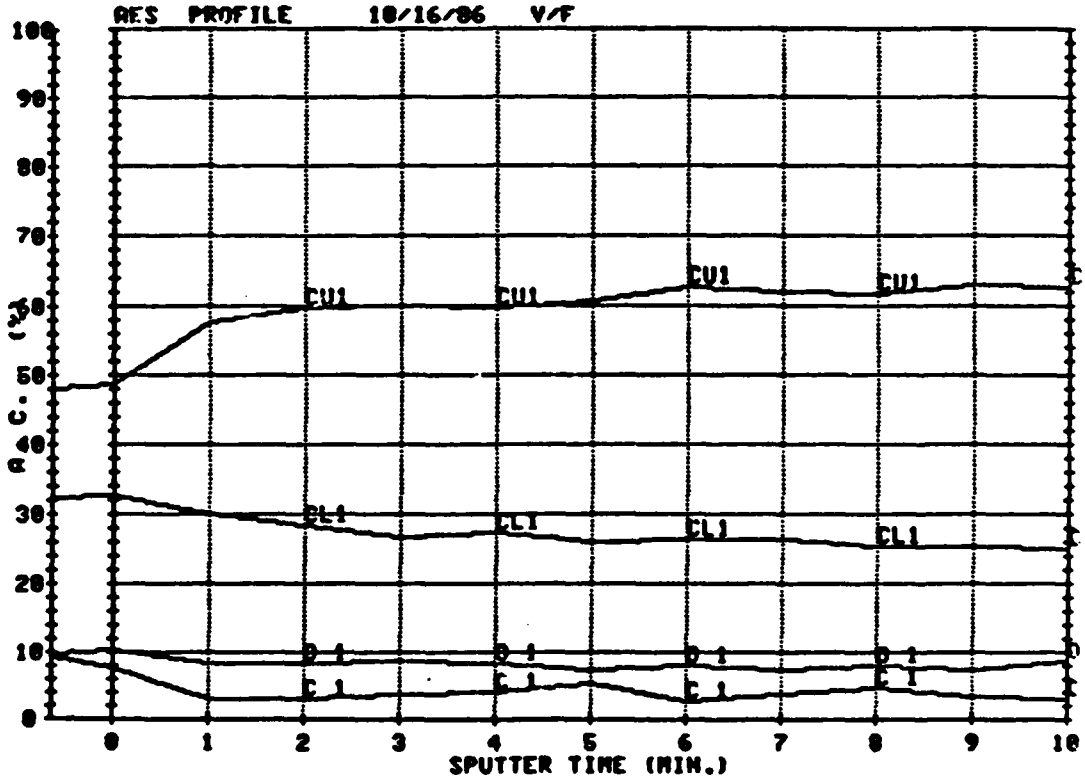

Figure 78: ADP: electroless 45C short etch

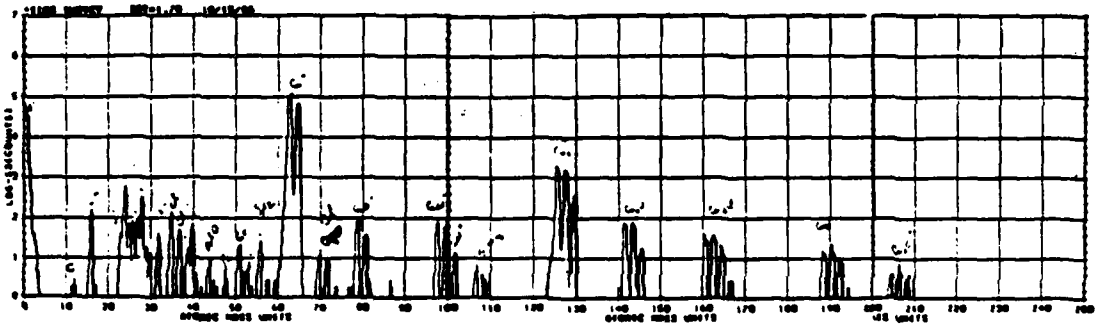

Figure 79: SIMS: electroless short etch

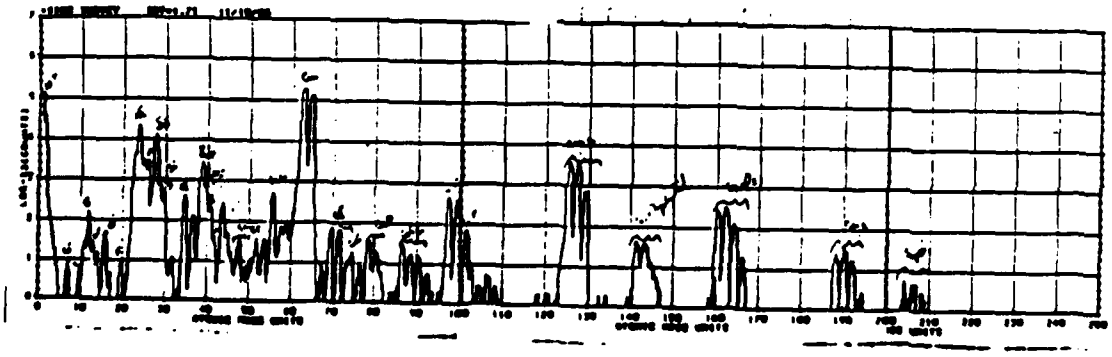

Figure 80: SIMS: electroplate short etch

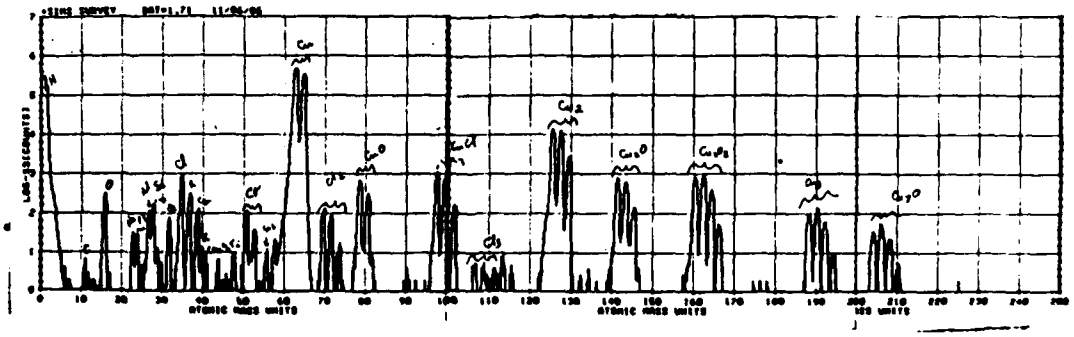

Figure 81: SIMS: evaporate short etch

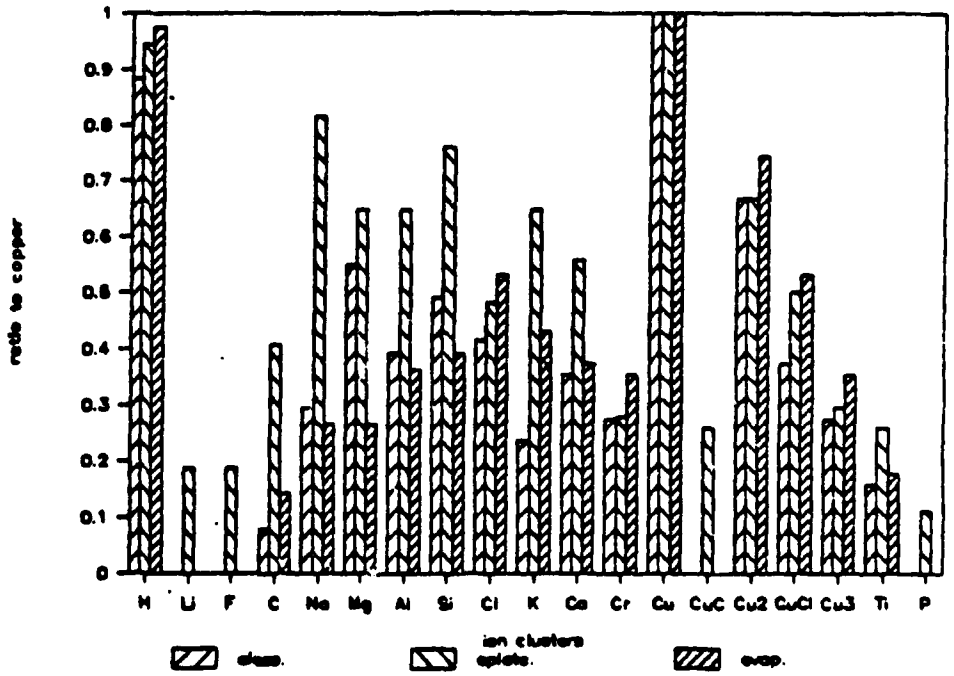

Figure 82: SIMS: comparison short etch

Figure 83: SEM: electroless long etch

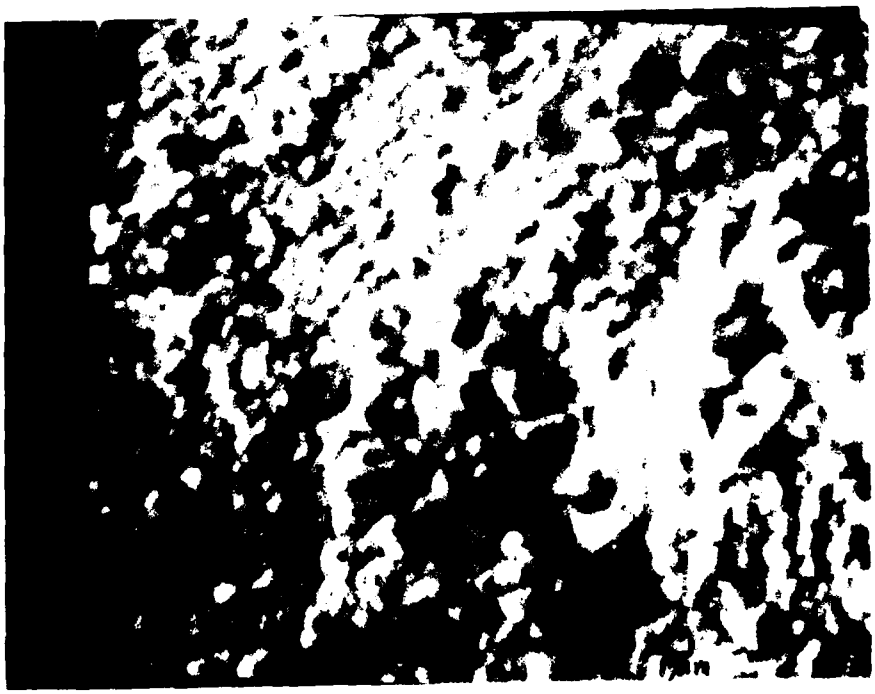

Figure 84: SEM: electroplate long etch

Figure 85: SEM: electroplate long etch

Figure 86: SEM: evaporate long etch

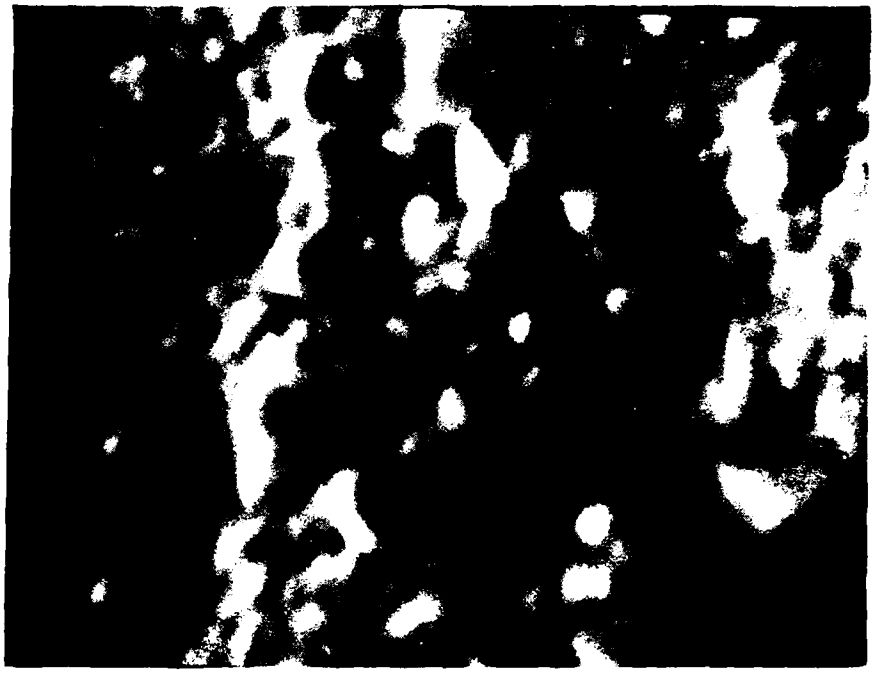

Figure 87: SEM: electroplate long etch

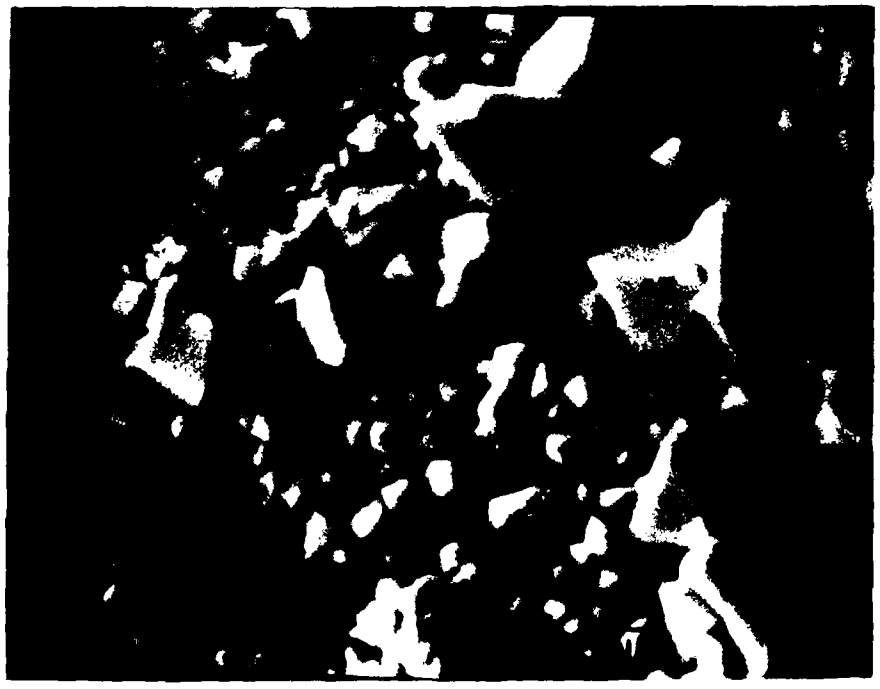

Figure 88: SEM: sputter long etch

Figure 89: SEM: electroless long etch

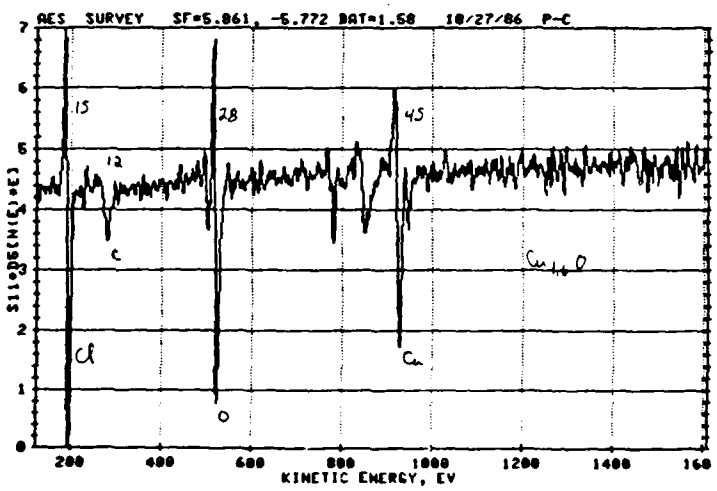

Figure 90: AES: electroless long etch

Figure 91: SEM: electroless long etch

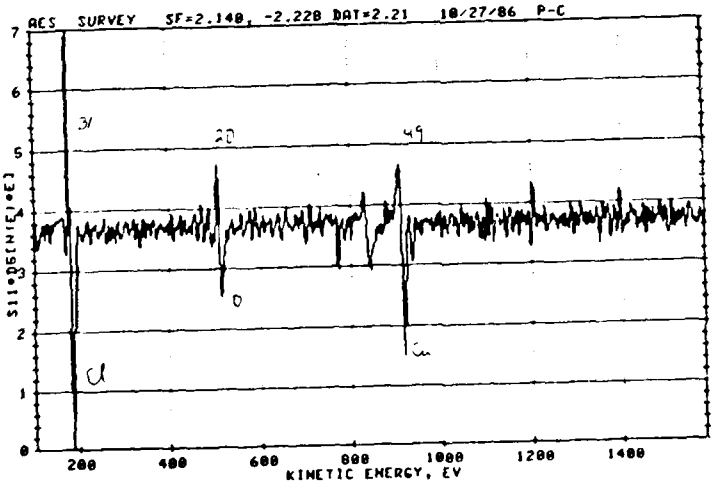

Figure 92: AES: electroless long etch point 1

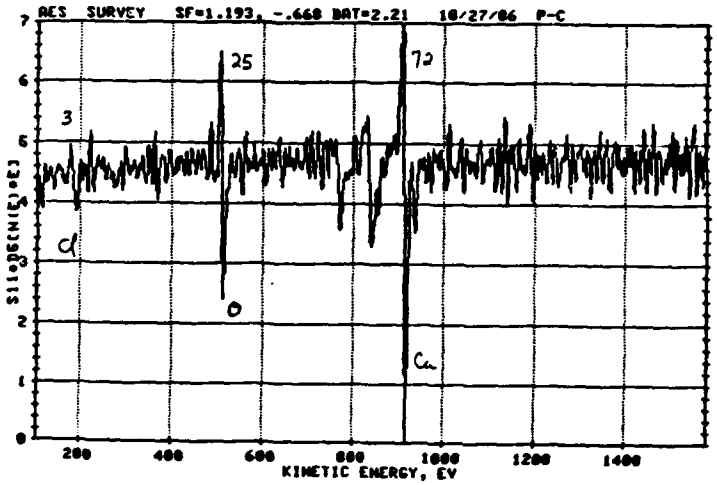

Figure 93: AES: electroless long etch point 2

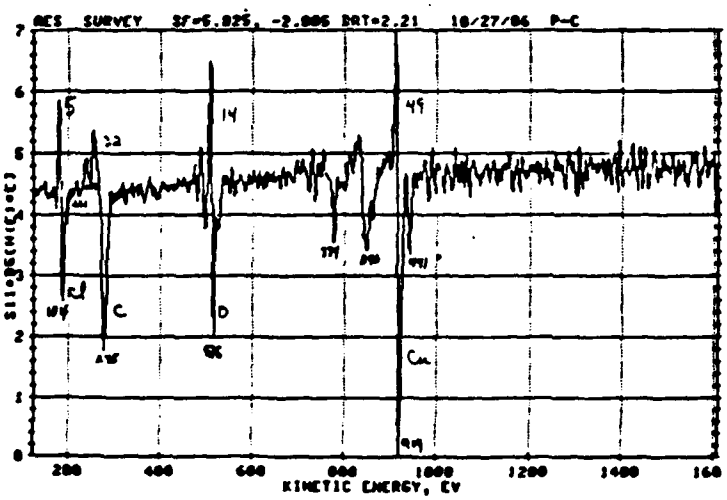

Figure 94: AES: electroless long etch

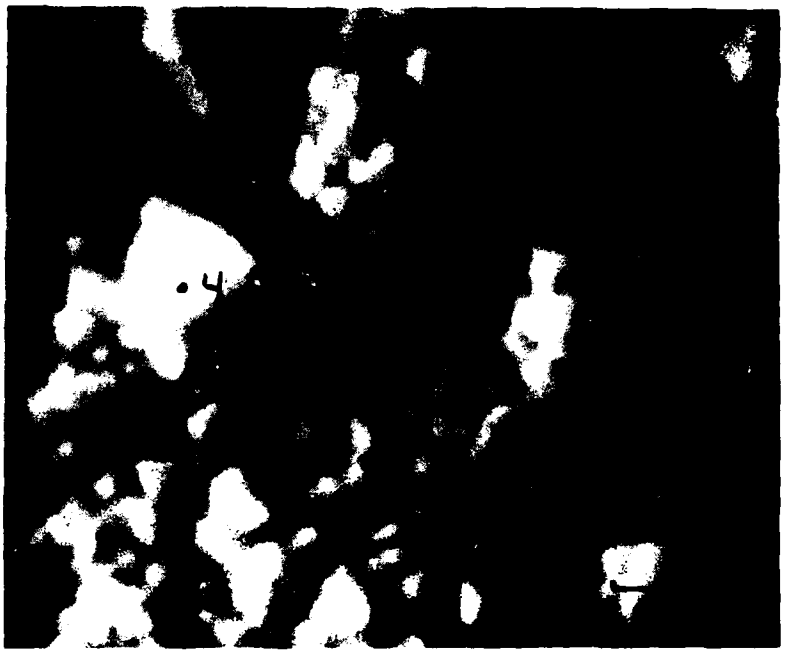

Figure 95: SEM: electroplate long etch

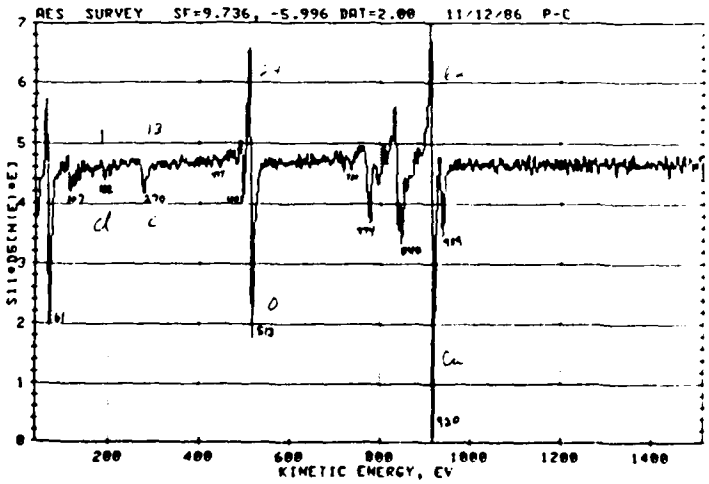

Figure 96: AES: electroplate long etch (area survey)

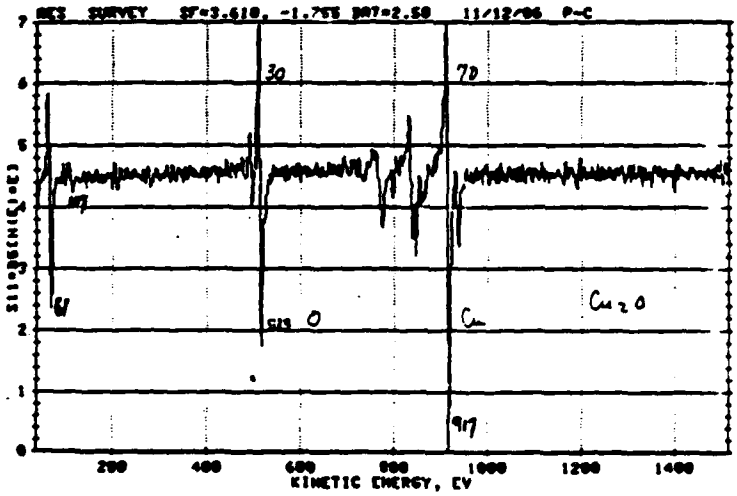

Figure 97: AES: electroplate long etch at point 1

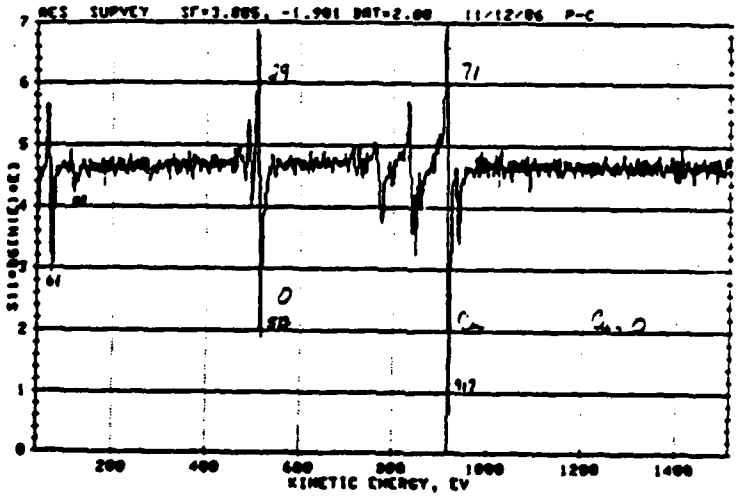

Figure 98: AES: electroplate long etch at point 2

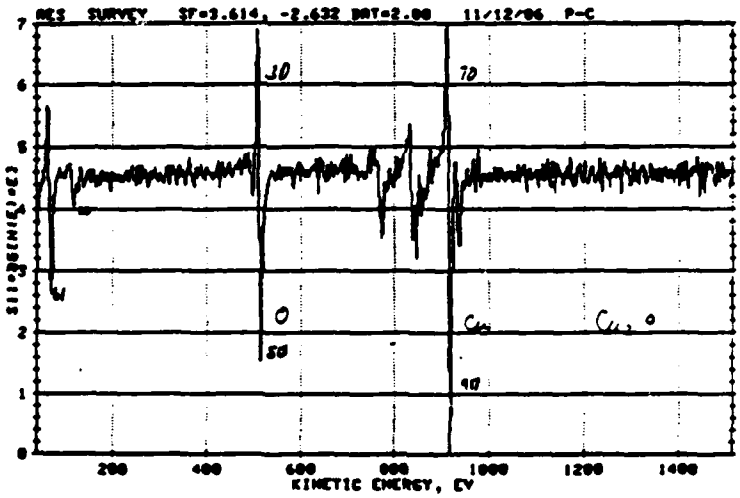

Figure 99: AES: electroplate long etch at point 3

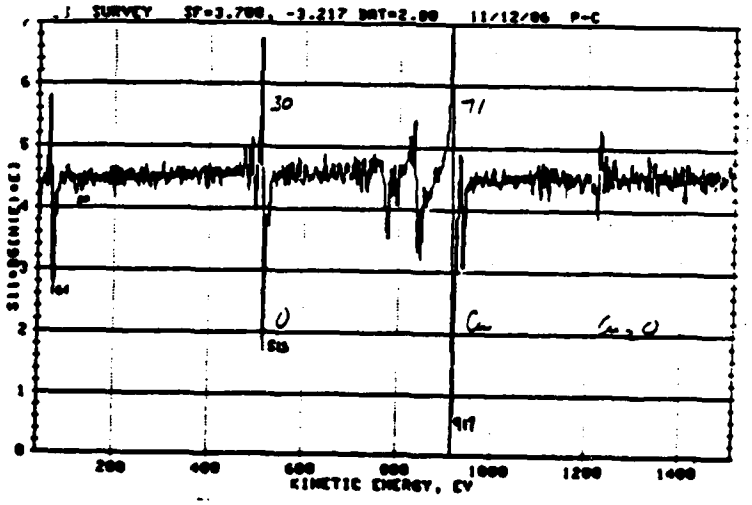

Figure 100: AES: electroplate long etch at point 4

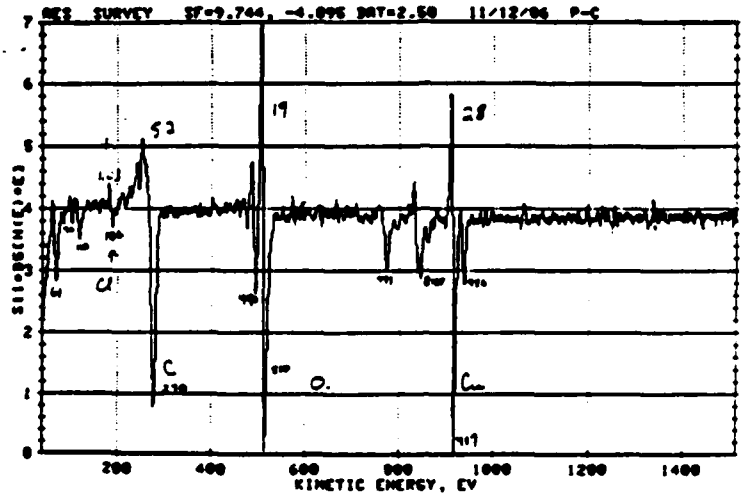

Figure 101: AES: electroplate long etch at center

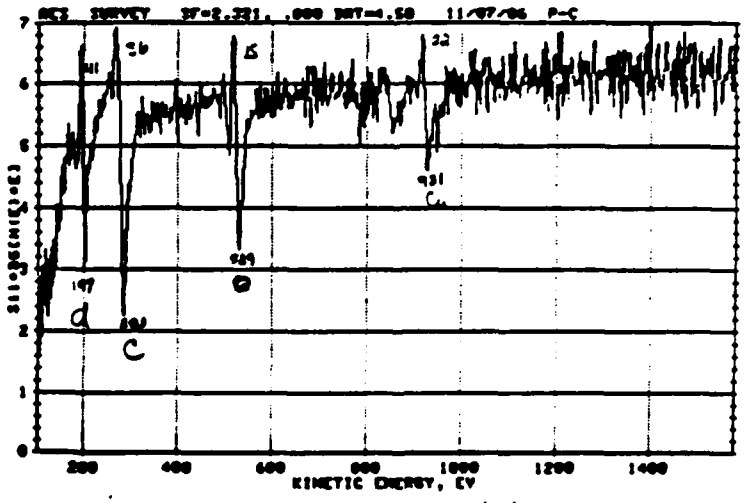

Figure 102: AES: evaporate long etch

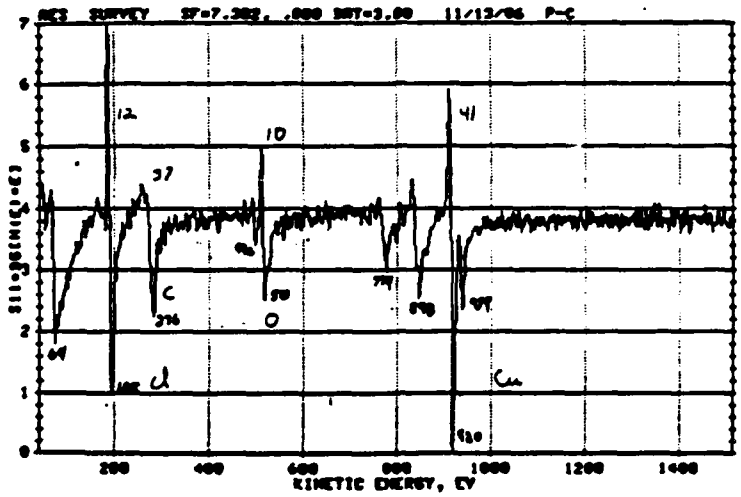

Figure 103: AES: sputter long etch

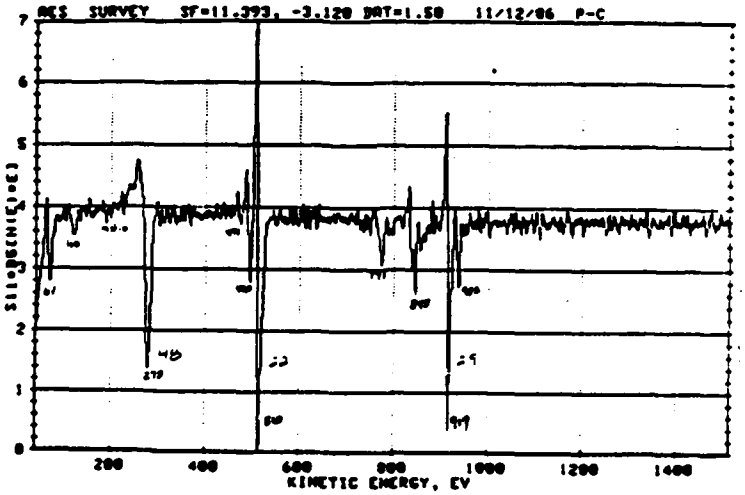

Figure 104: AES: electroplate long etch

after 0.5 min. ion beam sputter

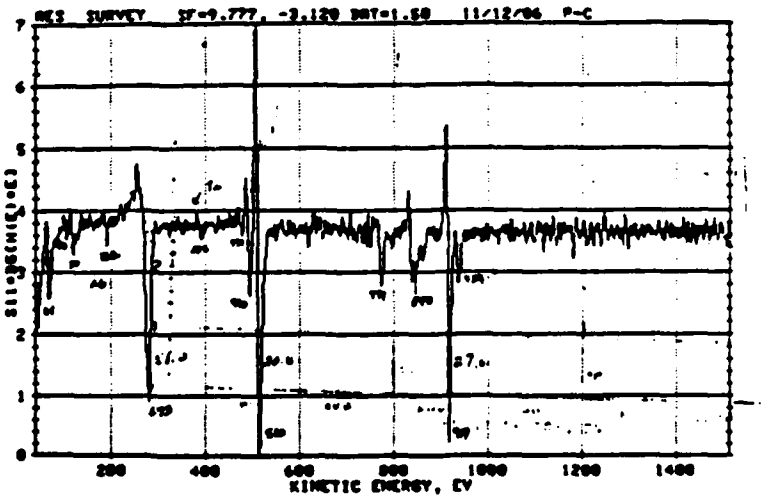

Figure 105: AES: electroplate long etch

after 1.0 min. ion beam sputter

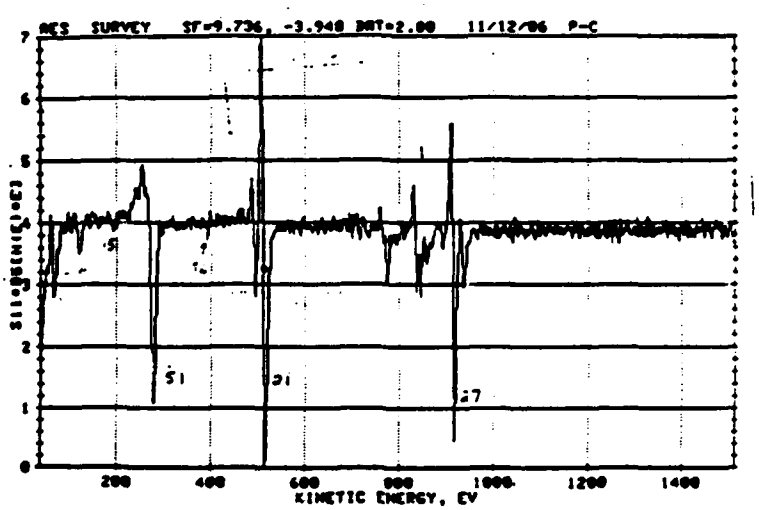

Figure 106: AES: electroplate long etch

after 1.5 min. ion beam sputter

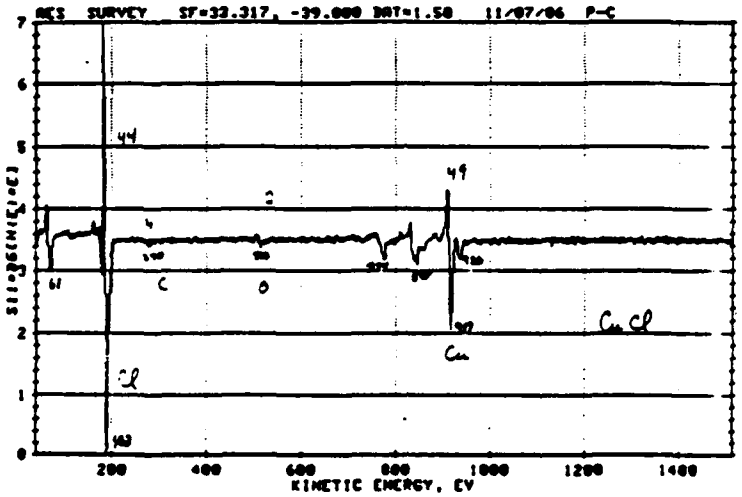

Figure 107: AES: evaporate long etch

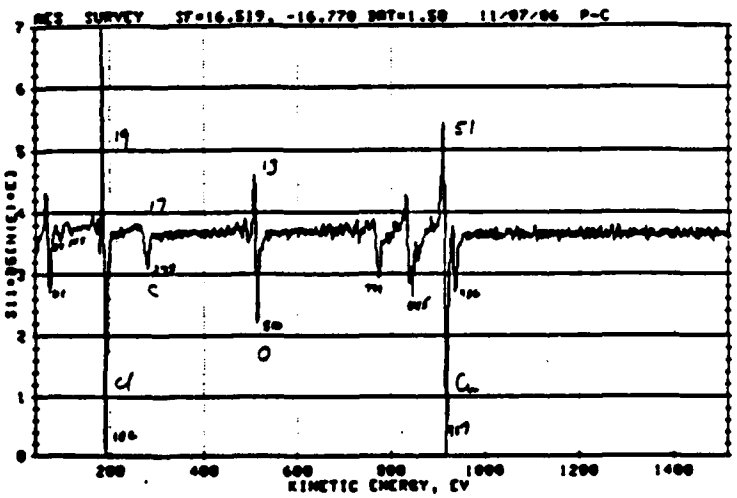

Figure 108: AES: evaporate long etch

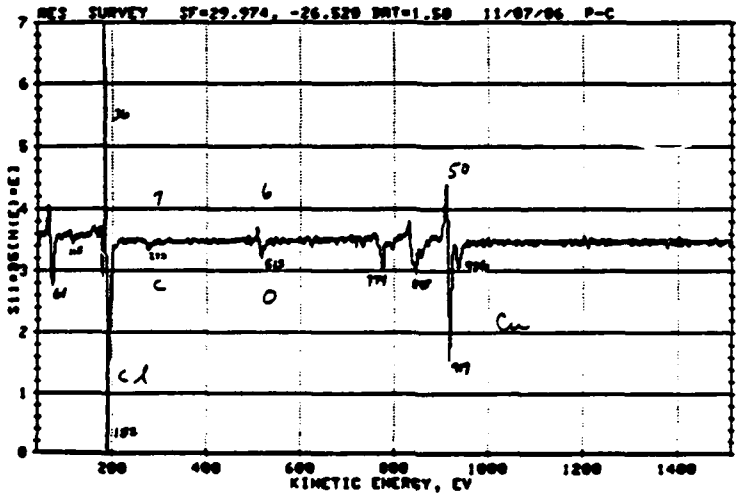

Figure 109: AES: evaporate long etch

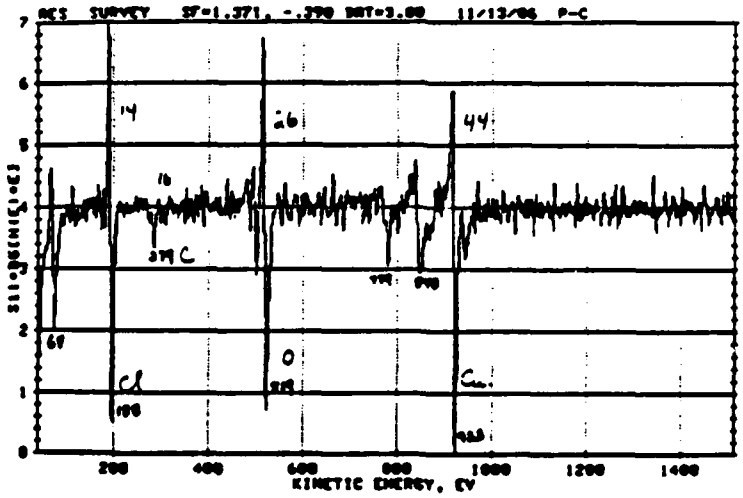

Figure 110: AES: sputter long etch at point 1

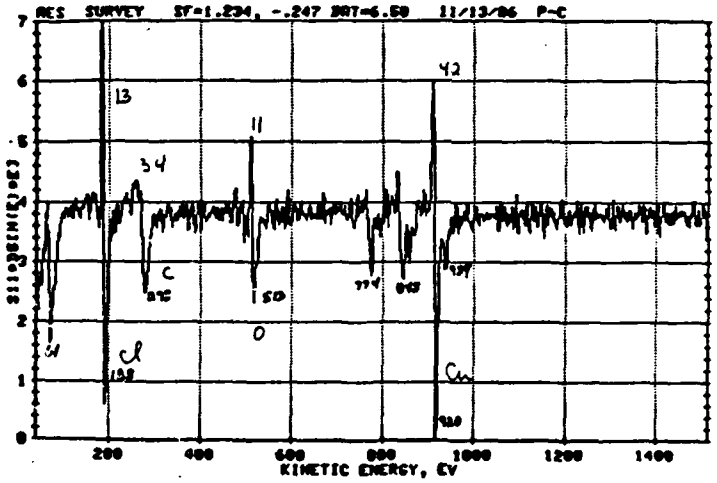

Figure 111: AES: sputter long etch at point 2

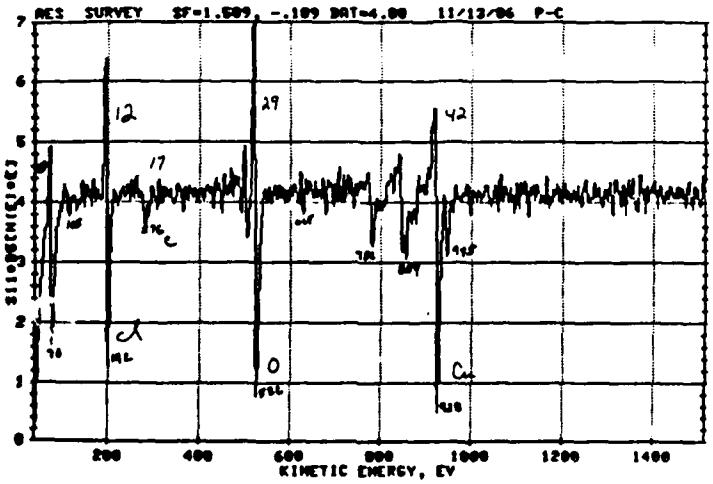

Figure 112: AES: sputter long etch at point 3

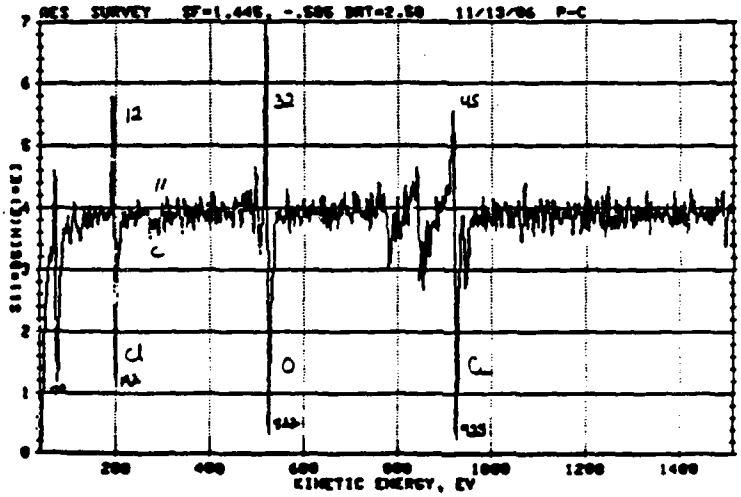

Figure 113: AES: sputter long etch at point 4

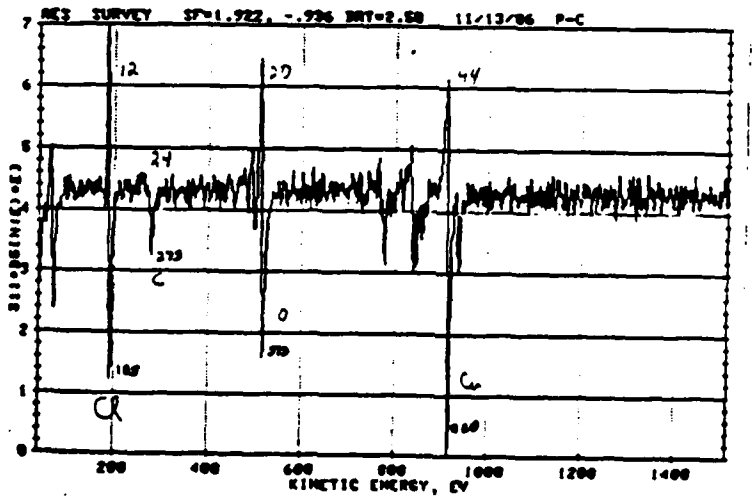

Figure 114: AES: sputter long etch at point 5

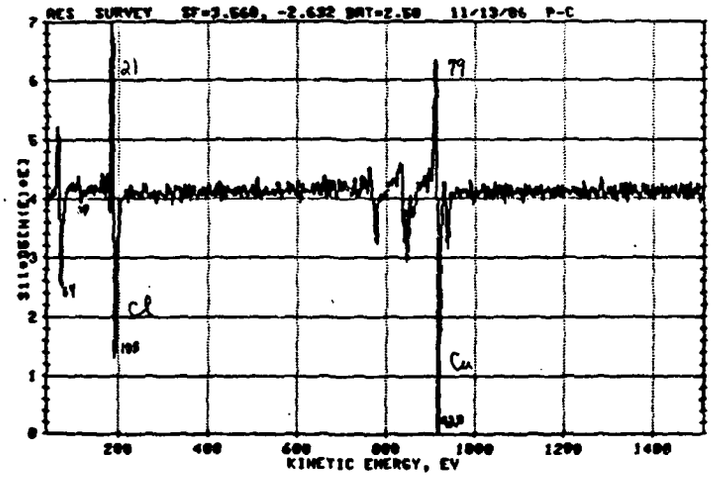

Figure 115: AES: sputter long etch at point 6

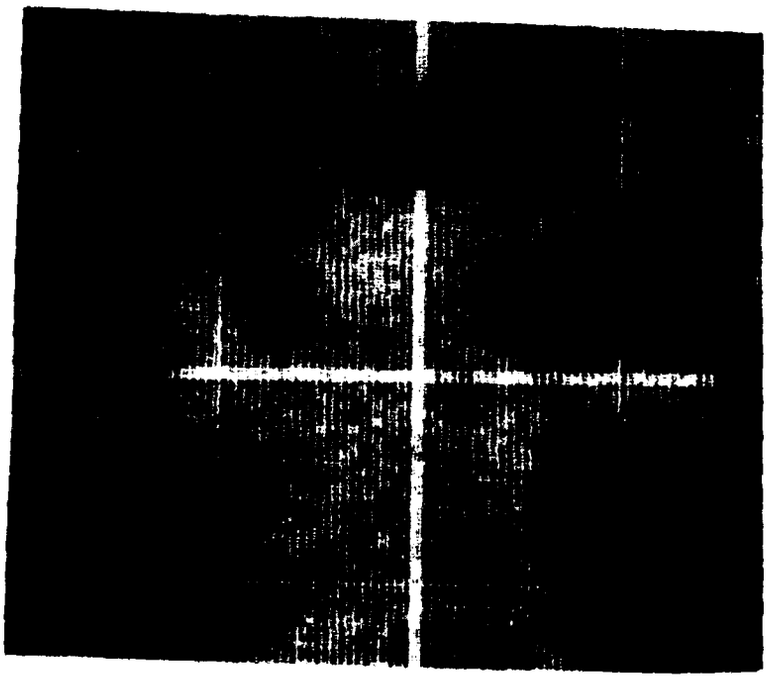

Figure 116: AES MAP: sputter long etch - chlorine

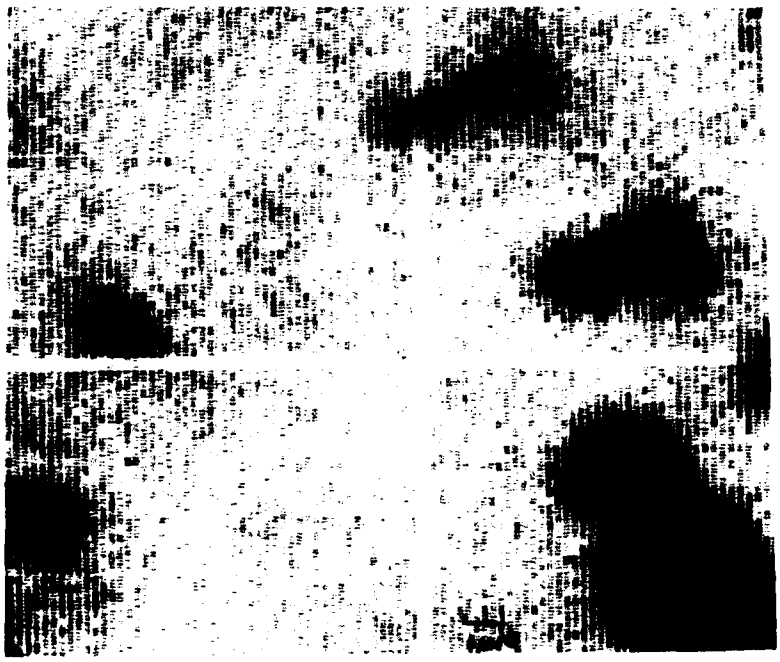

Figure 117: AES MAP: sputter long etch - copper

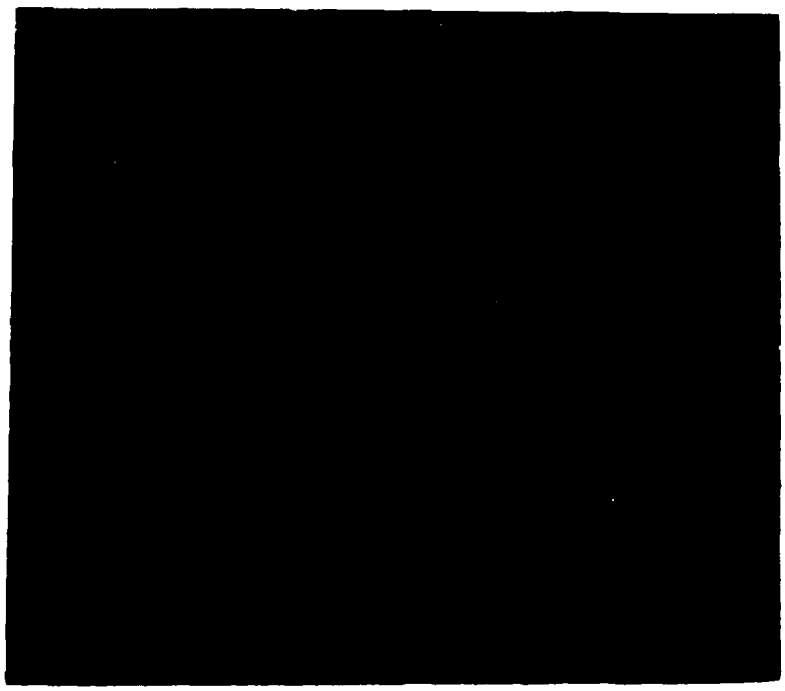

Figure 118: AES MAP: sputter long etch - oxygen

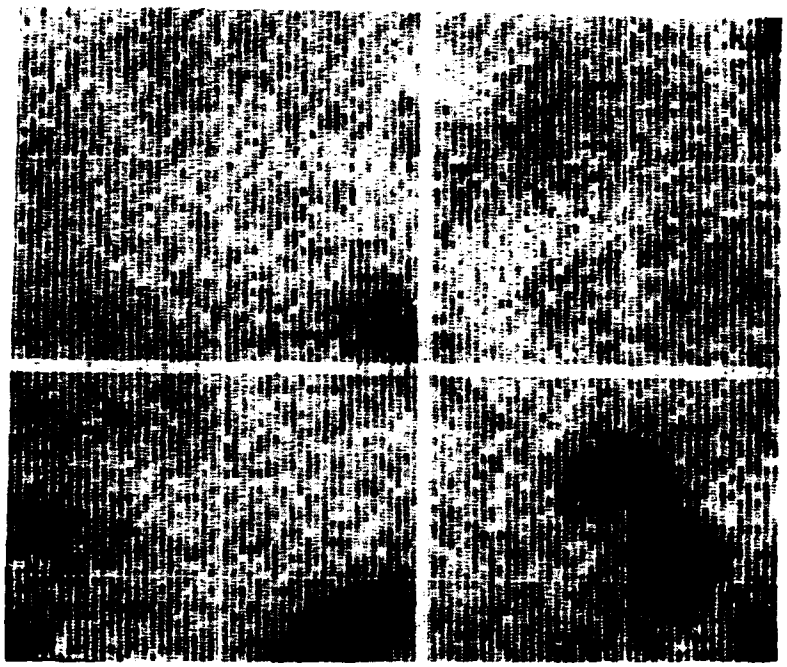

Figure 119: AES MAP: sputter long etch - carbon

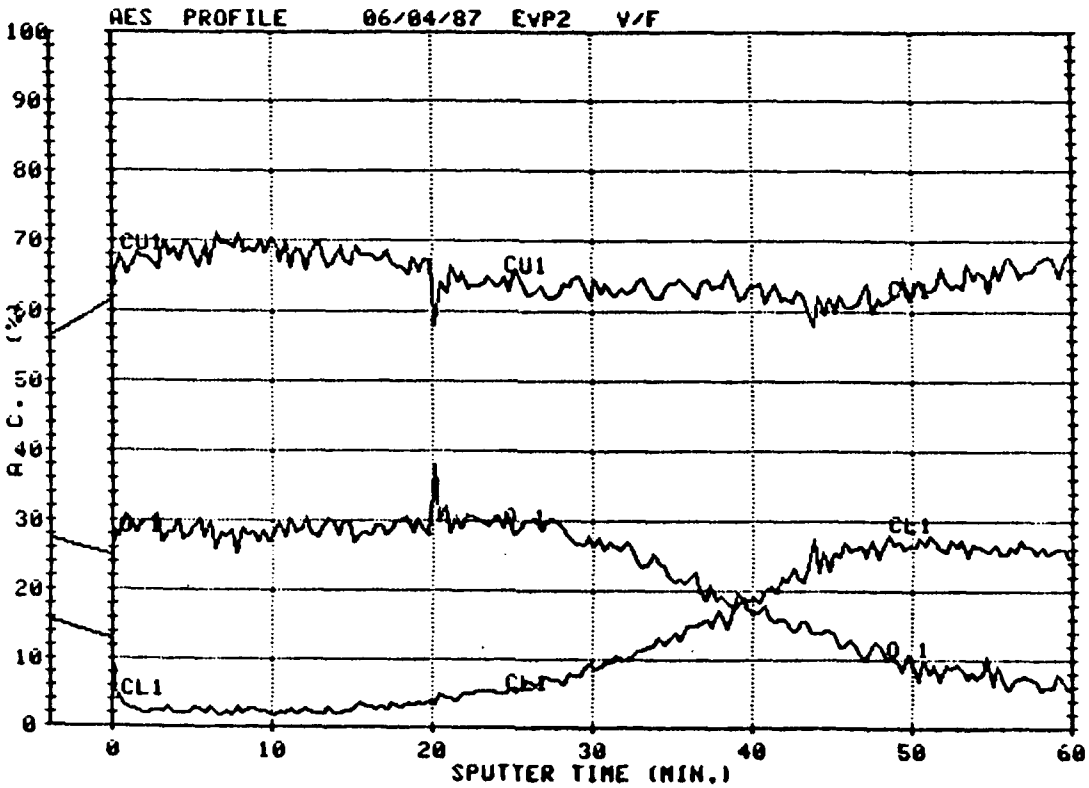

Figure 120: ADP: evaporate long etch 45C closed system

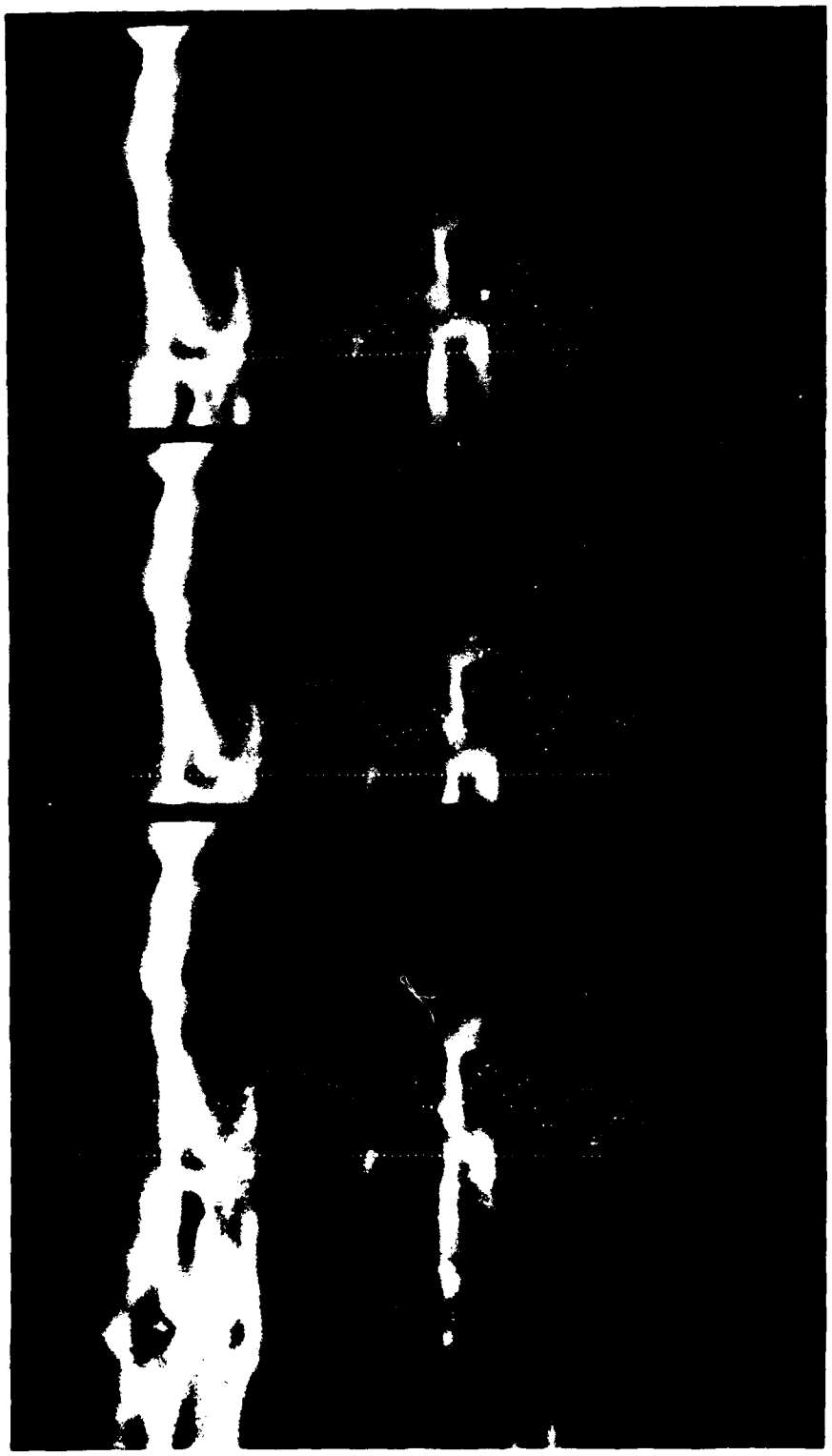

Figure 121: AES: fracture cross-section line profile

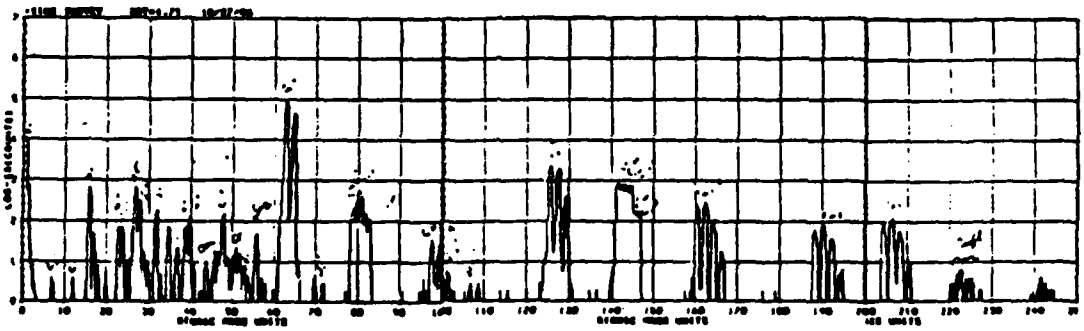

Figure 122: SIMS: electroless long etch

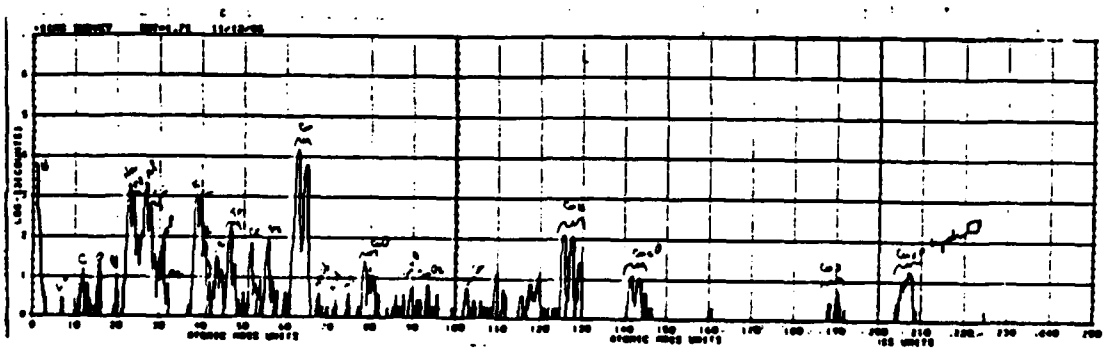

Figure 123: SIMS: electroplate long etch

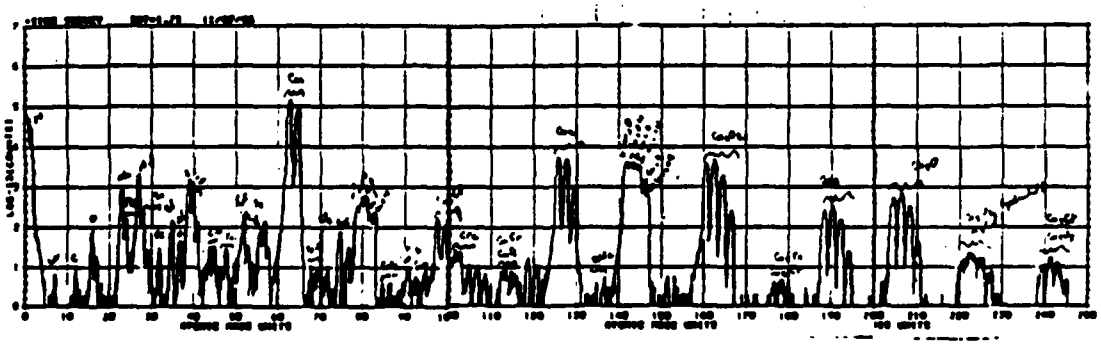

Figure 124: SIMS: evaporate long etch

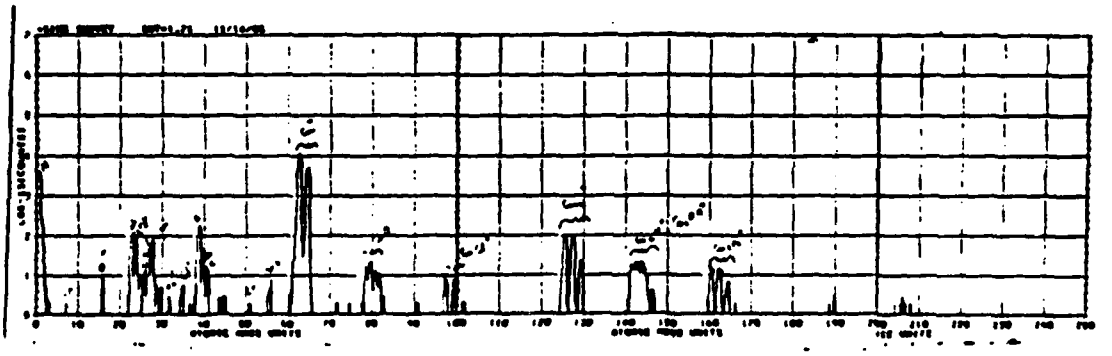

Figure 125: SIMS: sputter long etch

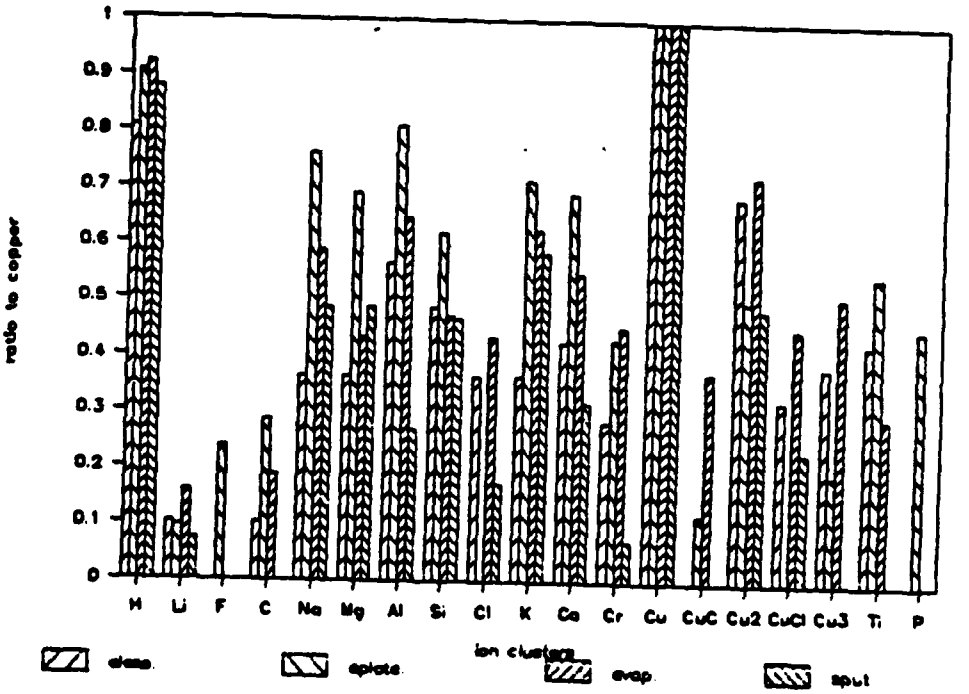

Figure 126: SIMS: comparison long etch

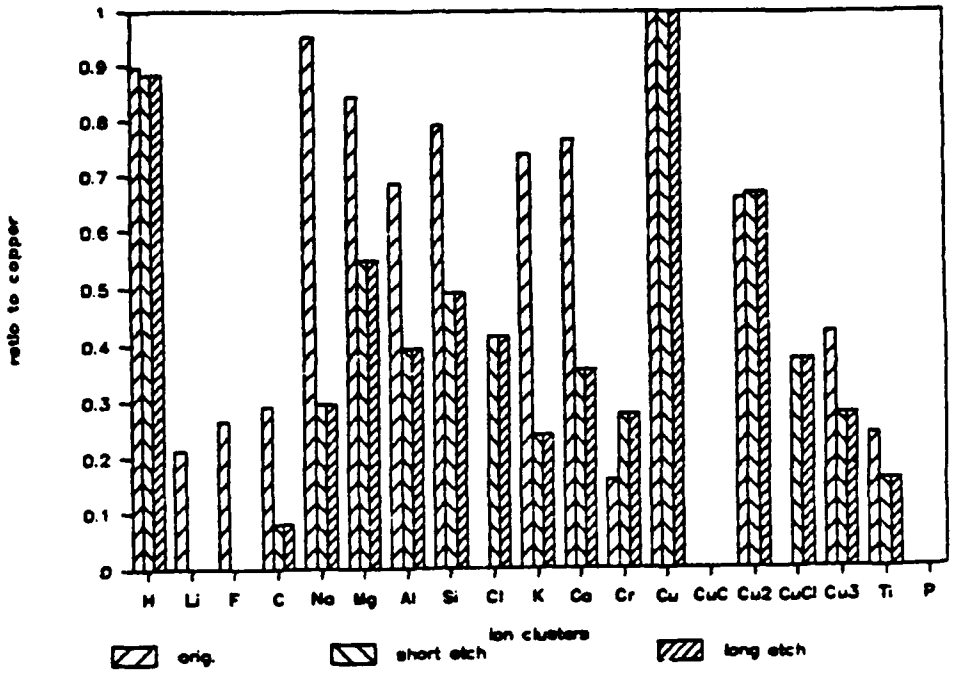

Figure 127: SIMS: comparison all electroless

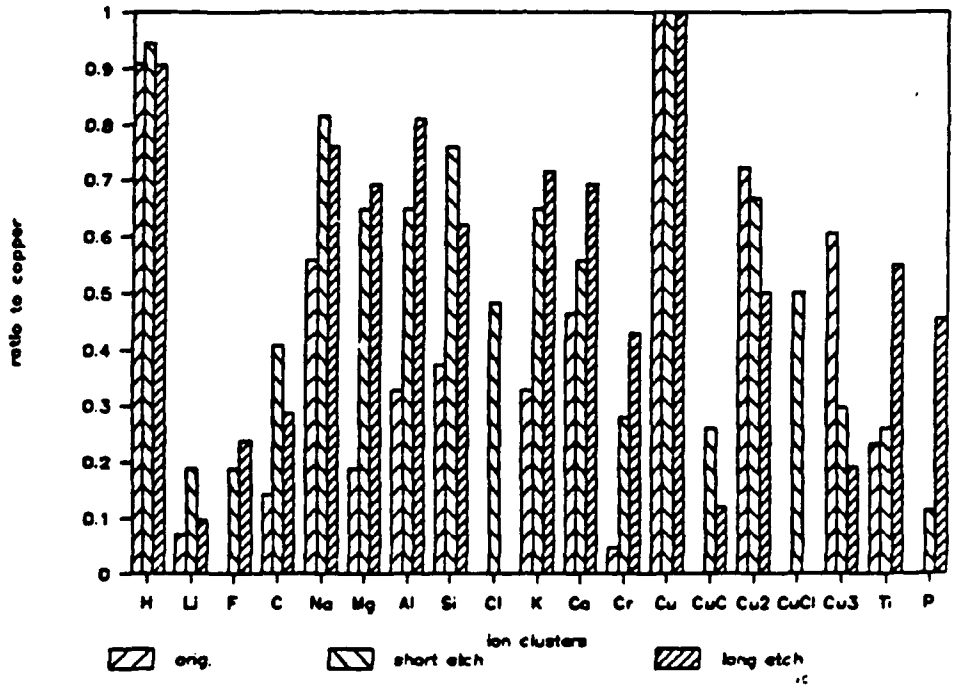

Figure 128: SIMS: comparison all electroplate

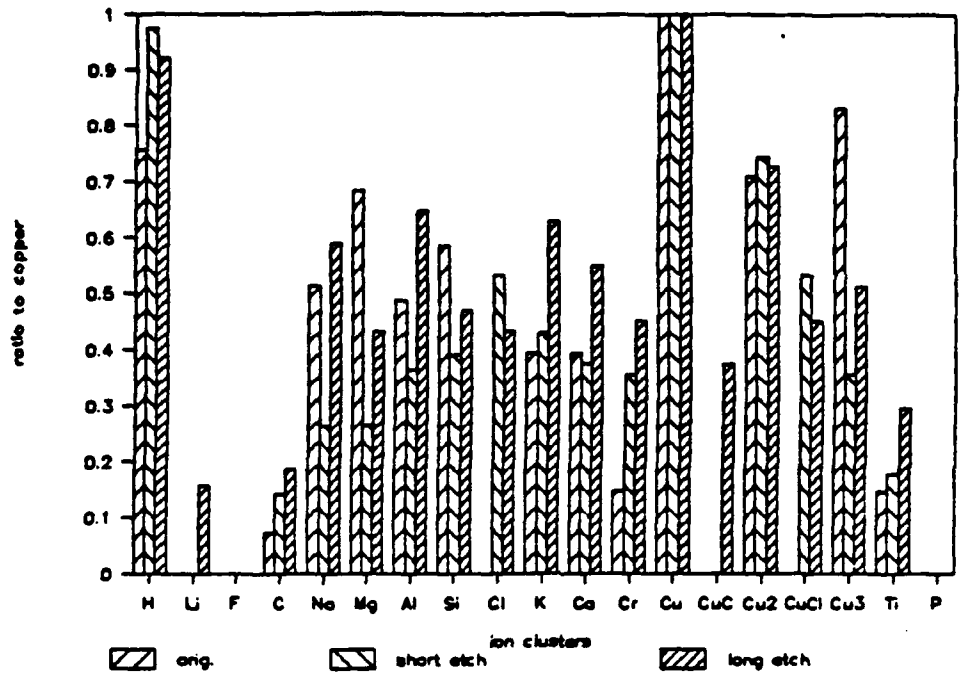

Figure 129: SIMS: comparison all evaporate

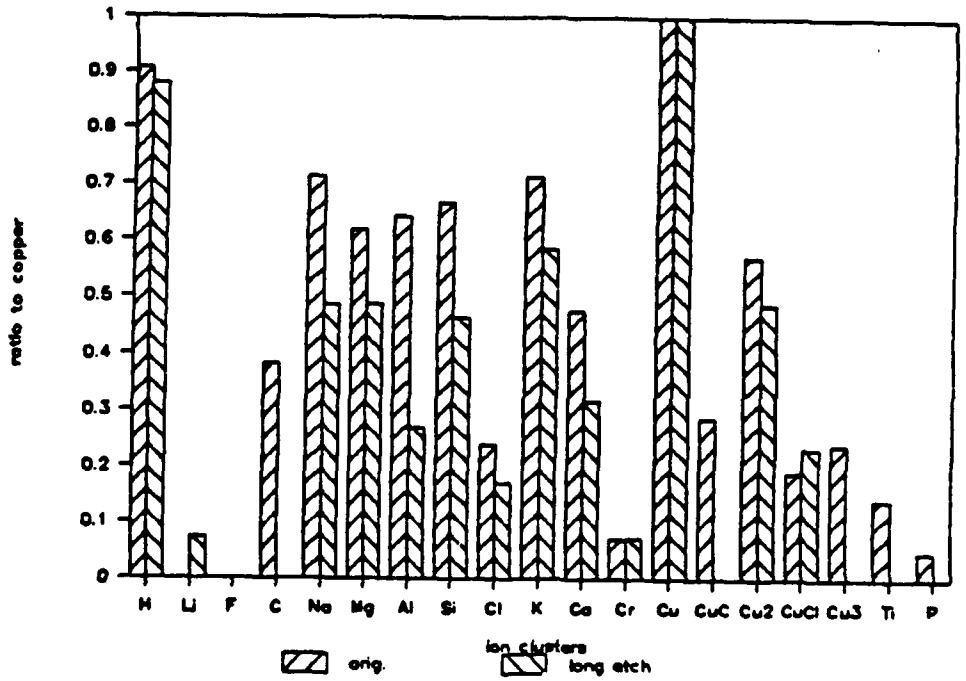

Figure 130: SIMS: comparison all sputter

BIBLIOGRAPHY

1. U. Erb, H. Gleiter, and G. Schwitzgebel, Acta Metallurgical, Vol.30, pp.1377-80, 1982

2. J.Schwarz, L.Walsh, unpublished research proposal to IBM, 1985

3. G.T.Miller,Jr. and K.R.Lawless, Journal Electrochemical Society, Vol. 106, No.10, pp.854-860,1959

4. M.R. Pinnel, H.C. Tompkins, and D.E. Heath, Journal Vacuum Science Technology, Vol.16, No.2, pp.161-3, Mar/Apr. 1979

5. H.A. Arbit and K. Nobe, Corrosion, Vol.24, p.17, 1968

6. D.D. Davis and D.L. Johnson, Journal of Electrochemical Society, Vol.125, No.11, pp.1889-91, 1978

7. M.E. Ghasby, G.A. Sedahmed, and I.A.S. Mansour, Br. Corrosion J., Vol.17, No.1, 1982

8. G. Bianchi and P. Longhi, Corrosion Science, Vol.13, pp.853-64, 1973

9. R.F. North and M.J. Pryor, Corrosion Science, Vol.10, p.297, 1970

10. A.J.Read, J.of Physical Chemistry, Vol.76, No.24, 1972

11. R.D. Granata, H. Vedage, and H. Leidheiser,Jr., Surface Technology, Vol.22, pp.39-50, 1984

12. S. N. Raicheva, Electrochemica Acta, Vol.29, No.8, pp.1067-73, 1984

13. H. Leidheiser, Jr., "The Corrosion of Copper, Tin, and Their Alloys", pp.72-7, John Wiley and Sons, N.Y., 1971

14. R. Perret and G. Joseph, Lab. Practice, Vol.32. No.10, pp.95-6, 1983

15. L.I. Maissel and R. Glang, "Handbook of Thin Film Technology", McGraw-Hill, N.Y., chapters 1&2, 1970

16. A.M. Wilson, "Polyimides Synthesis, Characterization, and Applications", editor K.L. Mittal, p.721, Plenum Press, N.Y., 1984

17. L.Walsh, Microstructural Characterization of Copper Films Deposited on Titanium Substrates, Unpublished Masters Thesis, 1984

18. K.Blackwell, IBM Endicott, Private Communication

19. L.E. Reichl, "Instabilities, Bifunctions and Flucations in Chemical Systems", 1st Edition, University of Texas Press, Austin, 1982

20. "Temporal Order: Proceedings of a Symposium on Oscillations in Heterogenous Chemical and Biological Systems", University of Bremen, Sept. 17-22, 1984, Berlin, Springer-Verlag, 1985

21. K.F.Bonhoeffer and H.Gerischer,Zeitschrift fur Elektrochemie and angewandte physikalische Chemie, Band 52, No.4, pp.149-160, Sept.1948

22. J.H.Hildebrand and R.E.Powell,Principles of Chemistry, Maxmillan Co., New York, p.265, 1964

23. P.G.Shewmon, Diffusion in Solids, J.William Book Company, Jenks, Ohio, p.66, 1983

24. H.Γ.Winters, J.Vac.Sci.Technol.B3(1),pp.9-15, Jan/Feb 1985

25. H.F.Winters and J.W.Coburn, J.Vac.Sci.Technol, B1(2),pp.1376-1383, Apr/Jun1983

26. H.F.Winters, J.W.Coburn, and T.J.Chuang, J.Vac.Soc.Technol. B1(2),pp.469-480, Apr/June 1983

27. L.G.M.Pettersson and P.S.Bagus, Physical Review Letters, Vol.56, No.5, Feb.1986

28. G.C.Schwartz and P.M.Schaible, Journal Electrochemical Society, Vol.130,No.8,pp.1777to1779,August 1983

29. S.Park, T.N.Rhodin, and L.C.Rathbun,J.Vac.Sci.Technol. A4(2),pp168-172, Mar/Apr1986

30. P.J.Goddard and R.M.Lambert, Surface Science 67,pp.180-194, 1977

31. M.F. Obrecht, Corrosion, Vol.18, No.5, p.189, 1962

32. W.Sesselmann and T.J.Chuang,Surface Science, 176,pp.66-90, 1986

33. R.W.Vook, X-Ray Diffraction, in Epitaxial Growth Part A, by J.W.Matthews(ed), Academic Press, NY,p360,1975

34. H. Galrm, F. Jeylitsch, and E. Horl, Pract. Metall., Vol.19, p.369, 1982

35. O. Kubaschewski and B.E. Hopkins, "Oxidation of Metals and Alloys", Academic Press, London, 1962

36. J. C. Scully, "The Fundamentals of Corrosion", Pergamon Press, N.Y., 1966

37. H.E. Buhler, "Atlas of Interference Layer Metallography", 1980

38. M. Francon, "Optical Interferometry", pp.79-81, Academic Press, N.Y., 1966

39. U.R. Evans, "Metallic Corrosion, Passivity, and Protection", pp.49,52,676,Edward Arnold & Co., London, 1937

40. C. F. Baes and A. Mesmer, "The Hydrolysis of Cations", Wiley, N.Y., 1976

41. B. Derby and E.R. Wallach, Journal of Materials Science, Vol.19, pp.3140-48, 1984

42. M. Turner, P.A. Brook, Corrosion Science, Vol.13, pp.973-83, 1973

43. M. Braun, K. Nobe, Journal of Electrochemical Society, Vol.126, No.10, pp.1666-71, 1979

44. H.P. Lee, K. Nobe, Journal of Electrochemical Society, Vol.131, No.6, pp.1236-43, 1984

45. R.J. Chin and K. Nobe, Corrosion, Vol.33, No.10, pp.364-69, 1977

46. B. Miller, Journal of Electrochemical Society, Vol.116, No.12, 1969

47. D.W. Shoesmith, T.E. Rummery, D. Owen, and W. Lee, Journal of Electrochemical Society, Vol.123, No. 6, pp.791-99, 1976

48. W.D. Bjorndahl, K. Nobe, Corrosion, Vol.40, No.2, pp.82-7, 1984

49. A.A. Kazantsev and V.A. Kuznetsov, Elecktrokhimija, Vol.19, No.1, pp.92-5, 1983

50. A. L. Bacarella and J.C. Griess Jr., Journal of Electrochemical Society, Vol.120, No.4, pp.459-65, 1973

51. C.H. Bonfiglio, H.C. Albaya, O.A. Cubo, Corrosion Science, Vol.13, pp.717-24, 1973

52. C. E. Guthrow,Jr. and G.T. Miller,Jr., Journal of Electrochemical Society, Vol.113, No.4, pp.415-23, 1966

53. F. DiQuarto and S. Piazza, Electrochima Acta, Vol.30, No.3, pp.315-24, 1985

54. G. Faita, G. Fiori, and D. Salvadore, Corrosion Science, Vol.15, pp.383-92, 1975

55. C. Ogden and D. T ıch, Journal of Electrochemical Society, Vol.128, No.3, pp.539-46,1981

56. R. Walker and S.J. Duncan, Surface Technology, Vol.23, pp.301-21, 1984

57. S.T. Rashkov and L. Vuchkov, Surface Technology, Vol.14, pp.309-21, 1981

58. S.C. Barnes, Journal of Electrochemical Society, Vol.111, No.3, pp.296-99, 1964

59. S. Nakahara and Y. Okinaka, Acta Metallurgical, Vol.31, No.5, pp.713-24, 1983

60. A.G. Dirks and J.J. VanDenBrock, Thin Solid Films, Vol.96, pp.257-63, 1982

61. S. Nakahara and A.F. Hebard, Thin Solid Films, vol.102, pp.345-60, 1983

62. C. Ogden, D. Tench, J. White, Journal of Applied Electrochemistry, Vol.12, pp.619-26, 1982

63. J.M. Nieuwenhuizen and H.B. Haanatra, Phillips Tech. Review, Vol.27, No.3/4, pp.87-91

64. K.I. Popov, M.G. Pavlovic, and M.D. Maksimovic, Journal of Applied Electrochemistry, Vol.12, pp.525-31, 1982

65. H.P. Dhar, R.E. White, G. Burnell, L.R. Cornwell, R.B. Giffen, and R. Darby, Corrosion, Vol.1, No.6, pp.317-23, 1984

66. J.W. Matthews, "Epitaxial Growth- Parts A & B", chapter 2, Academic Press, N.Y., 1975

67. H.S. Potdar, N. Pavaska, A. Mitra, A.P.B. Sinha, Solar Energy Material, Vol.4, p.291, 1981

68. A. Aveline and I.R. Bonilla, Solar Energy Material, Vol.5, pp.211-20, 1981

69. V.F. Drobny and D.L. Pulfrey, Thin Solid Films, Vol.61, pp.89-98, 1979

70. S. Haupt, U. Collisi, H.D. Speckmann, H.H. Strehblow, Journal of Electroanalytical Chemistry, Vol.194, pp.179-90, 1985

71. L. Paoletti, P.A. Rosa, P. Picozzi, and S. Santucci, Journal Vacuum Science Technology A, Vol.2, No.4, pp.1471-4, 1984

72. D. W. Bullett, Philosphical Magazine B., Vol.51, No.2, pp.223-4, 1985

73. C.R. Tellier, Journal of Material Science, Vol.20, pp.1901-19, 1985

74. T.M. Mayer, M.E. Harper, J.J Cuomo, Journal Vacuum Science Technology A, Vol.3, No.4, pp.1779-83, 1985

75. A.T. D'Agostino and P.N. Ross Jr., Journal of Electroanalytical Chemistry, Vol.189, pp.371-77, 1985

76. J. Kim and D.S. Yee, Thin Solid Films, Vol.128, pp.67-78, 1985

77. G.J.M. Janssen and W.C. Nieuwpont, Philosphical Magazine B, Vol.51, No.2, pp.127-35, 1985

78. C.H. Ling, C.W. Kwok, and T.M. Tay, Journal Physics D: Applied Physics, Vol.18, pp.671-75, 1985

79. W. Davison and C. Woof, Analytical Chemistry, Vol.57, pp.2567-70, 1985

80. M. Pourbaix, "Thermodynamics of Dilute Aqueous Solutions", pp.384-92, Edward Arnold and Co., London, 1949

81. J.P. Dahl and A.C. Switendick, Journal Physics and Chemistry of Solids, Vol.27, pp.931-42, 1966

82. S.M. Wilhelm, Y. Tanizawa, Chang-YiLee, and N. Hackerman, Corrosion Science, Vol.22, No.8, pp.791-805, 1982

83. G. Wrangln, "An Introduction to Corrosion and Protection of Metals", p.4, Chapman and Hall, N.Y., 1985

84. H.J. Fischbeck and K.H. Fischbeck, "Formulas, Facts, and Constants for Students and Professionals in Engineering, Chemistry, and Physics", p.34, Springer-Verlag, N.Y., 1982

85. L.E. Davis, N.C. MacDonald, P.W. Palmberg, G.E. Riach, and R.E. Weber, "Handbook of Auger Electron Spectroscopy", Physical Electronics Industries, Inc., Minnesota, 1976

86. C. Barrett, T.B. Massalski, "Structure of Metals", 3rd Revised Edition, pp.463-5, Pergamon Press, N.Y., 1980

87. American Society for Metals, "Metals Handbook Ninth Edition, Volume 10, Materials Characterization", pp.395-6, ASM, Metals Park, 1986

88. B.D. Cullity, "Elements of x-ray diffraction", 2nd edition, p.517, Addison-Wesley, Reading, Massachuetts, 1978

89. Joint Committee on Powder Diffraction Standards, 1601 Park Lane, Swarthmore, Pa. 19081

90. D.W.Bullett, Solid State Communication, Vol. 38, pp.969-972, 1981

91. G.Martin and B.Perrailon, Measurements of Grain Boundary Diffusion in Grain-Boundary Structure and Kinetics, Metals Park, Ohio, p269, 1980

MISSION
of
Rome Air Development Center

RADC plans and executes research, development, test and selected acquisition programs in support of Command, Control, Communications and Intelligence (C^3I) activities. Technical and engineering support within areas of competence is provided to ESD Program Offices (POs) and other ESD elements to perform effective acquisition of C^3I systems. The areas of technical competence include communications, command and control, battle management information processing, surveillance sensors, intelligence data collection and handling, solid state sciences, electromagnetics, and propagation, and electronic reliability/maintainability and compatibility.